Portions of this dissertation were adapted from the following publications:

doi: 10.1371/journal.pone.0129055

doi: 10.1128/mBio.01168-17

Defining mechanisms of disease initiation through analysis of *Helicobacter pylori* interactions with gastric microbial communities and the host

Alevtina A. Gall

A dissertation

submitted in partial fulfillment of the

requirements for the degree of

Doctor of Philosophy

University of Washington

2018

Reading Committee:

Nina R. Salama, Chair

Daniel B. Stetson

Lucas R. Hoffman

Program Authorized to Offer Degree:

Molecular and Cellular Biology

University of Washington

Abstract

Defining mechanisms of disease initiation through analysis of *Helicobacter pylori* interactions with gastric microbial communities and the host

Alevtina A. Gall

Chair of the Supervisory Committee:

Professor Nina Salama

Molecular and Cellular Biology, University of Washington

Division of Human Biology, Fred Hutchinson Cancer Research Center

Helicobacter pylori is an exceptionally prevalent bacterial pathogen that colonizes the human stomach where it can cause inflammation, and in some cases lead to gastric ulcers and cancer. *H. pylori* infection also seems to protect against development of certain diseases such as esophageal adenocarcinoma. The prevalence of *H. pylori* has been rapidly declining in economically developed countries and the disappearance of infection tracks with the reciprocal rise in esophageal adenocarcinoma.

H. pylori may be modulating esophageal adenocarcinoma risk through its interactions with members of the upper gastrointestinal microbial communities. Before that hypothesis can be tested, a comprehensive survey of which microbial community members are present in health and disease is needed. Barrett's esophagus, a metaplastic transition of the normal squamous epithelial lining of the esophagus to mucus-producing columnar epithelium, is the only known precursor lesion to esophageal adenocarcinoma. Using high throughput sequencing, we characterized the microbial composition of the upper gastrointestinal tract in individuals with Barrett's esophagus. We found that bacterial communities of the stomach and esophagus showed overlapping community membership. Despite closer proximity, the stomach antrum and corpus communities were less similar than the antrum and esophageal samples. In this Barrett's esophagus cohort, *Streptococcus* and *Prevotella* species dominated the upper GI and the ratio of these two species was associated with waist-to-hip ratio and hiatal hernia length, two known esophageal adenocarcinoma risk factors. Genomic instability is a predictor of cancer development in Barrett's esophagus. We found that *H. pylori*-positive individuals had a significantly decreased incidence of aneuploidy and a trend toward lower incidence of esophageal adenocarcinoma. Our analysis also revealed that *H. pylori* can be found in esophageal tissues of infected individuals. The protective effect of *H. pylori* carriage on risk of esophageal adenocarcinoma development may be explained by *H. pylori*'s influence on members of the esophageal microbiota and/or direct interaction with esophageal epithelial cells.

In the stomach, *H. pylori* is recognized by both the innate and adaptive immune system, but this rarely results in bacterial clearance. *H. pylori* establishes chronic colonization, in part, by evading numerous host defense strategies. However, *H. pylori* also seems to benefit from a restricted inflammatory response. During *H. pylori* infection cytotoxin associated gene A (CagA)

is delivered to gastric epithelial cells through a type 4 secretion system (*cag*-T4SS). Along with CagA, proinflammatory bacterial factors gain access to the host cell cytosol through the *cag*-T4SS. Detection of those bacterial factors leads to activation of global transcription factor NF-κB, which regulates production of proinflammatory cytokines key for recruitment of immune cells to the site of infection. Until recently, the entire *cag*-T4SS-dependent inflammatory response in gastric epithelial cells was attributed to detection of bacterial cell wall fragments by host pathogen recognition receptor nucleotide-binding oligomerization domain 1 (NOD1). When we CRISPR/Cas9 targeted NOD1 in gastric epithelial cells, we found that the NF-κB mediated inflammatory response was attenuated, but not eliminated, suggesting that other pathogen recognition pathways play a role in *H. pylori* detection. We determined that bacterially-derived heptose-1,7-bisphosphate (HBP), a metabolic precursor in lipopolysaccharide (LPS) biosynthesis, is delivered to the host cytosol through the *cag*-T4SS, where it activates the host tumor necrosis factor receptor-associated factor (**T**RAF)-**i**nteracting protein with **f**orkhead-**a**ssociated domain (TIFA)-dependent cytosolic surveillance pathway. We also found that CagA toxin contributes to the late NF-κB-driven response. The sequential activation of TIFA, NOD1, and CagA delivery drives the initial inflammatory response in gastric epithelial cells. To determine the *in vivo* relevance of NOD1 signaling, we infected *Nod1*$^{-/-}$ mice with a mouse adapted strain of *H. pylori*. We found that *Nod1*$^{-/-}$ mice were more susceptible to *H. pylori* infection than wild-type mice. Despite the modest contribution of NOD1 signaling that we observed in the gastric epithelial cell line, Nod1 appears to be important in restricting bacterial growth in a mouse model of infection.

The discrepancy between our *in vitro* and *in vivo* findings motivated us to develop a better gastric epithelial cell model to study innate immune signaling pathways involved in *H.*

pylori detection. Using mouse and human gastric tissues, we selected, expanded and propagated Lgr5-expressing progenitor cells in the presence of stem cell growth factors Wnt, R-spondin and Noggin. We differentiated these gastric organoids into primary-like gastric epithelial cells by withdrawing stem cell growth factors from the culture media. When we seed gastric organoids on a permeable support, they form a polarized gastric epithelial monolayer that can then be used for infection studies where bacteria are added to the apical side of the transwell. This novel *ex vivo* system enables host-pathogen interaction studies in a physiologically more relevant setting.

Myeloid-derived cells detect *H. pylori* via pathogen recognition pathways that are distinct from those activated in gastric epithelial cells. We found that monocytes initiate a type I interferon (IFN) response following *H. pylori* exposure and that the response is *cag*-T4SS dependent. It remains unclear which bacterial factor(s) is initiating the type I IFN response and whether the response is synergistic or antagonistic of the NF-κB-driven inflammatory response. We can begin addressing these questions by using the gastric organoid co-culture system where we infect polarized epithelial cells with *H. pylori* and add myeloid-derived cells to the basal compartment to investigate the cross talk between bacteria, gastric epithelial cells and recruited immune cells. The studies presented in this dissertation enhance our understanding of how *H. pylori* initiates a proinflammatory signaling cascade in the host and better defines pathways that can be manipulated for therapeutic purposes.

TABLE OF CONTENTS

LIST OF FIGURES

LIST OF TABLES

ACKNOWLEDGEMENTS

First and foremost, I would like to thank my thesis advisor, Nina Salama, who has been a wonderful role model and has pushed me to learn and grow as an independent researcher. I am deeply grateful for her support and guidance throughout my graduate school career. I would like to thank all of the members of the Salama Lab, past and present, who made even the most frustrating and long days in lab so much more enjoyable. I would particularly like to thank Christina Leverich for all of her help with various experiments and keeping our lab organized and running smoothly. A big thanks to Desirée Yang, for teaching me how to make bacterial mutants.

I am grateful to the members of my thesis committee, David Fredricks, Jessica Hamerman, Luke Hoffman and Dan Stetson, who kept me on track and encouraged me to think critically about my data and how it fits in a larger context.

I was also fortunate to work with a number of wonderful collaborators throughout my graduate career. I am grateful to members of the Reid lab, particularly Brian Reid, Carissa Sanchez, Patty Blount, Christine Karlsen and Xiaohong Li for their contributions to our project characterizing microbial communities in the upper gastrointestinal tract of individuals with Barrett's esophagus. Thank you to Erick Matsen, Brian Claywell and Connor McCoy for providing the computational biology expertise that allowed us to make sense of our sequencing data. I really appreciate all of the help that members of Dan Stetson's lab provided, especially Elizabeth Gray and Hannah Volkman, who supplied critical reagents and helpful suggestions for CRISPR targeting mammalian cells and probing type I IFN responses in *H. pylori* infection. A big thank you to Scott Gray-Owen and Ryan Gaudet for being so generous with their time and

tools/reagents, which enabled us to more fully dissect the contribution of TIFA to *H. pylori* detection. I am also very grateful to members of Thad Stappenbeck's lab, particularly Christina Hickey, Nicole Malvin, Kelli VanDussen and Naomi Sonnek, for teaching me how to isolate and culture gastrointestinal organoids. Thank you to Jason Smith and Mayumi Holly for their experimental advice for optimizing gastric organoid growth conditions in our lab.

I am extremely grateful to the UW MSTP, particularly Julie Overbaugh and Marshall Horwitz, for always being supportive of their students and ensuring that all of us make the most of our time in the program. Thank you to UW Molecular and Cellular Biology Program, particularly, Maia Low, Andrea Brocato and Michelle Karansevalos for providing the administrative support to get me to the finish line.

This project was supported by NIH NIAID grants R01A1094839, R01AI054423 and P30 CA015704NIH (N.R.S.), as well as the Bacterial Pathogenesis Training Grant T32 AI55396-10 and MSTP training grant T32 GM007266 (A.A.G.) Work presented in this thesis are the responsibility of the author and do not necessarily represent the official views of the NIH.

DEDICATION

To my mom, Svetlana, for instilling in me the value of hard work and dedication and for encouraging me to pursue my dreams

To my husband, Martin, for being a constant source of support and encouraging me to overcome challenges even when they seemed insurmountable

To my daughter, Maya, for always reminding me what is important in life

CHAPTER 1: Background

Helicobacter pylori pathogenesis

Helicobacter pylori is a Gram negative bacterial pathogen notorious for its role in development of peptic ulcer disease, gastric adenocarcinoma and MALT lymphoma. Asymptomatic infection is exceptionally prevalent among the world's population resulting in gastric inflammation in virtually all infected individuals. However, only about 10% develop gastric ulcers, < 3% develop gastric adenocarcinoma and < 0.1% develop mucosa-associated lymphoid tissue (MALT) lymphoma (*1*). Chronic inflammation caused by *H. pylori* contributes to the development and progression of all *H. pylori*-associated diseases (*2*). Gastric adenocarcinoma is the third leading cause of cancer death worldwide and 89% of all gastric cancers result from chronic *H. pylori* infection (*3*). Seventy-nine percent of gastric MALT lymphomas, which are B-cell malignancies, are associated with *H. pylori* infection (*4*). Antibiotics to eradicate *H. pylori* are the first line of treatment and typically result in complete remission of MALT lymphoma in 70-80% of cases (*5*). Interestingly, a well characterized translocation in *H. pylori*-associated MALT lymphomas is a fusion oncogene between *MALT1* (essential for activation and proliferation of T and B cells) and *API2* (inhibitor of apoptosis), which leads to constitutive NF-κB stimulation, a major inflammatory pathway activated by *H. pylori* (*6*).

H. pylori uses flagellar motility and urease, an enzyme that locally buffers stomach acid, to escape the stomach lumen and colonize a narrow strip of mucus overlaying the gastric epithelium. The bacteria adhere to gastric epithelial cells, but remain primarily extracellular (*7*). *H. pylori* can also induce apoptosis in gastric epithelial cells (*8*, *9*) and disrupt cell-cell junctions

(*10*, *11*), allowing the bacteria to gain access to the submucosal space where they can directly interact with recruited immune cells. *H. pylori* typically infects the stomach antrum where it can lead to development of duodenal ulcers, however, this pattern of infection is associated with a lower risk of cancer progression. Individuals who are predominantly infected in the stomach corpus or have inflammation throughout the stomach are at a greater risk of developing gastric cancer (*12*). A complex interplay of bacterial, host genetic and environmental factors may explain why some individuals develop disease, while in others chronic colonization is protective.

Protective associations with *H. pylori* infection

A growing body of literature suggests that colonization with *H. pylori* can be protective against development of certain diseases such as allergy, asthma (*13*), esophageal adenocarcinoma (*14*), inflammatory bowel disease (*15*), multiple sclerosis (*16*) and obesity (*17*). *H. pylori* rates have steadily declined in economically-developed countries over the last 100 years, mirroring a decline in peptic ulcer and gastric cancer rates. However, a reciprocal increase in some allergic and inflammatory diseases is well documented (*18-20*).

Evidence from animal studies suggests that regulatory T cells (Tregs), which secrete anti-inflammatory cytokines, such as IL-10 and are induced by *H. pylori* infection, suppress inflammatory responses to allergens in the airway and pathogen-induced or sodium dextran sulphate-induced intestinal inflammation (*21*, *22*). *H. pylori*-positive individuals have higher frequencies of IL-10 producing Tregs in peripheral blood (*23*) and lower systemic type I interferon (IFN) levels (*24*). *H. pylori* genomic DNA contains much higher frequency of immunoregulatory than immunostimulatory sequences, as compared to *E. coli* or probiotic bacteria *B. infantis*, *B. longum*, *L. reuteri* and *L. acidiphillus*. Bone marrow derived dendritic

cells (BMDCs) transfected with *H. pylori* genomic DNA produce less IL-12 and type I IFN compared to *E. coli* DNA transfected BMDCs (*24*). Based on these data several, non-mutually exclusive, mechanisms may explain *H. pylor*i's protective effects. Peripheral *H. pylori*-induced Tregs may be maintaining an overall anti-inflammatory state by suppressing activation of effector T cells. Tregs may directly interact with immature dendritic cells causing downregulation of their co-stimulatory molecules and preventing their maturation, which leads to the inability of DCs to efficiently prime effector T cells that drive inflammatory responses (*21*, *25*). Bacterial factors, such as immunoregulatory DNA may directly tolerize antigen presenting cells, which in turn induce more naïve T cells to become Tregs rather than effector T cells.

H. pylori interactions with gastrointestinal microbial communities

Disease can be caused not only through pathogen interaction with the host, but also through pathogen interaction with other microbes. The stomach was originally believed to be a sterile site due to the presence of digestive enzymes and its highly acidic, inhospitable environment. It is now evident that the gastric mucosa supports a diverse range of bacterial species. One recent study determined that the number of cultivatable bacterial species present in the healthy human stomach ranges from 10^2 to 10^4 colony forming units (CFU)/g stomach tissue and is comprised of four main genera: *Propionibacterium*, *Lactobacillus*, *Streptococcus* and *Staphylococcus* (*26*). Loss of microbial diversity along the gastrointestinal (GI) tract has been associated with a number of disease states (*27*). When *H. pylori* is present, it dominates all other bacterial species and in high-throughput sequencing studies 93-99% of reads from stomach samples map to *H. pylori* (*28-32*). Although *H. pylori* clearly contributes to development of gastric cancer, *H. pylori* infection seems to protect against esophageal adenocarcinoma (*14*). It is

possible that *H. pylori* modifies esophageal adenocarcinoma risk through its effect on upper GI tract microbial communities.

Barrett's esophagus is the only known precursor lesion to esophageal adenocarcinoma and is characterized by metaplasia of a normal squamous epithelium to a mucus-secreting simple columnar epithelium. One of the largest studies characterizing the microbial constituents in the distal esophagus found that samples from individuals with esophagitis and Barrett's esophagus contained high frequency of Gram-negative organisms from the phyla *Bacteroidetes*, *Proteobacteria*, *Fusobacteria*, and *Spirochaetes,* whereas Gram-positive organisms from the Firmicutes phyla dominated samples from healthy esophagus. It has been proposed that one way in which the Gram-negative microbiota may contribute to progression to esophageal adenocarcinoma is through production of pro-inflammatory bacterial factors such as LPS. LPS detection activates NF-κB, leading to production of cytokines that drive inflammation, which may increase risk for cancer development. Furthermore, NF-κB activation increases levels of inducible nitric oxide synthase and nitric oxide relaxes the lower esophageal sphincter allowing the acidic gastric refluxate to damage the lower esophageal epithelial lining. There are several potential mechanisms by which *H. pylori* may protect against development of esophageal adenocarcinoma: 1) chronic *H. pylori* colonization may lead to atrophic gastritis and loss of acid producing parietal cells, which results in a less acidic gastric refluxate 2) Tregs induced by *H. pylori* infection prevent inflammation driven damage of the esophagus 3) *H. pylori* occupies the niche of disease modulating microbes in the esophagus 4) *H. pylori* directly interacts with esophageal epithelial cells affecting pathways involved in cancer progression. More in depth studies aimed at understanding the interaction of *H. pylori* with the host and upper GI microbial

communities are needed in order to determine which mechanisms contribute to esophageal cancer development.

Transmission and adaptation of *H. pylori* to the human host

H. pylori has resided with its human host for at least 100,000 years, predating modern human migration out of Africa (*33*, *34*). The bacterium is likely transmitted within families via the oral-oral, gastro-oral or fecal-oral route, most commonly from parent to child. Mother-to-child transmission appears to be the most common (*35*). A recent study, analyzing *H. pylori* 16S ribosomal subunit DNA sequences in stool samples from 30 Iranian families, determined that 33% of children harbored sequences identical to their mother's strain and 7% identical to their father's strain (*36*). Colonization typically occurs before the age of 5 (*37*). Interestingly, colonization in children can be transient or persistent (*38*), whereas colonization of adults is typically persistent (*39*). Limited evidence also suggests that viable *H. pylori* may be present in drinking water in areas of the world with high infection burden (*40*).

Bacterial sequence identity within families lends support for the idea that *H. pylori* is vertically transmitted. Numerous studies analyzing *H. pylori* DNA sequences from the same individual over time have confirmed that genetic changes occur in the bacteria in the form of single nucleotide polymorphisms and recombination events (*41*, *42*), especially in cases of mixed infection with two or more distinct strains (*43*). *H. pylori* utilizes a number of strategies that increase genetic diversity within the bacterial population, including natural transformation, point mutations, intra and inter-genomic recombination, as well as slipped-strand mispairing (*44*). These changes can lead to bacterial progeny that are better adapted to deal with threats within the

host environment. Children are genetically similar to their biological parents and, therefore, may be more susceptible to colonization with strains that have adapted in their parents for decades.

Cag pathogenicity island

Cytotoxin-associated gene A (CagA) has been extensively characterized as a major contributor to epithelial cell transformation that can result in gastric cancer. Infection with *cagA+* strains is associated with increased inflammation and subsequent development of peptic ulcers and gastric adenocarcinoma (*45*, *46*). CagA is encoded within a region of the chromosome known as the *cag* pathogenicity island (*cag*-PAI). Along with *cagA*, the *cag*-PAI contains genes required for assembly of a type IV secretion system (T4SS). CagA is injected directly into epithelial cells via the *cag*-T4SS, which acts as a molecular syringe (*47*). After several months of experimental infection with a single *H. pylori* strain, mice and rhesus macaques accumulated bacterial strain variants that contained mutations in the *cagY* gene, which render the *cag*-T4SS non-functional. Interestingly, strains with functional *cag*-T4SS were also recovered from the same animals (*48*, *49*) suggesting that the ability to switch the *cag*-T4SS "on" or "off" is advantageous for the bacteria.

Presence of a functional *cag*-T4SS and CagA allows *H. pylori* to gain nutrients from host gastric epithelial cells. $CagA^-$ *H. pylori* or mutants lacking a functional *cag*-T4SS are unable to form microcolonies on the apical surface of gastric epithelial cells and replicate in iron-limiting conditions. CagA+ strains cause mislocalization of host transferrin, a host protein used to transport iron, to the apical surface of gastric epithelial cells (*50*). Furthermore, in the setting of iron-deficiency, CagA+ *H. pylori* strains become hyper-virulent with increased translocation of CagA into host cells and subsequent increased production of pro-inflammatory cytokines. In

contrast, CagA$^-$ strains undergo changes from wild type helical to coccoid morphology, a change known to be induced by environmental stress. Addition of exogenous iron reverses the coccoid phenotype (*51*).

Along with CagA, the *cag*-T4SS delivers bacterial factors into the gastric epithelial cell cytosol where they activate an NF-κB-dependent immune response, leading to production of proinflammatory cytokines such as interleukin 8 (IL-8), a key neutrophil chemoattractant (*52*). Thus, the bacteria are continuously balancing the beneficial effects of CagA translocation, namely nutrient acquisition, and the deleterious host immune response induced by a functional *cag*-T4SS. Interestingly, a study analyzing *H. pylori* prevalence in a Finish cohort between 1973 and 1994 found that CagA+ *H. pylori* strains declined more rapidly than CagA$^-$ strains (*39*). Furthermore, a number of the protective effects ascribed to *H. pylori* are specifically associated with CagA$^+$ strains (*53*, *54*).

Innate immune response to *H. pylori*

Gastric epithelial cells initiate the earliest immune response to *H. pylori*. The bacteria attach to host epithelial cells via a suite of outer membrane proteins. For example, adhesin BabA binds fucosylated Lewis^B antigen and SabA binds sialyl-Lewis^X antigen on gastric epithelial cells (*55*). Direct contact with the host cell induces the assembly of the *cag*-T4SS, which translocates CagA into host cells (*47*). Along with CagA, bacterial factors are delivered inside the gastric epithelial cell where they induce an NF-κB-dependent pro-inflammatory response (*52*). Until recently, the majority of the *cag*-T4SS-dependent NF-κB-driven immune response in gastric epithelial cells was attributed to the intracellular delivery of peptidoglycan cell wall fragments which are recognized by host nucleotide-binding oligomerization domain 1 (NOD1)

(*3*, *56*, *57*). Activation of NOD1 leads to induction of NF-κB, a global transcription factor that drives the production of pro-inflammatory cytokines, such as IL-8 and release of antimicrobial peptides, such as β-defensins (*56*-*58*). IL-8 is a potent neutrophil chemoattractant that recruits neutrophils and monocytes to the site of infection (*59*). In a mouse model of *Helicobacter* infection neutrophils were required for bacterial clearance, but were only able to do so in the absence of IL-10 (i.e. *Il10*$^{-/-}$ mice) or when Tregs were depleted (*60*, *61*).

H. pylori also initiates a pro-inflammatory immune response independent of the *cag*-T4SS. Toll-like receptor 2 (TLR2) recognizes a number of *H. pylori* ligands including LPS (*62*), neutrophil activating protein (NAP) (*63*), heat shock protein 60 (HSP60) (*64*) and urease (*65*). The NLRP3 inflammasome has been shown to play a role in controlling *H. pylori* infection, possibly through the TLR2-dependent detection of *H. pylori* LPS and urease (*65*). NLRP3 deficient mice are less susceptible to *H. pylori* infection and induce fewer Tregs in response to infection than wild type mice (*66*). Activation of the NLRP3 inflammasome by *H. pylori* leads to the production of active IL-1β and IL-18 and in a mouse model of infection IL-18 is required for inducing regulatory T cells, which dampen inflammatory responses, while IL-1β-driven inflammation contributes to bacterial clearance and tissue damage (*67*). Importantly, polymorphisms in human *NOD1, IL8* (*68*, *69*), *IL1B* and its receptor (*70*) have been linked to increased degree of gastritis, risk of developing ulcers and gastric cancer. These data provide further evidence that host genetic factors, particularly those underlying the innate immune response to *H. pylori*, play a key role in disease susceptibility and severity.

Adaptive immune response to *H. pylori*

The adaptive, mostly T cell-mediated inflammatory response depends on the events of the early innate immune response, which is initiated by gastric epithelial cell detection of *H. pylori* and subsequent recruitment of neutrophils, macrophages and dendritic cells (DCs) to the gastric mucosa (Fig. 1.1). DCs, in particular, bridge the innate and adaptive immune responses to *H. pylori*. During *H. pylori* infection, DCs are recruited to the gastric mucosa and are activated by the presence of *H. pylori* pathogen associated molecular patterns (PAMPs). DCs have been shown to respond to *H. pylori* in a TLR-dependent and independent manner, with specific pattern recognition receptors (PRRs) triggering pro-inflammatory, while others triggering anti-inflammatory responses (*71*). Prolonged activation of DCs with *H. pylori* leads to a decrease in IFNγ production and hyporesponsiveness to co-stimulation, thereby compromising DC ability to induce a Th1 response (*72*).

Th1, IFNγ-producing and Th17, IL-17-producing T cells infiltrate the gastric mucosa of *H. pylori* – positive humans and in animal models of infection. *H. pylori*-infected, T cell-deficient mice do not develop gastritis and adoptive transfer of CD4+ cells leads to inflammation in the gastric mucosa (*73*). IL-17 deficient mice infected with *H. pylori* have decreased gastritis and decreased gastric neutrophil infiltration, as compared to wild type mice (*74*). While Th1 and Th17-mediated immune responses have been implicated in bacterial clearance, they are also key drivers of host damaging inflammation. To counterbalance the pro-inflammatory Th1/Th17 response, Tregs are induced by *H. pylori* infection. Dendritic cells exposed to *H. pylori* induce T reg differentiation, which in turn dampen the pro-inflammatory T cell mediated immune response (*61*). Subsequently, *H. pylori* clearance in animal models of infection has only been achieved in the absence of Tregs or their anti-inflammatory cytokine, IL-10 (*60*, *61*).

B cells are also activated during *H. pylori* infection, but the antibody responses that are induced appear to promote bacterial persistence rather than clearance. B cell deficient mice show reduced *H. pylori* colonization and increased T cell infiltration of the gastric mucosa, which corresponds to bacterial clearance. It has been suggested that the IgA and IgG antibodies induced by *H. pylori* infection may bind to and hide pro-inflammatory bacterial factors thereby making *H. pylori* more difficult to detect by recruited immune cells (*75*).

H. pylori's strategies to evade the host immune response

H. pylori achieves chronic infection, in part, due to its ability to evade the host immune response. A number of *H. pylori* PAMPs avoid stimulation of their cognate PRRs. *H. pylori*'s tetra-acetylated LPS is one thousand-fold less stimulatory than *E. coli*'s hexa-acetylated LPS. It also carries less negative charge, which further interferes with TLR4 binding (*76*). Additionally, *H. pylori* evades recognition via an N-terminal domain modification in the flagellin protein, abrogating its interaction with TLR5 (*77*, *78*). TLR9 stimulation by *H. pylori* genomic DNA, which carries immunoregulatory sequences, suppresses inflammation potentially through direct induction of tolerogenic dendritic cells (*24*, *79*). *Tlr9*$^{-/-}$ mice show increased gastric inflammation that appears to be Th17 cell mediated (*80*). DC-SIGN, a C-type lectin receptor, is expressed by macrophages and dendritic cells and recognizes mannosylated or fucosylated pathogen-derived ligands. DC-SIGN mediated recognition of *H. pylori* Lewis Y antigen leads to production of IL-10 and dampening of the NF-κB-driven proinflammatory immune response (*81*).

Later host inflammatory responses are also manipulated by *H. pylori*. The predominant T cell response in infected gastric tissue is Th1 and Th17 skewed. However, *H. pylori* secretes virulence factors, such as vacuolating cytotoxin A (VacA) and γ-glutamyl transpeptidase that

inhibit T cell proliferation and normal effector function. Furthermore, dendritic cells that are exposed to *H. pylori* fail to induce naïve T cell differentiation into effector T cells, but rather promote Treg differentiation (*61*). Treg infiltration of infected gastric mucosa leads to reduced inflammation and prevents an effective T-cell mediated response that can lead to bacterial clearance (*52*).

H. pylori treatment – challenges for vaccine development

H. pylori infection can be treated with a combination of antibiotics (clarithromycin and amoxicillin) and a proton-pump inhibitor. In many cases, eradication of *H. pylori* leads to resolution of gastritis and, in some cases, cancer regression. This treatment strategy is becoming more challenging with the rapid increase of antibiotic resistant *H. pylori* (*82*). Sterilizing immunity to *H. pylori* has not been achieved in human clinical trials despite vigorous efforts and promising results in animal models (*83*-*85*). Most successful vaccines induce neutralizing antibodies, however, in the case of *H. pylori*, the antibody responses generated seem to be detrimental (*75*), thus efforts have been focused on developing vaccines that induce a protective T cell-mediated response. Clinical trials have focused on multiple antigens, including urease, CagA, VacA and NAP in combination with various adjuvants. One phase III trial conducted in Chinese children tested the efficacy of an oral vaccine, containing *H. pylori* urease fused to *E. coli* heat labile toxin. Infection with *H. pylori* was reduced by 72% one year post-immunization and 55% three years post-immunization. Although the vaccine did not provide full protection, it demonstrates that protection from natural infection in humans can be achieved (*86*). One promising approach for vaccine development is to target bacterial factors that evade or suppress an effective immune response. For example, Imevax has recently completed a phase I trial with a

vaccine targeting *H. pylori*'s γ-glutamyl transpeptidase, a secreted factor that blocks T cell proliferation (*87*). While the results of that trial have not been published, this approach aims to boost T cell mediated responses that are capable of clearing *H. pylori* (*88*). Another approach would be to pursue treatment strategies aimed at bacterial factors that modulate the innate immune response.

Project Aims

The regulatory adaptive immune response induced by *H. pylori* enables chronic colonization. Treatment strategies that overcome the immunosuppressive host response to *H. pylori* must be employed in order to achieve sterilizing immunity to *H. pylori*. PRRs on host cells orchestrate the earliest immune response to pathogens and set the stage for the subsequent adaptive immune response. *H. pylori* interactions with members of the upper GI microbial community may also modulate disease susceptibility. The goal of this thesis is to provide insight into how *H. pylori* influences the upper GI microbiota and the host immune response. To that end, the following project aims were pursued:

1) Define how presence of *H. pylori* shapes microbial communities in the upper gastrointestinal tract
2) Identify mechanisms by which *H. pylori* triggers an innate immune response in gastric epithelial cells
3) Identify mechanisms by which *H. pylori* triggers an innate immune response in myeloid-derived cells

A comprehensive understanding of the early immune response is ultimately required in order to achieve an effective immune response that leads to bacterial clearance while limiting host-damaging inflammation.

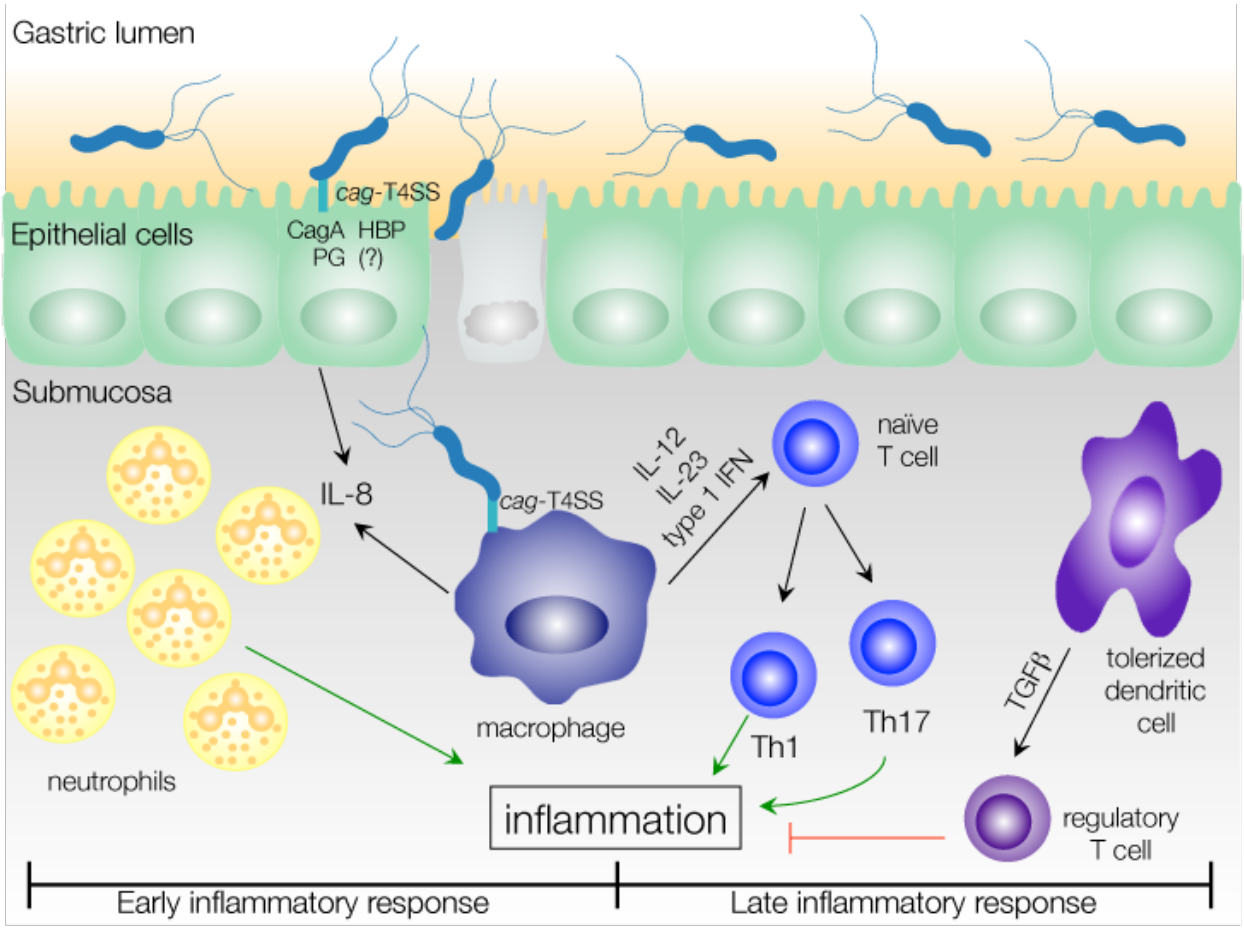

Figure 1.1. Summary of *H. pylori* induced immune response
H. pylori initiates an early inflammatory response in gastric epithelial cells that recruits innate immune cells to the site of infection. Macrophages and dendritic cells shape the late inflammatory response through activation and differentiation of naïve T cells. Figure adapted from (*89*).

CHAPTER 2: Bacterial composition of the human upper gastrointestinal tract microbiome is dynamic and associated with genomic instability in a Barrett's esophagus cohort

PREFACE

The data presented in this chapter has been previously published in Gall *et al. PLoS ONE* 2015 (*31*). We are grateful to the Seattle Barrett's Esophagus Research Program (SBERP) participants who enabled us to conduct this study. We thank Dr. Sujatha Srinivasan for providing procedural guidance, Lynn Onstad for helpful suggestions with data analysis and Christine Karlsen for her role as the clinical coordinator for SBERP.

INTRODUCTION

The incidence of esophageal adenocarcinoma (EAC) has increased by 463% from 1979 to 2004, making it one of the most rapidly increasing cancers in the United States (*90*). Barrett's esophagus (BE) is the only known precursor of EAC and is characterized by replacement of the stratified squamous epithelium with a metaplastic columnar epithelium. Barrett's epithelium secretes bicarbonate and mucus, which may be a protective adaptation against gastroesophageal reflux disease. Continued acid exposure and subsequent inflammation has been suggested to induce proliferation of BE cells, which may contribute to the development of EAC (*91*). *Helicobacter pylori*, a Gram-negative bacterium, has a well-documented role in the development of gastric and duodenal ulcers, as well as gastric adenocarcinoma (*1*). Intriguingly, several studies have shown that infection with *H. pylori*, is inversely correlated with the development of EAC (*92-95*). While the prevalence of *H. pylori* carriage worldwide remains at about 50%,

infection rates and incidence of gastric adenocarcinoma have declined sharply in the United States and Europe (*96*). This decline preceded the increase in EAC incidence. Inflammation caused by chronic *H. pylori* infection can lead to gastric atrophy and loss of acid-producing parietal cells, which predisposes the stomach to cancer (*97*). Some studies have suggested that the subsequent hypochlorhydria results in a refluxate that is less damaging to the esophageal epithelium and thus less likely to induce progression to EAC (*98*). A more recent case-control study involving over 600 participants found that *H. pylori* mediated protection is independent of gastric atrophy, suggesting other consequences of *H. pylori* infection should be considered (*93*). In the majority of *H. pylori* positive individuals, *H. pylori* was the most abundant species detected in stomach biopsies (*28*, *29*), but the ability of this organism to interact with tissues in the esophagus and the role(s) of other bacteria present in the stomach and esophagus in modifying disease risk at these sights remain unclear.

While the microbiome of the oral cavity and the lower GI tract have been more thoroughly investigated, relatively little is known about the microbial communities that reside within the esophagus and the stomach. A recent study surveying bacteria present in the oral cavity, lower GI and skin in healthy human volunteers showed that the mouth is dominated by members of the *Firmicutes* and *Proteobacteria* phyla, with *Bacteroidetes* being the third most common. The gut microbiome, on the other hand, was primarily dominated by *Bacteroidetes* and to a lesser extent, *Firmicutes* (*99*). Another study comparing throat, stomach and fecal microbiota in healthy individuals concluded that stomach and throat communities are more closely related (in the absence of *H. pylori* infection) than lower GI communities as measured by UniFrac distance, a phylogeny based metric. Although the *Firmicutes* and *Bacteroidetes* phyla are well represented in the upper and lower gastrointestinal tract, their members differ. The

prominent genera in the upper GI are *Streptococcus*, *Gemella* and *Prevotella*, while the lower GI is dominated by *Ruminococcus*, *Clostridium*, *Eubacterium* and *Bacteroides* (*29*).

The microbial residents of the stomach and esophagus differ from those found in the mouth and the lower GI tract. Using a 16S rRNA gene clone library approach, Bik and colleagues isolated 128 different phylotypes from corpus and antrum biopsies. Most of the sequences were assigned to *Proteobacteria*, *Firmicutes*, *Actinobacteria*, *Bacteroidetes* and *Fusobacteria* phyla. A subset of the patients sampled in the study were confirmed *H. pylori* carriers and in these individuals *H. pylori* was the most abundant species detected (*28*). One of the first studies to use a culture independent method to survey the microbiome of the distal esophagus in healthy individuals determined that the most prevalent genera residing at this site are *Streptococcus* (39%), *Prevotella* (17%) and *Veillonella* (14%) (*100*). Another recent study concluded that individuals with Barrett's esophagus or esophagitis are more likely to harbor Gram-negative anaerobic or microaerophilic organisms, such as *Prevotella*, *Veillonella*, *Haemophilus*, *Neisseria* and *Rothia*. Healthy individuals, on the other hand, were much more likely to be dominated by *Streptococci* species (*101*).

In the present study, we sought to investigate the relationships between microbial communities found in the distinct tissues of the esophagus and stomach in a Barrett's esophagus cohort undergoing regular endoscopic surveillance. We compared tissue sampling methods to determine which would maximize recovery of bacterial DNA from upper GI samples. Mucosal brush sampling allowed us to enrich for species abundance and diversity. We reliably mapped greater than 90% of the pyrosequencing reads of amplified 16S rRNA gene fragments down to the species or genus level and found that *Streptococcus* and *Prevotella* species were the most abundant organisms detected in the upper GI tract. We also observed an association between the

Streptococcus to *Prevotella* species ratio and known risk factors for development of Barrett's esophagus. We specifically examined the association of *H. pylori* with EAC disease progression. Almost all participants in our study utilize one or more acid suppression medications, allowing us to begin addressing *H. pylori*'s protective role independent of its role in acid suppression. We found that *H. pylori* positive individuals had a decreased incidence of aneuploidy in Barrett's esophagus tissue.

RESULTS

Mucosal brush samples enhance detection of bacterial diversity in the esophagus and stomach

To explore bacterial community composition in the upper GI tract in the context of Barrett's esophagus, we took advantage of the longstanding Seattle Barrett's Esophagus Research Program (SBERP). SBERP has undertaken surveillance biopsy sampling of participants with Barrett's esophagus to study the evolution of esophageal adenocarcinoma over several decades. We collected upper GI samples from a subset (n=12) of SBERP participants (Table 2.1). To determine the optimal method for surveying the upper GI, we used two sampling methods: tissue biopsies and mucosal brush samples using cytology brushes. One possible advantage of brush sampling relates to cross contamination between samples. The brush resides in a protective sheath while it is threaded through the endoscope channel, is deployed at the site of sampling and is then re-sheathed before being retracted through the endoscope. We also hypothesized that brush sampling would enrich for bacterial cells that, presumably, are exclusively associated with the epithelial surface. The order of sample collection was Barrett's esophagus, normal squamous esophagus, stomach antrum and stomach corpus (Fig. 2.1A). In cases where both biopsy and brushes were collected, the biopsy samples were collected first and

then a brush sample was collected at the same endoscope position. Biopsy forceps were rinsed in sterile water between samples.

To identify bacteria present in each sample, we isolated total DNA and used broad range PCR amplification of the 16S rRNA with subsequent 454 pyrosequencing of the amplified products. Operational taxonomic units (OTUs) were defined by phylogenetic classifications (not percent identity), where ambiguous assignment to a set of taxonomic groups was considered to be a classification. We compared DNA recovered from tissue biopsy versus cytology brushes. Consistent with previous findings in the stomach and esophagus (*28*, *100*, *101*), tissue biopsies yielded bacterial DNA representing 282 OTUs, but contained a very high ratio of human to bacterial DNA (as high as 100000:1). Compared to biopsies, brush sampling yielded up to one log increase in bacterial 16S copy per sample and lowered human DNA (measured by 18S) recovery by up to two logs (Fig. 2.1B & C). For participants where we obtained simultaneous brush and biopsy samples, brushes consistently yielded all of the OTUs found in the biopsy samples, as well as additional OTUs (Table 2.2 and Fig. 2.2). The dataset generated from our study contained a total of 296,042 reads with 67.8% of sequences classified at a species level, 23.0% at a genus level and 9.2% at a higher taxonomic level. We did not observe a statistically significant difference between the number of reads detected at each of the sampled sites (Fig. 2.3) or the number of OTUs in technical replicate samples (Table 2.3). Furthermore, the proportion of different OTUs was consistent between the two sampling methods (Fig. 2.3) and brush and biopsy samples from the same patient showed co-clustering by KR distance metric (Fig. 2.3). However as shown in Fig. 2.1D, diversity measured by brush sampling was greater than with biopsy sampling, likely because more OTU were detected. Our data suggest that brush

sampling is superior to biopsies for maximizing the quantity and quality of recovered bacterial DNA. Thus, in subsequent analyses, we utilized brush samples when available.

Bacterial communities in the upper GI tract display high inter-individual variation but overlapping community membership between sites

The most abundant bacterial groups observed in our upper GI microbiome samples were members of the *Firmicutes* and *Bacteriodetes* phyla (Fig. 2.4). Two sets of samples deviated from this pattern. One participant had recorded *H. pylori* infection based on prior histologic examination. Consistent with previous reports (*28*), both stomach samples from this participant had abundant *H. pylori* reads (99% in stomach corpus). In the stomach antrum sample, in addition to *H. pylori* (28% of total reads), a high proportion of other *Proteobacteria* were detected including *Enterobacteriaceae* [exclusively *E. coli* and *Shigella*] (Fig. 2.4B). While *H. pylori* was also detected in the esophageal samples (5% of total reads), the majority of bacterial reads from the esophageal sites belonged to the *Firmicutes* and *Bacteriodetes* phyla. The second set of outliers constituted samples abundant in *Enterobacteriaceae* from all four sites of individual P9 taken at a 3-year follow-up appointment. With the exception of *Shigella* species, all of the *Enterobacteriaceae* species represented at the 3-year time point were also present at the initial upper GI sampling (t=0) although at a 10-1000 fold lower abundance (Fig. 2.4B and Table 2.4).

We used principal component analysis to examine the relatedness of our samples. As shown in Fig. 2.5A, the majority of patient samples tended to cluster together. Overall, samples from the same individual were more phylogenetically similar to each other than to samples from the same anatomic site in a different individual (Fig. 2.5B). Among samples within an individual, the stomach corpus samples tended to be the most distinct, while samples from the stomach

antrum and esophagus were more similar to each other (Fig. 2.5C). Thus the acidic environment of the corpus may drive the distinct composition at this site but does not prevent seeding of the stomach antrum with organisms present further upstream in the GI tract.

Community composition similarity with replicate sampling

Three participants in our study were sampled at two time points. The upper GI of individuals P7, P2 and P9 were sampled 4 months, 2 and 3 years apart, respectively. Although the total number of reads per sample varied between individuals across time, particularly when biopsy samples from the initial collection were compared to brush sampling at the second time point, the number of represented species remained stable over time (Table 2.4). The upper GI microbiome of individual P7 showed the least amount of change over a 4 month time period (Fig. 2.6A & D). Individual P2 (surveyed 2 years apart) showed greater fluctuation in the relative abundance of certain species than P7, but did not display a dramatic shift in microbial community members (Fig. 2.6B & D). Individual P9, on the other hand, showed a dramatic expansion in the members of the *Enterobacteriaceae* phylum (Fig. 2.6C). Moreover, a second set of samples obtained at each site from individual P9 were more phylogenetically distinct with respect to the first set than the average inter-subject difference for all samples where two time point collections were available (Fig. 2.6D).

To further examine changes in bacterial community composition among these samples, we narrowed our analysis to the OTUs that increased or decreased in frequency by ≥ 5% between the two time points sampled. We chose 5% as the threshold because the average change in OTU relative abundance between the initial and subsequent sampling was 1.1% with a standard deviation of 3.9%. This allowed us to focus on the OTUs that exhibited a change that was 1 standard deviation or more away from the mean (Table 2.4). Of the sixty-one OTUs that changed

by ±5% across all sites, fifty were found in either individual P9 or P2. Interestingly, in individual P9 *Shigella* spp. were undetectable at the initial sampling but were detected at all four sites at the second time point with the most dramatic increase (9.6%) seen in the squamous esophagus tissue sample. Similarly, in individual P2 *Neisseria flavescens/subflava* were not detected initially, but were subsequently detected at all four sites with the greatest difference in relative abundance (5.5%) observed in Barrett's esophagus tissue. Individual P2 also exhibited a loss of *Lactobacillus* and *Paralactobacillus spp*. across all four sites, but most dramatically in the stomach corpus (*Lactobacillus reuteri* and *Paralactobacillus* decrease in relative abundance by 23.8% and 13.9%, respectively). We speculate that this change may have occurred because individual P2 discontinued acid suppression medication (Omeprazole) prior to collection of the second time point specimens. It is unclear, however, how long this participant abstained from proton-pump inhibitor treatment. Indeed, a recent study comparing the composition of the upper GI microbiome before and after PPIs found an increase in members of the *Lactobacillales* family after PPI treatment was initiated (*102*).

Although the clinical status of individual P7 did not change over a 4-month time period (metaplasia at the initial and follow-up sampling), individuals P2 and P9 both regressed from a diagnosis of high grade to low grade dysplasia. This change in clinical diagnosis was accompanied by an expansion in members of the *Proteobacteria* phylum. Individual P2 experienced an expansion of *Betaproteobacteria* (*Neisseria* species) and *Gammaproteobacteria* (*Chelonobacter* and *Haemophilus* species). In individual P9, however, *Klebsiella* and *Escherichia* species, members of the *Gammaproteobacteria* class, underwent an expansion (Table 2.4).

Streptococcus to _Prevotella_ ratio is associated with waist to hip ratio and hiatal hernia length, two known Barrett's esophagus and EAC risk factors

Given that *Firmicutes* or *Bacteroidetes* constituents dominated the majority of the samples in our study, we wanted to investigate the key species in our samples within each of these phyla. Based on the relative abundance of all members of the *Firmicutes* and *Bacteriodetes* phyla, we determined that either the *Streptococcus* (*Firmicutes*) or the *Prevotella* (*Bacteriodetes*) genera dominate within individuals and across anatomic sites (Fig. 2.4). We preformed a cluster analysis based on the phylogenetic placement of sequences for all study samples and observed that participant samples roughly segregated into four groups based on their *Streptococcus* to *Prevotella* ratios [ratio <0.5, 0.5-1.5, 1.5-4.0 & >4.0] (Fig. 2.7). We confirmed the *Streptococcus*:*Prevotella* ratios determined through pyrosequencing by quantifying all *Streptococcus* and *Prevotella* species in our samples using droplet digital PCR. In order to do so, we designed pan-*Streptococcus* and pan-*Prevotella* primers that bind to a species-conserved region of the 16S rRNA outside of the sequence used to amplify the 16S rRNA for our pyrosequencing studies (Fig. 2.8). There was no statistical difference between the *Streptococcus:Prevotella* ratios as determined by pyrosequencing and ddPCR (Fig. 2.7B). We then investigated correlations between the *Streptococcus:Prevotella* ratios and clinical features of the participants in our study. A high waist-to-hip ratio has been associated with an increased risk for progression to EAC in our study cohort (*103*) as well as others (*104*). The presence of a hiatal hernia is independently associated with an increased risk of Barrett's esophagus (*105*). We found that *Streptococcus*:*Prevotella* ratios in the stomach corpus positively correlated with waist-to-hip ratios of the male study participants (Fig. 2.7C), although the correlation was not statistically significant. We also found a highly statistically significant inverse correlation of

Streptococcus:*Prevotella* ratios in the stomach corpus (p=0.002) and Barrett's esophagus (p=0.001) with hiatal hernia length, and a slightly weaker inverse correlation in the stomach antrum (p=0.02) (Fig. 2.7D). Notably, we did not observe a similar correlation between waist-to-hip ratio and hiatal hernia length in this population ([$r^2 = 0.12$] Fig. 2.9), indicating that these two clinical parameters are independently associated with *Streptococcus*:*Prevotella* ratios. An increased Barrett's segment length has been associated with progression to high grade dysplasia and EAC (*106*). We noted a negative correlation between the *Streptococcus*:*Prevotella* ratio in the stomach corpus and increased Barrett's segment length ([$r^2 = 0.28$, p=0.07] Fig. 2.9). We observed no appreciable correlations between *Streptococcus*:*Prevotella* ratio and clinical diagnosis, inflammation score, age or tobacco use (Fig. 2.9).

H. pylori carriage is associated with decreased genomic instability among individuals with Barrett's esophagus

Limited by sample size, we were unable to explore the effect of *H. pylori* carriage on bacterial members of the esophagus. However, given that we detected *H. pylori* reads in esophageal samples of individual P6, we wondered if *H. pylori* status correlated with disease progression in the larger Barrett's esophagus cohort. As of 2004, baseline *H. pylori* infection status was available from histologic evaluation of stomach antrum biopsies for 433 participants. Prevalence of *H. pylori* infection is low in this cohort (9%). As shown in Fig. 2.10A, a trend towards a lower incidence of esophageal adenocarcinoma development among *H. pylori* positive participants was observed (Log-rank test p>0.69), but was not statistically significant. Genomic instability has emerged as an important predictor of subsequent cancer development in the context of Barrett's esophagus (*107*). Average DNA content measured by flow cytometry was available for a subset (78%) of participants for which *H. pylori* infection status had been

measured. Interestingly, *H. pylori* positive participants showed a lower incidence rate of DNA content aneuploidy than *H. pylori* negative participants, which was statistically significant (Fig. 2.10B; Log-rank test $p<0.045$). These results suggest that *H. pylori* may directly or indirectly influence cancer progression in the esophagus.

DISCUSSION

Here, we found that infection with *Helicobacter pylori* in a Barrett's esophagus cohort was associated with decreased incidence of aneuploidy, a measure of genomic instability that predicts progression to esophageal adenocarcinoma (*107*). Infection with *H. pylori*, and particularly *cagA*-positive strains, is associated with development of gastric adenocarcinoma (*108*), but is inversely associated with development of EAC (*93-95*). CagA protein is delivered to the host epithelial cell via the *cag*-type IV secretion system, where it is phosphorylated and activates a variety of oncogenic pathways including the host oncoprotein SHP-2 (*109*). Consistent with previous studies (*28*), we found that, when present, *H. pylori* was 99% and 24% abundant in the stomach corpus and antrum, respectively. Intriguingly, we also detected *H. pylori* reads in both of the sampled esophageal sites (5% relative abundance). This is consistent with a recent study utilizing a culture-based method to probe esophageal microbiota where *H. pylori* was detected in biopsies collected from healthy, reflux esophagitis and Barrett's esophagus tissues (*110*). These findings raise the possibility that *H. pylori* may be directly interacting with host epithelial cells in the esophagus and/or other bacterial members residing in the tissue. Whether *H. pylori* is able to deliver CagA protein to esophageal epithelial cells by the same mechanism as in the stomach remains unclear. Mutations in SHP2 and aberrant activation of this protein have been implicated in squamous head and neck cancer (*111*), but not esophageal adenocarcinoma. Due to the limited number of *H. pylori* positive samples in our study we were

unable to evaluate CagA status in our study cohort. However, whether CagA plays a role in EAC remains an important and unanswered question. Perhaps CagA protein is not translocated or phosphorylated in the context of the esophagus and *H. pylori* interaction with the host cells is tissue specific. Further work is necessary to address these questions and shed more light on *H. pylori*'s role in development of EAC.

Numerous studies in recent years have contributed to our understanding of the human microbiome, however, the upper GI has not received as much research focus as sites which are easier and less invasive to sample (*e.g.* skin, oral mucosa, lower GI via stool sampling, etc.). Questions remain whether the esophagus and the stomach are host to distinct microbial communities or if these sites are an extension of each other. It is also unclear whether the upper GI communities are more similar to bacteria found in the oral cavity or the lower GI tract. The overlap in membership of the oral, pharyngeal, esophageal and intestinal microbiota has been well documented and it has been suggested that the oral mircobiota substantially contributes to the seeding of downstream sites in the gastrointestinal tract (*28*, *29*, *112-116*). The oral cavity is dominated by *Streptococcus* and *Veillonella* (*Firmicutes*), *Neisseria* and *Haemophilus* (*Proteobacteria*) and *Prevotella* (*Bacteroidetes*) species, which vary less over time than gut communities. The gut microbiome is more diverse and consists largely of *Bacteroides* and *Prevotella* (*Bacteroidetes*), as well as *Ruminococcus* (*Firmicutes*) species (*99*, *112*, *117*, *118*). Our findings suggest that esophageal and stomach communities are more similar in composition to the oral cavity than the lower GI and support the idea that the upper GI is seeded, in part, by oral communities. One study investigating the composition of bacterial communities in the oral cavity, gut, skin, nostril, hair on head and external auditory canal observed that the strongest sample clustering occurred by anatomic site rather than sex, individual or time point (*99*).

Moreover, distinct distribution of species at different oral sites (*i.e.* keratinized vs. non-keratinized squamous epithelium and gingival plaque) have been suggested to be shaped by localized environmental factors (*112*). We, however, did not observe a substantial difference in microbial community membership or diversity in the squamous esophagus versus bacteria associated with columnar Barrett's epithelium. Among the twelve individuals studied, sequences from the various upper GI sites sampled within a given individual were phylogenetically closer to each other than they were to sequences from the same site in another individual. Of the upper GI sites sampled, the stomach corpus tended to be most distinct and antrum communities were more similar to those found in the esophagus, rather than the stomach corpus that is immediately proximal. While association with different types of epithelial surfaces did not appear to select for different community membership, the low pH associated with the stomach corpus compared to the antrum and esophagus may be a major factor underlying intra-individual variation in our study. Indeed, changes in pH have been shown to modify microbial communities in the stomach and esophagus of a Barrett's esophagus and esophagitis cohort (*102*).

Temporal studies of the gastrointestinal microbiota have shown that commonly shared taxa across individuals at different body sites, referred to as the core microbiome, remain stable over time (*99*, *117*, *119-121*). In the lower GI tract, factors such as long-term diet and weight stability are strong predictors for maintaining the taxonomic core (*117*, *120*). Two of the three participants in our study who were sampled at a second time (4 months and 2 years) showed high phylogenetic similarity between samples from the two time points. Interestingly, P2 had stopped PPI therapy at the second time point, yet the community looked quite similar to the first time point with the exception of a few specific species noted above.

A third participant (P9) who was sampled after three years had a microbiome composition that was phylogenetically distinct between the two sampling times. At the initial sampling, the upper GI of individual P9 was dominated by *Streptococci* species with members of the *Klebsiella* and *Escherichia* species present at a much lower abundance. At the second sampling, we observed a substantial expansion in the relative abundance and diversity of the *Enterobacteriaceae* family. A similar expansion of *Enterobacteriaceae* members has not been documented in Barrett's esophagus or stomach microbiome studies. Given the available data, it is impossible to determine what factors contributed to the microbial shift observed in individual P9. Interestingly, a study investigating the role of fecal microbiota composition and frailty found that a decrease in *Lactobacilli* (*Firmicutes*), *Bacteroides* and *Prevotella* (*Bacteroidetes*) species, accompanied by an increase in *Enterobacteriaceae* species was significantly associated with a higher frailty score in elderly individuals (*122*, *123*). An overall decrease in species richness in the lower GI has also been associated with aging (*124*).

A handful of recent studies have sought to determine the core microbiome of the upper GI tract in healthy and disease states. One study investigating the microbiome of the esophagus found differences in the microbial composition of healthy individuals versus those with esophagitis or Barrett's esophagus. They proposed a distinction between a type 1 microbiome of healthy individuals, dominated by *Streptococci* species, and a type 2 microbiome of individuals with esophagitis and Barrett's esophagus with an increased relative abundance of Gram-negative, anaerobic/microaerophilic species (including *Prevotella*, *Veillonella*, *Haemophilus*, *Neisseria* and *Rothia*) (*101*). Another study observed a similar enrichment of *Veillonella*, *Prevotella*, *Fusobacterium* and *Neisseria* in Barrett's but not normal esophagus (*110*). Our data suggest that the relative abundance of *Streptococci* species can vary substantially in individuals with Barrett's

esophagus and that the balance of *Streptococcus* and *Prevotella* species in the upper GI may be associated with Barrett's esophagus risk factors, such as central obesity (*103*). An increase in *Bacteroidetes* species in the lower GI has been linked to an increase in lean body mass. While an increase in *Firmicutes* species, and corresponding decrease in *Bacteroidetes* species, has been linked to obesity (*113*, *125-127*). It has been postulated that members of the *Firmicutes* phylum are better suited for metabolizing short-chain fatty acids and extract more energy from the host diet than their *Bacteroidetes* counterparts (*113*, *128*). It is unclear how well the ratio of *Firmicutes* to *Bacteroidetes* species in the upper GI mirrors that found in the lower GI. However, given our findings, it is possible that the relative abundance of bacterial members in these two phyla may be similarly linked to obesity in the upper GI.

As discussed above, our study was limited by its small sample size. *H. pylori* status was known for a larger subset of the Seattle Barrett's cohort study participants (n=433) allowing us to evaluate aneuploidy incidence and progression to EAC in relation to *H. pylori*, though we only observed a statistically significant association with aneuploidy incidence. We evaluated the rest of the bacterial microbiome of a much smaller subset of the cohort (n=12) which precluded us from making definitive conclusions regarding the role of other bacterial species present in Barrett's esophagus and progression to EAC. The small number of individuals evaluated may also have obscured tissue specific associations of bacterial communities that have been observed in other larger studies at other anatomic sites. Our small sample size precludes any conclusions concerning upper GI microbiome stability over time. Future studies will be focused on obtaining more samples from individuals over time, as well as greater representation of shorter (months) and longer (years) timespans between samplings. From a technical standpoint, we were not always able to map 16S reads to a genus or species level. Future studies may benefit from

additional metagenomic sequencing platforms that incorporate larger portions of the 16S gene combined with additional genomic sequences and computational analysis methods to improve resolution and distinguish among similar organisms. All of the participants in our study had Barrett's esophagus, thus we were unable to investigate how the upper GI microbiome differs from that of healthy individuals. Although we detected *H. pylori* in the esophageal samples, this study did not evaluate whether the bacteria were directly interacting with the epithelium or if they were transiently present in the esophagus due to regurgitation of the stomach contents.

Despite the limitations, our study presents several strengths. The prospective nature of the Seattle Barrett's cohort and regular endoscopic surveillance of participants, allowed us to sample multiple sites in the upper GI tract over time. Although constrained by the number of study samples, we were able to focus our study on characterizing the microbial community in the esophagus and the stomach of individuals with Barrett's esophagus. Piloting the use of cytology brushes to sample the upper gastrointestinal tract, we found that this method enriches for both bacterial abundance and diversity. Although each of the four anatomic sites sampled were distinct from each other within a given individual (especially the stomach corpus), the high inter-individual variability observed in our study suggests that the microbiome of the esophagus and the stomach is more of a continuous site in terms of bacterial diversity and composition. We also found that *Streptococcus* and *Prevotella* species numerically dominate the upper GI in this study cohort, but the ratio of the two varies from person to person and across anatomic sites. Follow-up studies with a larger sample size will evaluate whether the *Streptococcus*:*Prevotella* ratio is of clinical significance for Barrett's esophagus and progression to EAC. Our analysis of the upper GI samples from an *H. pylori*-positive individual suggest that *H. pylori* can be found in the esophagus of infected individuals. Future studies will validate these findings, as well as assess

the role *H. pylori* plays in the upper GI, particularly, the esophagus. *H. pylori* may be directly modifying the esophageal microbial community or it may simply be coming along for the ride in the stomach refluxate. Additionally, it may be interacting with esophageal tissues via different mechanisms than the stomach, which may, in part, explain its inverse association with EAC.

EXPERIMENTAL PROCEDURES

Ethics statement

Written and oral consent was obtained from each individual prior to sample collection. Institutional Review Board approval was obtained for this study through the University of Washington and Fred Hutchinson Cancer Research Center.

Study participants and sample collection

Study participants described in the present study (n=12) are a subset of individuals enrolled in the Seattle Barrett's Esophagus Research Program (SBERP). Established in 1983, SBERP is a prospective cohort of BE patients that undergo periodic endoscopic surveillance via collection of tissue biopsy samples from the Barrett's segment as previously described (*129*, *130*). Individuals were recruited to participate in SBERP between 1983-2008 and were included in the study if they provided consent, were at least 18 years of age, were medically fit to undergo endoscopy, and had Barrett's esophagus but not esophageal adenocarcinoma at baseline endoscopy. If a prospective participant did not have high grade dysplasia at baseline, the length of his/her Barrett's segment had to be 3 cm or longer. If high grade dysplasia was present, then the Barrett's segment length requirement did not apply. A subset of the cohort presented in this study is comprised of participants who underwent initial endoscopy between 1985 and 2008 and were in active surveillance between 2009-2012, when our study was conducted. As part of this

study, additional samples from normal squamous esophagus, stomach corpus and antrum were collected from each study participant for a total of four samples after an initial survey of the upper GI tract (stomach to esophagus). Esophageal samples were collected first (Barrett's then squamous) before stomach samples (antrum then corpus) to avoid contamination of the esophagus with stomach bacteria. In addition to tissue biopsies, mucosal tissue was also sampled using a flexible 1.5 mm x 140 cm cytology brush (Boston Scientific, Boston, MA) threaded through one of the endoscope working channels. Normal squamous esophagus, Barrett's esophagus, stomach corpus and stomach antrum were sampled via the brush method in 9 out 12 participants. Biopsy forceps were washed in sterile water between samples and a new cytology brush was used for each sample. Prior to sample collection, each participant was subject to a short interview in which information regarding changes in his/her medications and habits (i.e. tobacco or alcohol use) was recorded. To obtain a waist-to-hip ratio, a trained staff member measured the waist circumference of each participant at the level of the iliac crest and hip circumference at the largest circumference around the buttocks. The diaphragmatic hiatus, distal end of the tubular esophagus and the squamocolumnar junction (SCJ) were measured at endoscopy, as previously described (*131*). Briefly, the distal end was defined as the endoscopic lower esophageal sphincter where the tubular esophagus joins the proximal margin of the gastric folds. The SCJ is defined as the location where the squamous-lined esophagus joins the columnar-lined esophagus. The Barrett's segment length was measured as the distance between the distal end and the SCJ. The hiatal hernia is defined as the distance from the diaphragmatic hiatus and the distal end of the tubular esophagus. Barrett's esophagus biopsies and control tissues were evaluated and scored individually by a pathologist blinded to participant clinical status. Biopsies were classified as squamous, metaplasia, low-grade dysplasia, high-grade

dysplasia or esophageal adenocarcinoma according to the highest degree of abnormality found in the biopsy. The extent of inflammation was similarly evaluated and graded as acute or chronic and mild, moderate or severe. Cell aneuploidy was measured by means of DNA content flow cytometry on nuclei isolated from frozen endoscopic biopsy samples and stained with 4',6-diamidino-2-phenylindole (10 μg/mL) as described previously (*130*).

DNA isolation

Each biopsy and brush sample was collected into a cryovial containing minimal essential media plus 10% DMSO, 5% fetal calf serum, 5mM HEPES and frozen at -80°C until further processing. Prior to DNA isolation, samples were thawed and brush samples unsheathed. Cryovials were then vortexed for 1 min each, centrifuged at 12800 rpm for 2 min and supernatant removed. Total genomic DNA was then isolated using UltraClean Microbial DNA Isolation Kit [MoBio, Carlsbad, CA] according to manufacturer's instructions. Mock digests containing only the media were used to assess contamination from extraction reagents. DNA extracted from biopsy and brush samples was eluted in 100 μl and 25 μl of UltraClean elution buffer, respectively.

Quantitative PCR

Total bacterial DNA concentrations (16S rRNA gene copies) in each sample were measured using quantitative PCR. TaqMan broad-range 16S rRNA gene primers and probe used were as follows: forward primer (343F) 5'-TACGGRAGGCAGCAG-3' (*132*); reverse primer (806R) 5' GGACTACCVGGGTATCTAAT-3'; probe 5'FAM-TKACCGCGGCTGCTGGCAC-TAMRA-3'. The master mix (Applied Biosystems, Carlsbad, CA) contained buffer A (1X),

magnesium chloride (3 μM), deoxynucleotide triphosphates (1 μM), forward primer (0.8 μM), reverse primer (1 μM), AmpErase uracil-N-glycosylase (0.05 U), probe (200 μM) and AmpliTaq Gold LD polymerase (2.2 U) per reaction. With the exception of water and Taq polymerase, all reagents were additionally filtered using a Microcon centrifugal filter unit (Millipore, Billerica, MA) with sequential centrifugation at 2000 rpm for 10 min, 4000 rpm for 10 min and 8000 rpm for 5 min. Samples were quantified on a 7900HT sequence detection system (Applied Biosystems, Carlsbad, CA) with *E. coli* plasmid ranging from 10^1 to 10^7 gene copies used to generate a standard curve. The 18S rRNA gene forward primer (5'-CTCTTAGCTGAGTGTCCCGC-3' [20 μM]) and reverse primer (5'-CTTAATCATGGCCTCAGTTCCGA-3' [20 μM]) were added to SYBR Green real-time PCR master mix (Invitrogen, Carlsbad, CA) and total human DNA concentrations were similarly measured using qPCR in each sample. *E. coli* transformed with plasmid expressing full-length 18S rRNA gene were used to generate a standard curve (ranging from 10^2 to 10^9 gene copies).

454 pyrosequencing and analysis

The V3-V4 16S rRNA hypervariable region was amplified in each study sample using broad-range PCR with 347F and 806R primers, as previously described (*132*, *133*). Three GS FLX+ Titanium forward primers (Roche, Basel, Switzerland) were used in combination to enrich for a broad range of bacterial taxa. Forward primers F1, F2 and F3 were used in a 3:1:1 ratio:

F1: 5'-CGTATCGCCTCCCTCGCGCCATCAG**GC**ggaggcagcagtrrggaat-3'

F2: 5'-CGTATCGCCTCCCTCGCGCCATCAG**GC**ggtggctgcagtrrgg-3'

F3: 5'-CGTATCGCCTCCCTCGCGCCATCAG**GC**ggtggcagcagtrrgg-3'

The uppercase sequence corresponds to the 454 Life Sciences FLX adapter, the bold face sequence represents the GC linker and lowercase sequence, the target specific 16S rRNA sequence. A Titanium reverse primer:

5'-CTATGCGCCTTCCAGCCCGCTCAGXXXXXX**GC**ggactaccvgggtatctaat-3'

containing an adapter sequence, 6bp barcode (represented by X) and a GC linker sequence, was added to each sample to allow for multiplexing the sequencing reactions. The barcode sequences used in this study are described in previously published work (*134*). Amplified 16S rRNA fragments were PCR purified using Agencourt AMPure beads (Beckman Coulter, Pasadena, CA) and quantified using a Quant-iT PicoGreen dsDNA assay kit (Invitrogen). Samples were diluted to 1 x 10^7 molecules/µl, pooled (16 samples per pool) and sequenced on a 454 FLX or GS Junior instrument (Roche).

The overall quality of sequencing reads had to meet specific criteria in order to be included in subsequent analyses. Sequences were filtered to include only those having no ambiguous base calls (N's), at least 228 nucleotides in length, a mean quality score of 25, and a match to a known barcode and primer. A single homopolymer error was allowed in the forward primer. 454 sequences were "placed" on a fixed reference tree built from full-length 16S sequences customized for the stomach and esophagus using pplacer (*135*) in posterior probability mode. Placed sequences were then classified to the most specific rank possible with high confidence using the pplacer "hybrid2" classifier, which refines a naïve Bayes classifier (*136*) with a classification based on phylogenetic placement location. When a sequence matched multiple taxa of the same rank with probability > 0.2, the sequence was assigned to a combination of all taxa. Mapped reads in our study ranged from 70-28,113 reads with a median 2969 reads per sample. Distances between samples were calculated using the phylogenetic

Kantorovich-Rubinstein (KR) metric, also known as the "earth-mover" distance. As described in (*137*), the KR metric in this context is a slight generalization of weighted UniFrac, allowing assignments to internal edges of the tree and for mass to be split according to probabilistic assignment. Clustering was performed using squash clustering and edge principal components (*138*), which are methods that take advantage of the underlying phylogenetic tree to provide more interpretable clustering and ordination results. Intra-sample diversity was measured using quadratic entropy (*139*).

The sequencing data presented in this study has been made publically available through the NCBI Sequence Read Archive (BioProject ID: PRJNA270661 available at http://www.ncbi.nlm.nih.gov/bioproject/270661). We used an HMP developed protocol to remove sequences of human origin from our dataset to protect participant privacy (*140*). The protocol entitled "Human Sequence Removal" is available at http://hmpdacc.org/tools_protocols/tools_protocols.php.

Droplet digital PCR

Total *Streptococcus* and *Prevotella* species were quantified from genomic DNA isolated from study biopsy and brush samples using droplet digital PCR (ddPCR). The following primers and probes were designed or modified for this study in order to amplify a species-specific portion of the 16S rRNA gene distinct from the region amplified for pyrosequencing. *Streptococcus spp.*:

forward primer (5'-AGATGGACCTGCGTTGT-3')

reverse primer (5'-TGCCTCCCGTAGGAGT-3') (*141*)

probe (5'-FAM-CGATACATAGCCGACCTGAGAGG-BHQ-3')

Prevotella spp.:

forward primer (5'-GATGCGTCTGATTAGCTTG -3')

reverse primer (5'-CCAATATTCCTCACTGCTG-3')

probe (5'-HEX-CGATACATAGCCGACCTGAGAGG-BHQ-3')

Commercially available genomic DNA from *Streptococcus mitis* and *Prevotella melaninogenica* (ATCC, Manasses, VA) were used as controls to optimize the ddPCR assay. Twenty-five microliter reactions containing 2X master mix (Bio-Rad, Hercules, CA), 20X primer/probe mix (900 nM forward and reverse primer, 250 nM probe) and 1 µl of DNA template were prepared in duplicate for each sample. Reaction droplets were generated by mixing 20 µl of each reaction mixture with 70 µl of droplet generation oil in a DG8 cartridge and emulsified in the QX100 Droplet Generator (Bio-Rad, Hercules, CA). Forty microliters of the completed emulsion were slowly transferred to a Twin.tec semi-skirted 96-well PCR plate (Eppendorf, Hamburg, Germany) and heat-sealed with a foil cover. The following thermal cycler program was used to amplify the species-specific 16S rRNA gene fragment: 10 min at 95℃; 40 cycles of 30 sec at 95℃ and 1 min at 55℃; 10 min at 98℃. Droplets containing amplified gene fragments were then acquired using the QX100 Droplet Digital PCR system (Bio-Rad). Positive and negative droplets were distinguished based on probe fluorescence amplitude and quantified using QuantaSoft software (Bio-Rad).

Statistical analysis

Statistical analysis was performed using R version 3.0.3 (http://www.R-project.org/) (*142*). Data was graphed using Prism 6 software for Mac OS X (GraphPad, La Jolla, CA). Statistical significance for Kaplan-Meier curves for incidence of cancer and DNA content

aneuploidy was assessed using the Log-rank test. Quadratic entropy was used as a measure of species diversity (*143*) and the difference between biopsy and brush samples was determined by Wilcoxon ranked sum test. Similarly, the phylogenetic distance was approximated using the KR distance metric (*137*) and distances were compared within and between individual samples using the Wilcoxon ranked sum test. Pearson's correlation test was used to determine the relationship between *Streptococcus* to *Prevotella* ratios and hiatal hernia length, waist-to-hip ratio, Barrett's segment length and participant age. Differences in read counts recovered across sites, as well as differences in 18S and 16S copy number were assessed using Freidman rank sum test. For all statistical tests results were considered significant if the p-value for the test was less than or equal to 0.05. In the case of Pearson's correlation analysis, an uncorrected p-value threshold of 0.05 was used to determine statistical significance.

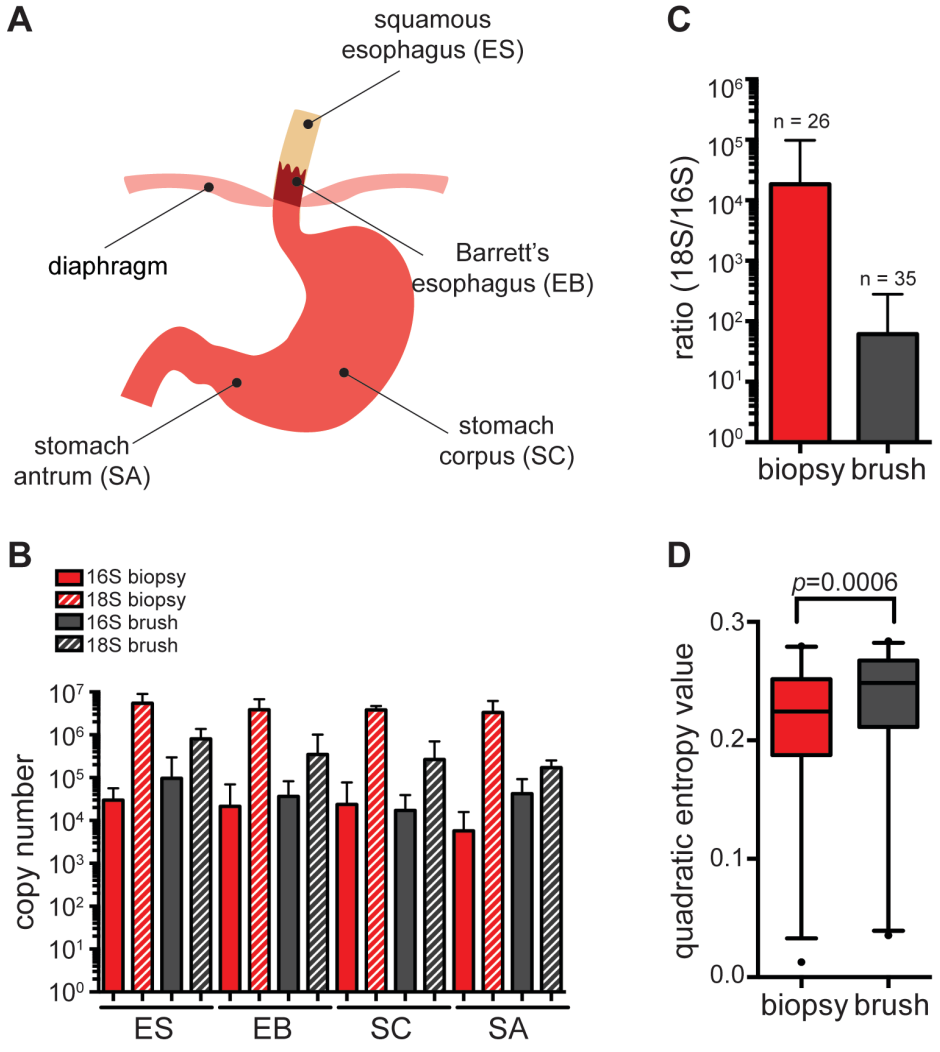

Figure 2.1. Brush sampling of the upper gastrointestinal tract enriches for bacterial abundance and diversity

(A) Diagram of the human upper gastrointestinal tract indicating regions sampled via biopsy or brush collection method. Anatomic sites were abbreviated with the first and second letter indicating the sampled organ and intra-organ tissue, respectively (ES – squamous esophagus; EB – Barrett's esophagus; SC – stomach corpus; SA – stomach antrum). (B) Total bacterial versus human DNA recovered from biopsy or brush samples segregated by anatomical site as measured by qPCR and plotted as copy number of bacterial 16S rRNA gene and human 18S rRNA gene. Error bars indicate standard deviation from the mean. (C) Ratio of human 18S rRNA to bacterial 16S rRNA copy number in all biopsy (n= 26) or brush (n=35) samples. Error bars indicate standard deviation from the mean. (D) Species diversity in biopsy and brush samples as measured by quadratic entropy analysis. The central line within each box represents the median of the data, the whiskers represent the 5th and 95th percentiles and data outside that range are plotted as individual points. Statistical difference between biopsy and brush samples was measured by Wilcoxon rank sum test with continuity correction (p = 0.000594)

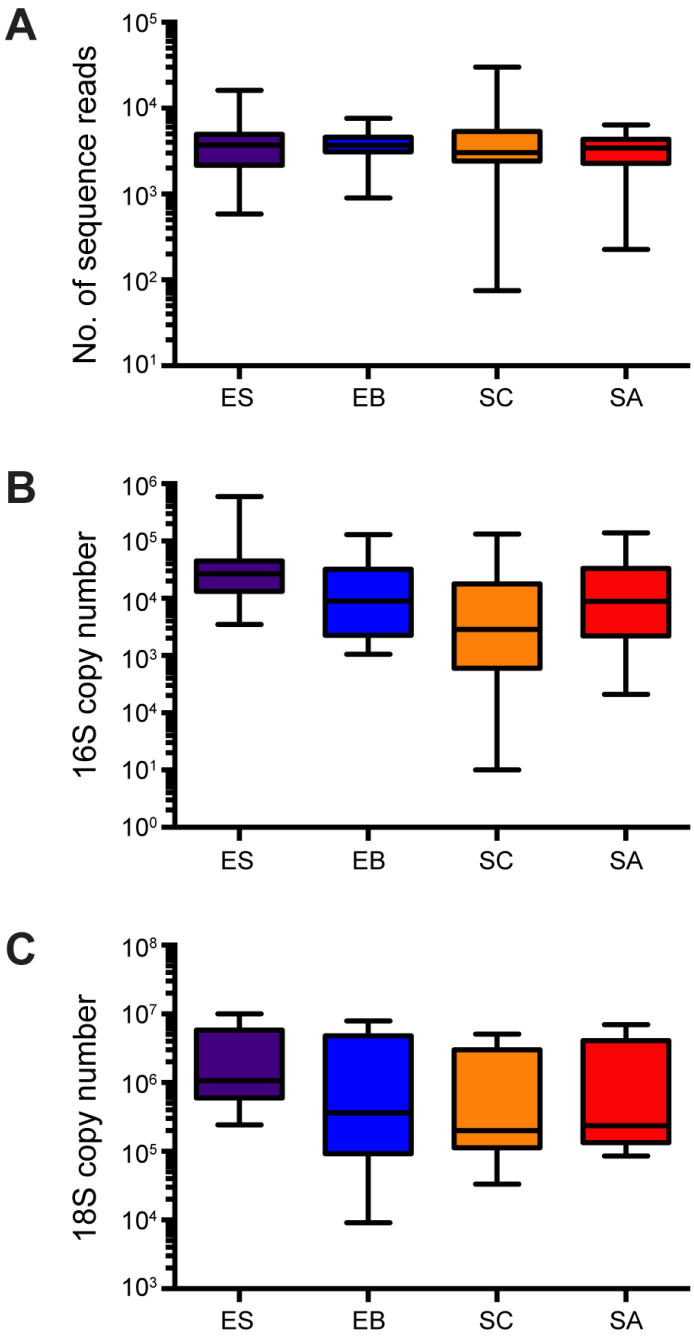

Figure 2.2. Observed sequencing depth and DNA recovered at each anatomic site
(A) Number of read counts from all study participants per site sampled. Statistical difference between sites was measured by Friedman rank sum test ($p = 0.55$). (B) Copy number of bacterial 16S rRNA per site sampled, as measured by qPCR. Statistical difference between sites was measured by Friedman rank sum test ($p = 0.004$). (C) Copy number of human 18S rRNA per site sampled, as measured by qPCR. Statistical difference between sites was measured by Friedman rank sum test ($p = 0.001$)

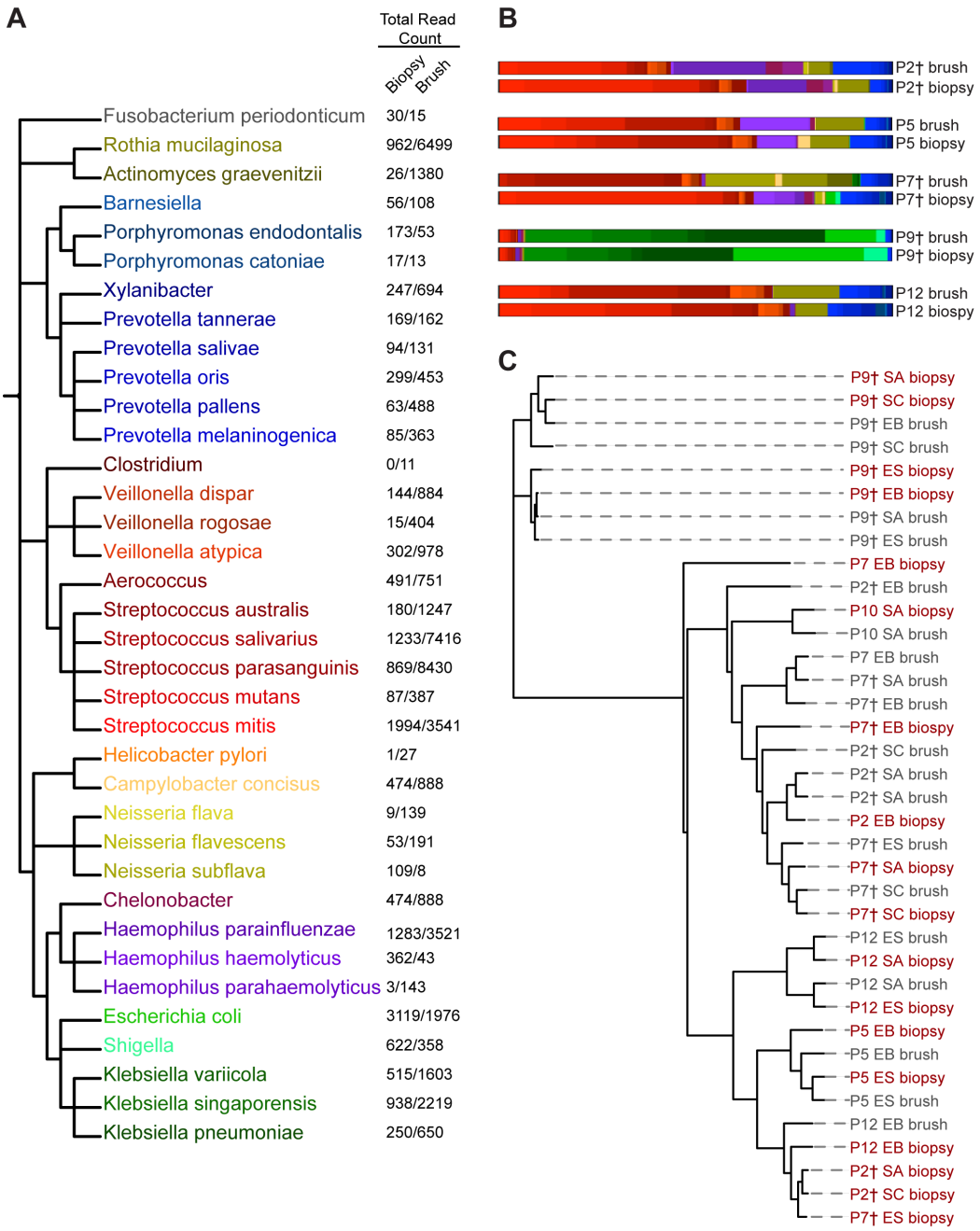

Figure 2.3. Comparison of OTUs detected in brush versus biopsy samples
(A) Phylogenetic relationship of the top 45 OTUs detected in samples where both a brush and biopsy specimen was available. Numbers in column represent the total number of reads detected for a given species or genera in brush and biopsy samples. (B) Combined species/genera-level profiles of top 45 OTUs detected by 454 sequencing at all four sites sampled via upper endoscopy in indicated participants. Data are color-coded according to scheme presented in (A). Species reads were normalized to the total number of reads per corresponding site in a given individual.† Denotes samples collected at a second time point (P2 [t=4 months]; P7 [t=2 years]; P9 [t=3 years]). (C) Cluster analysis of KR distances between microbial communities detected in brush or biopsy samples of indicated individuals.

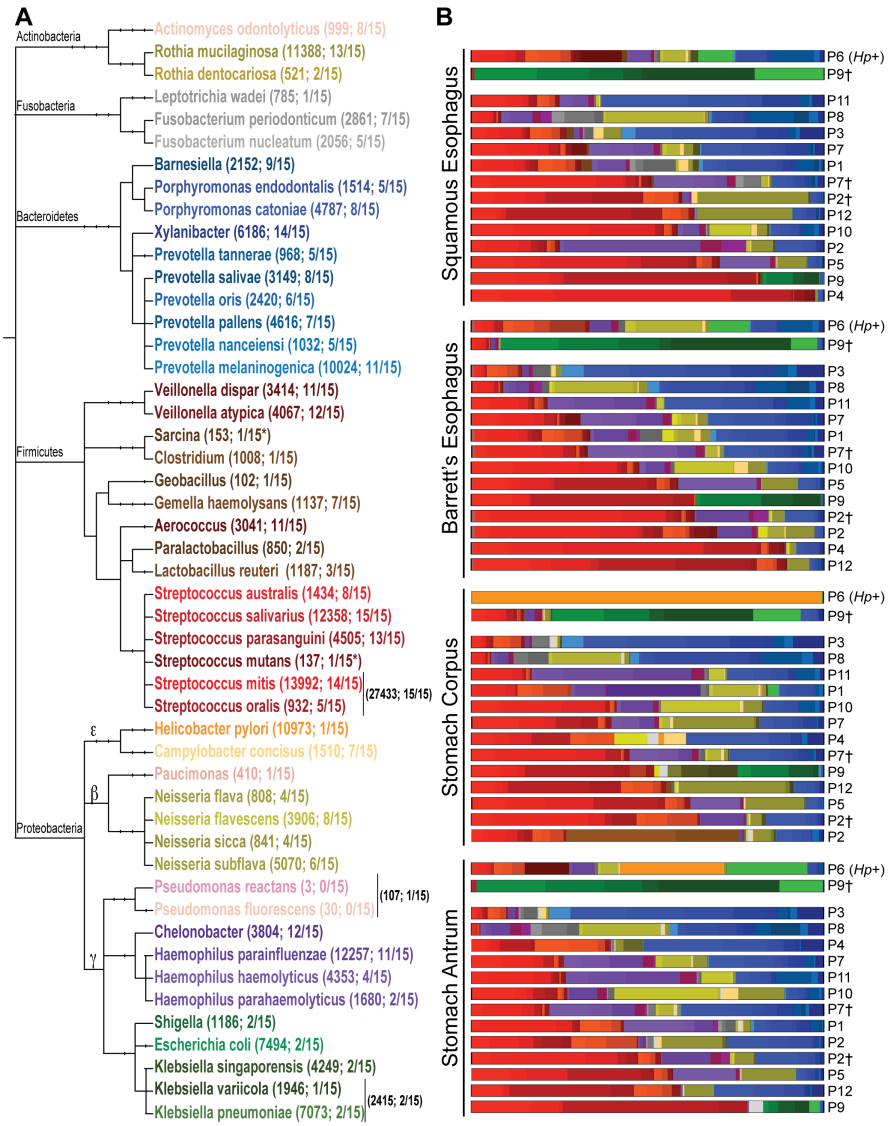

Figure 2.4. Members of the *Firmicutes* or *Bacteroidetes* phyla dominate the upper gastrointestinal tract microbiome

(A) Phylogenetic relationship of the top 45 OTUs recovered from each of the four sites sampled in individual participants. Respective phyla are noted above main branches of the phylogenetic tree. Numbers in parentheses represent total number of pyrosequencing reads recovered for a given species or genera across all samples followed by the fraction of participants in whom a relative abundance of ≥ 1.3% of a given species or genera were detected. (B) Species/genera-level profiles of top 45 OTUs detected by 454 sequencing in squamous esophagus, Barrett's esophagus, stomach corpus and stomach antrum of indicated participants. Data arranged in order of increasing *Firmicutes* dominance. Individual species/genera are color-coded according to scheme presented in (A). Sequencing reads from brush samples were used when available, otherwise, data from biopsy samples are shown. Species reads were normalized to the total number of reads per corresponding site in a given individual. †Denotes samples collected at a second time point (P2 [t=4 months]; P7 [t=2 years]; P9 [t=3 years]); *Hp*+ indicates *H. pylori*-positive individual. Italicized participant IDs denote data from biopsy samples in cases where brush samples were not available for analysis.

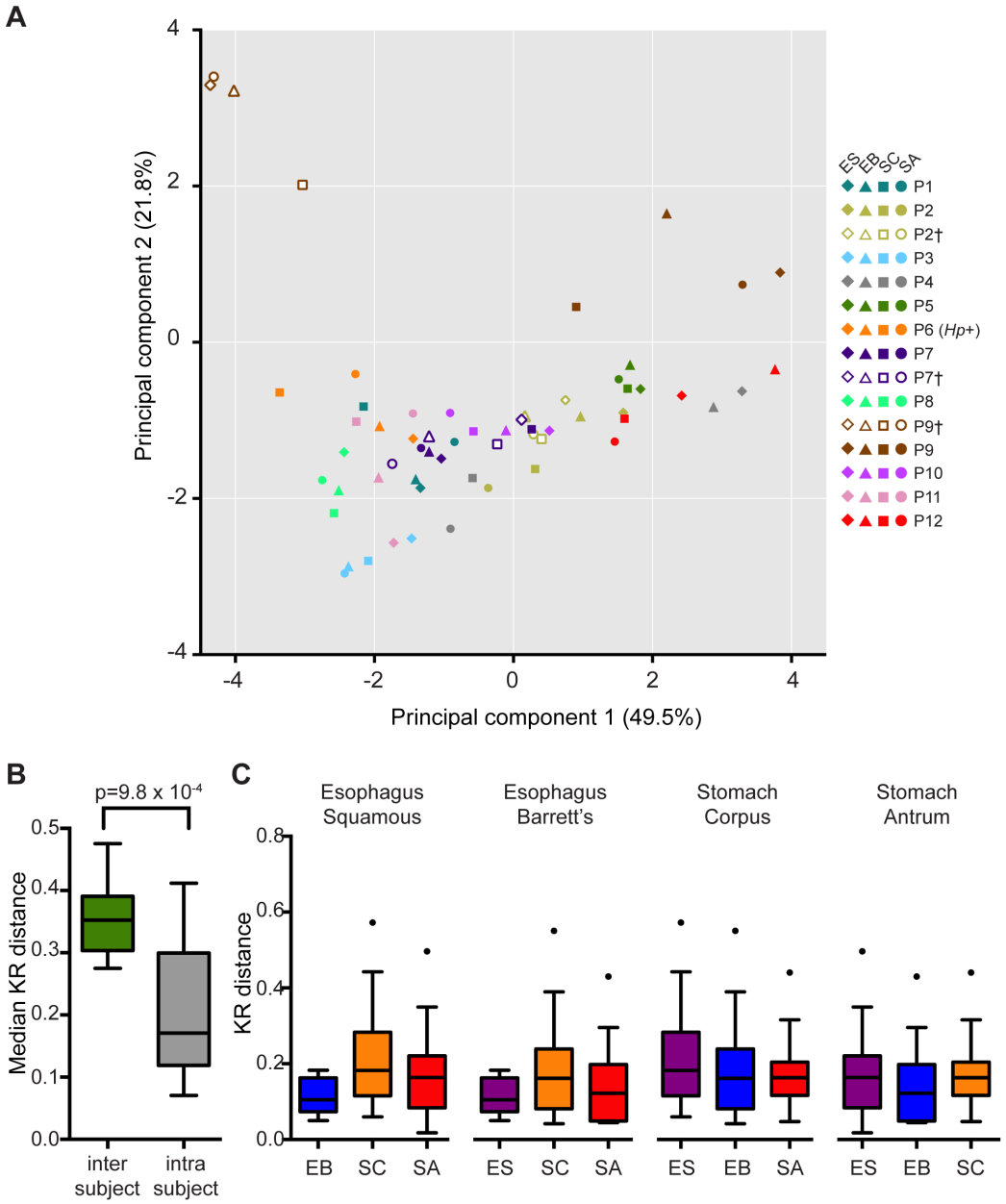

Figure 2.5. Phylogenetic sample profiles are most similar within individuals rather than across anatomic sites

(A) Principal component analysis of phylogenetic similarity among samples from each of the four anatomic sites of indicated participants. The number in parentheses corresponds to the percent variance of the data assigned to each indicated principal component. (B) Median KR distance across all samples between individuals (inter) and across sites within individuals (intra). Statistical significance was determined by Wilcoxon rank sum test with continuity correction. (C) Intra-individual KR distance of the three anatomic sites relative to the site indicated at the top of each graph. For B & C, the central line within each box represents the median of the data, the whiskers represent the 5th and 95th percentiles and data outside that range are plotted as individual points.

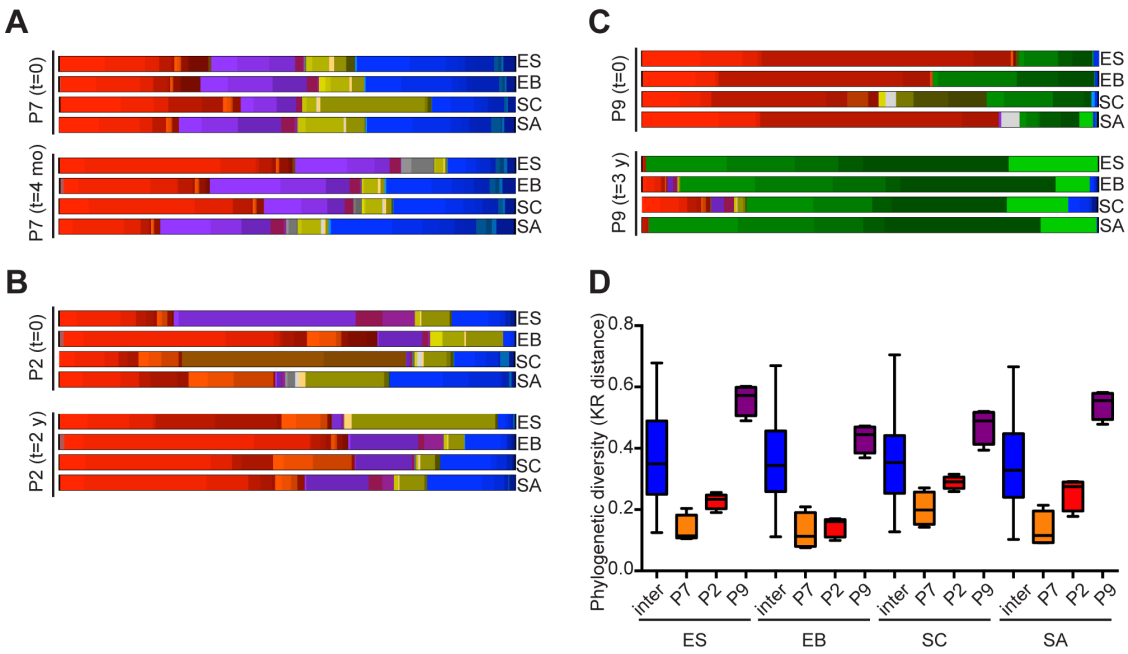

Figure 2.6. Upper gastrointestinal microbiome similarity with replicate sampling
(A-C) Species/genera-level profiles of microbiota detected by 454 sequencing in squamous esophagus, Barrett's esophagus, stomach corpus and stomach antrum of individuals P7 at the time of first [t=0] and second sample collection [t=4 months] (A), P2 at t=0 and t=2 years (B) and P9 at t=0 and t=3 years (C). Individual species/genera are presented according to coloring scheme described in Fig. 2.2. (D) Phylogenetic KR distance between (inter) samples from participants P2, P7 and P9 at both time points and within those individuals comparing the 1st and 2nd time points from the indicated anatomic site. The central line within each box represents the median and the whiskers represent the minimum and maximum values.

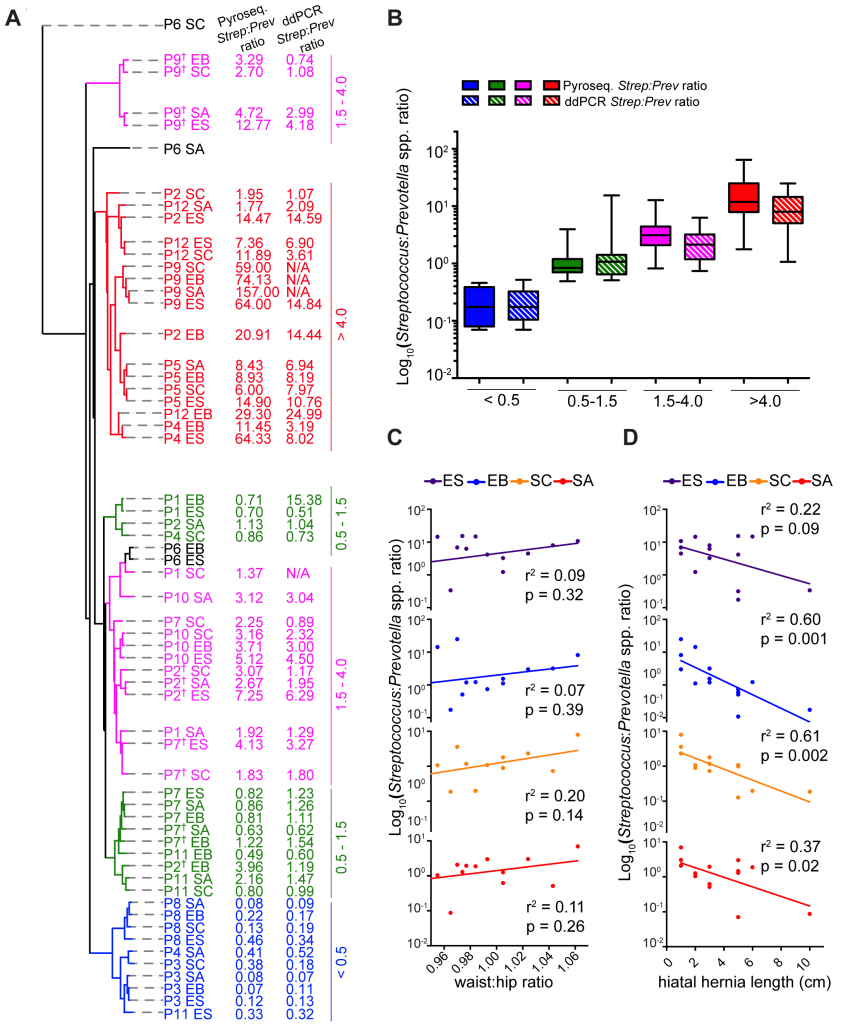

Figure 2.7. *Streptococcus* to *Prevotella* species ratio corresponds to phylogenetic distance sample clustering and correlates with Barrett's esophagus risk factors

(A) Cluster analysis of KR distances between microbial communities of individual study samples. Pyroseq. *Strep*:*Prev* ratio was calculated using relative abundance of mapped reads for all *Streptococcus* and *Prevotella* species as determined by pyrosequencing. ddPCR *Strep*:*Prev* ratio was calculated using copies/µl of a *Streptococcus* or *Prevotella*-specific 16s rRNA gene segment as determined by droplet digital PCR. Samples color-coded based on the majority of calculated Pyroseq. *Strep*:*Prev* ratios in a group being <0.5 (blue), 0.5-1.5 (green), 1.5-4.0 (magenta) or >4.0 (red). (B) Boxplots comparing *Streptococcus* to *Prevotella* ratio as determined by pyrosequencing and ddPCR. The central line within each box represents the median of the data, the whiskers represent the 5th and 95th percentiles and data outside that range are plotted as individual points. (C) Relationship of *Streptococcus* to *Prevotella* ratio (measured by ddPCR) and waist-hip ratio of all male participants segregated by anatomic site. Strength of association between these two variables was determined by Pearson's correlation test with correlation coefficient squared (r^2) values as indicated. (D) Relationship of *Streptococcus* to *Prevotella* ratios (measured by ddPCR) and hiatal hernia length in all participants segregated by anatomic site. Strength of association tween these two variables was determined by Pearson's correlation test with correlation coefficient squared (r^2) values as indicated.

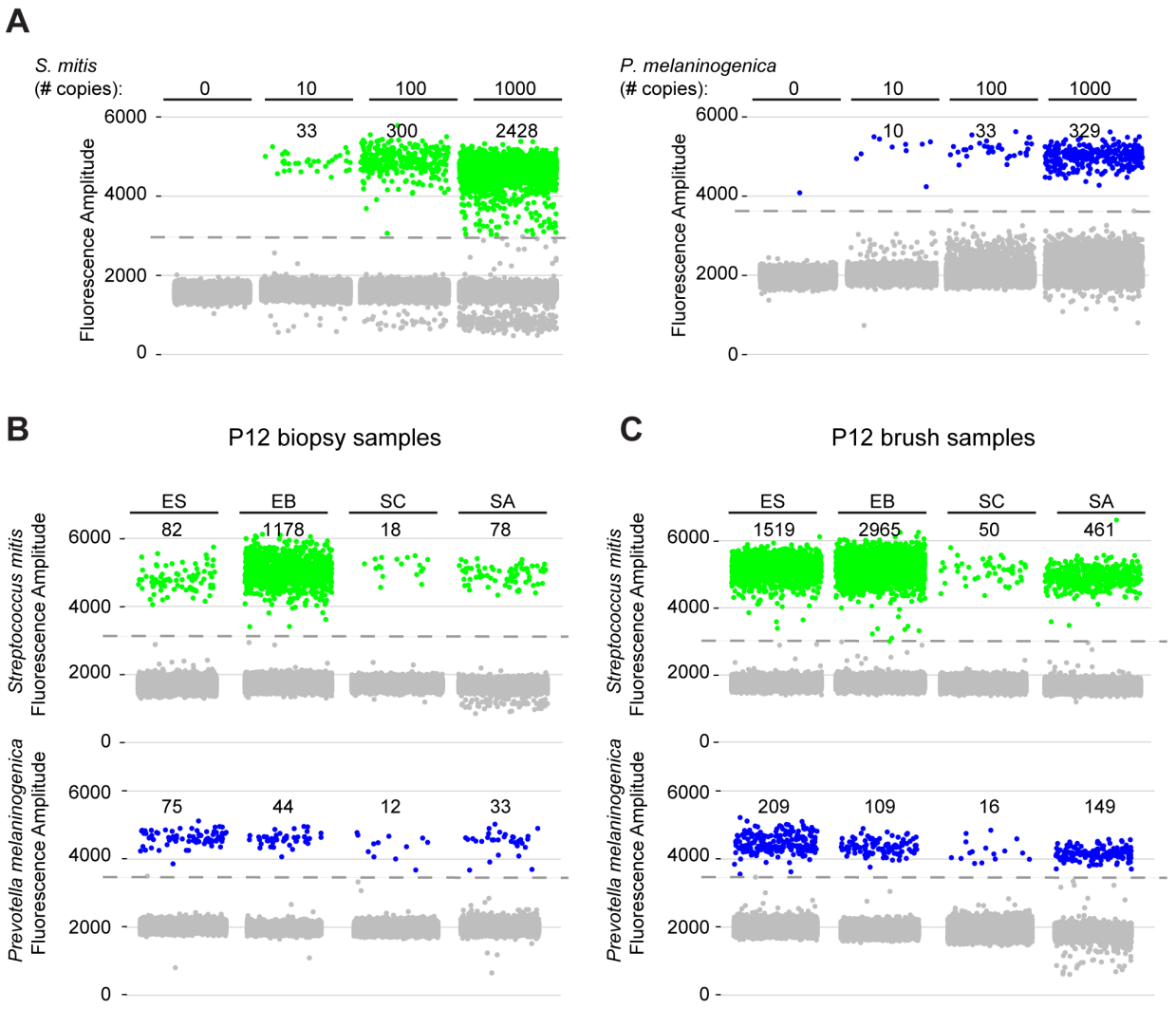

Figure 2.8. Droplet Digital PCR assay for detection of *Streptococcus* and *Prevotella* species in study samples

(A) Detection and quantification of *S. mitis* and *P. melaninogenica* genomic DNA using pan-*Streptococcus* and pan-*Prevotella* primers. Number of genome copies added to a background of AGS cell genomic DNA is indicated above horizontal bar at the top of each panel. Number of copies/ µl detected in each sample is indicated above positive events (green or blue droplets). Gray, dashed line represents the threshold above which an event was counted as positive. Negative events are depicted in gray. All experiments were performed in duplicate with a representative plot shown. (B) Quantification of *Streptococcus* and *Prevotella* species in biopsy samples from squamous esophagus (ES), Barrett's esophagus (EB), stomach corpus (SC) and antrum (SA) in individual P12. Number of copies/ µl detected in each sample is indicated above positive events (green or blue droplets). Gray, dashed line represents the threshold above which an event was counted as positive. Negative events are depicted in gray. All experiments were performed in duplicate with a representative plot shown. (C) Quantification of *Streptococcus* and *Prevotella* species in brush samples from ES, EB, SC and SA in individual P12.

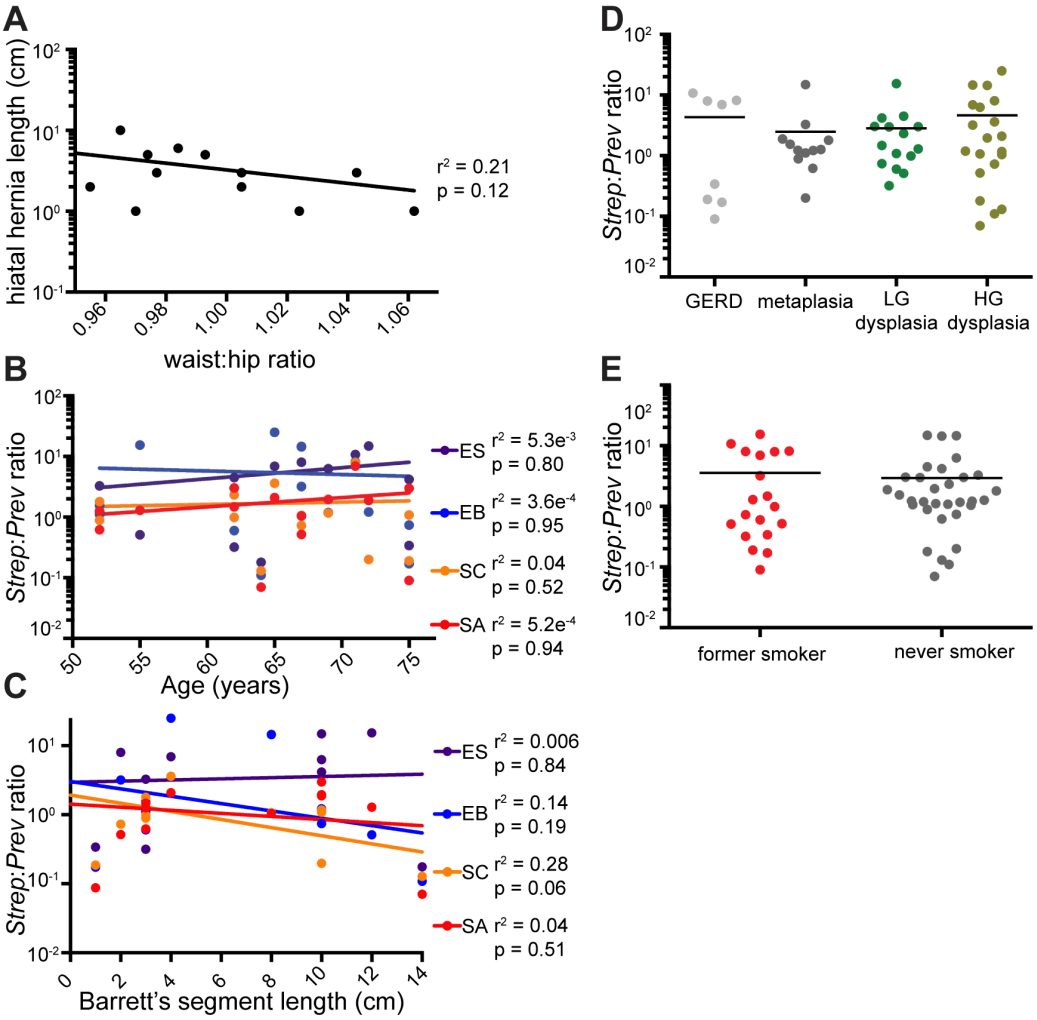

Figure 2.9. Correlation of *Streptococcus*:*Prevotella* ratio with participant demographics and Barrett's esophagus risk factors.

(A) Relationship of hiatal hernia length and waist to hip ratio. Strength of association between these two variables was determined by Pearson's correlation test with correlation coefficient squared (r^2) value and p value as indicated. (B) Relationship of *Streptococcus* to *Prevotella* ratio at each anatomic site and participant age. Association between variables was determined by Pearson's correlation test with r^2 and p values as indicated. (C) Relationship of *Streptococcus* to *Prevotella* ratio at each anatomic site and Barrett's segment length. Association between variables was determined by Pearson's correlation test with r^2 and p values as indicated. (D) *Streptococcus* to *Prevotella* ratio at each anatomic site and clinical diagnosis determined by histological assessment of Barrett's esophagus biopsy samples. LG = low grade HG = high grade. (E) *Streptococcus* to *Prevotella* ratio at each anatomic site and participant smoking history.

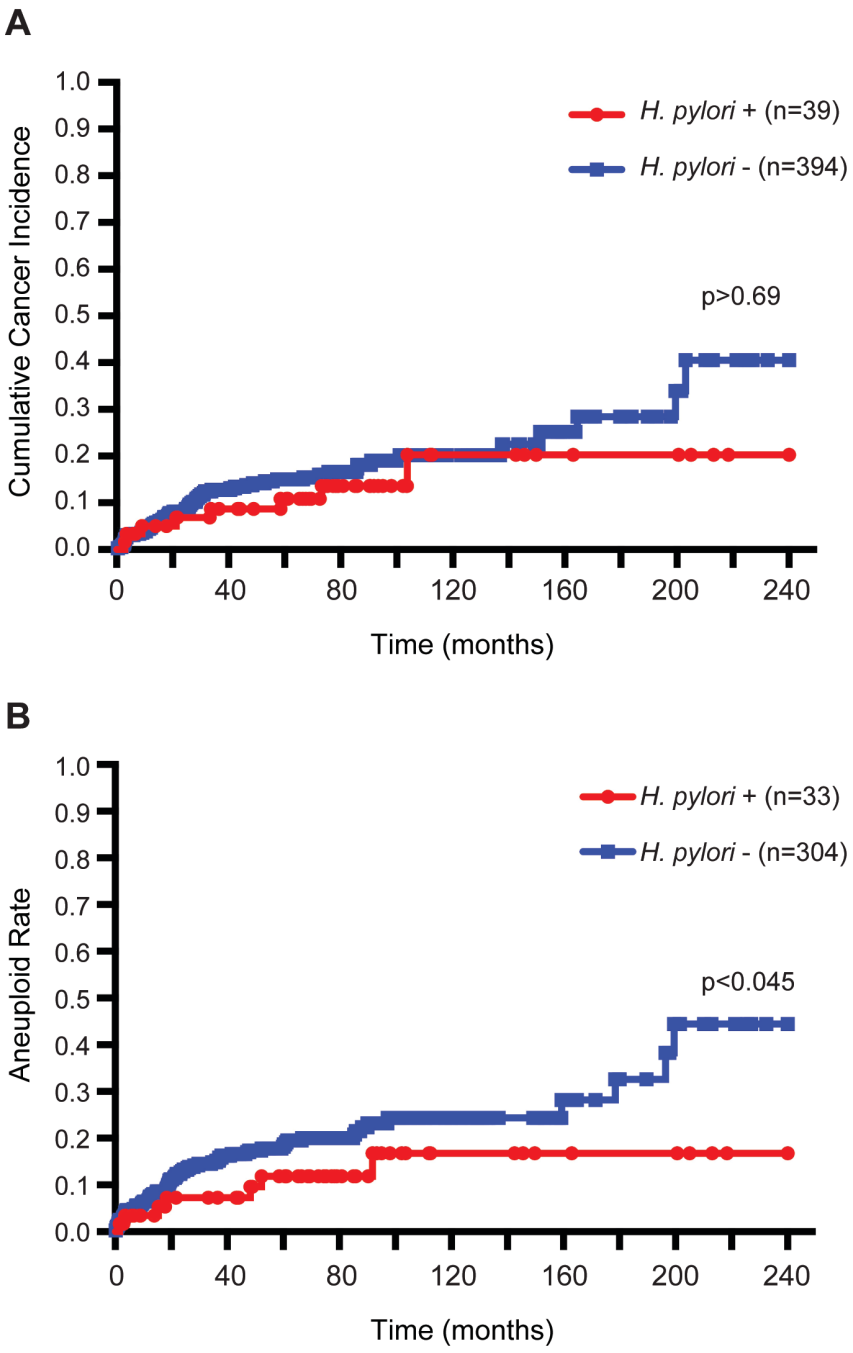

Figure 2.10. Incidence of cancer and aneuploidy in Seattle Barrett's Esophagus Research Program cohort

Kaplan-Meier curves for participants within the cohort for (A) cancer incidence (n=433, 39 infected) and (B) aneuploidy as measured by DNA content flow cytometry (n=337, 33 infected). *H. pylori* infection was assessed by histology of antral biopsies. Note aneuploidy information was not available for all research participants. Statistical significance was determined using the Log-rank test.

Table 2.1. Participant Demographics

Participant ID	Diagnosis	Sex	Age (yrs)	Acid suppression (number)	Antibiotic	Steroid	NSAID	Statin
P1	LG[a] dysplasia	M	55	Y (1)	N	N	Y (1)	N
P2	Metaplasia	M	67	Y (1)	N	N	Y (1)	Y (1)
P2[b]	Metaplasia	M	69	N	N	N	Y (1)	Y (1)
P3	Metaplasia	F	64	N	N	N	N	N
P4	Metaplasia	M	67	Y (1)	N	N	Y (1)	Y (1)
P5	GERD	M	71	Y (1)	N	Y (1)	Y (1)	Y (1)
P6[c]	Metaplasia	F	80	Y (1)	N	N	Y (1)	Y (1)
P7	HG[a] dysplasia	M	52	Y (2)	N	N	N	N
P7[b]	LG dysplasia	M	52	Y (2)	N	N	N	N
P8	GERD	M	75	Y (1)	N	N	Y (1)	Y (1)
P9	HG dysplasia	M	72	Y (1)	N	N	Y (1)	Y (1)
P9[b]	LG dysplasia	M	75	Y (1)	N	N	Y (2)	N
P10	LG dysplasia	M	62	Y (1)	N	N	Y (1)	N
P11	LG dysplasia	M	62	Y (1)	Y (1)	N	N	N
P12	Metaplasia	M	65	Y (1)	N	N	Y (1)	N

[a] LG = low grade HG = high grade

[b] Denotes samples collected at a second time point (P2 [t = 2 years]; P7 [t = 4 months]; P9 [t = 3 years])

[c] Denotes *H. pylori*-positive participant

Table 2.2: OTUs detected in brush versus biopsy samples

Species	P2* biopsy	P2* brush	P5 biopsy	P5 brush	P7* biopsy	P7* brush	P9* biopsy	P9* brush	P12 biopsy	P12 brush
Streptococcus mitis/oralis	2144	3080	37	879	3197	0	77	174	747	291
S. parasanguinis	78	367	15	285	33	6488	40	54	203	1236
Streptococcus salivarius	185	283	131	2802	209	1376	92	142	616	2813
Rothia mucilaginosa	515	778	63	1698	21	2263	34	50	329	1710
K. pneumoniae/variicola	0	0	0	0	0	125	2054	4521	0	0
Streptococcus mitis	779	935	31	2051	462	3	51	91	671	461
Escherichia coli	0	0	0	15	171	26	2948	1934	0	1
H. parainfluenzae	979	3393	1	0	165	1	92	117	46	10
Streptococcus	429	697	90	1522	304	71	70	178	334	1050
Prevotellaceae	190	1403	39	407	278	570	64	113	96	470
Klebsiella	0	0	0	0	0	40	957	2511	0	0
Neisseria flava/sicca	2	4	0	0	1	3444	0	0	0	0
Klebsiella singaporensis	0	0	0	0	0	0	938	2219	0	0
Haemophilus	27	101	62	2419	364	10	1	2	1	1
Klebsiella variicola	0	0	0	0	0	217	515	1386	0	0
Actinomycetales	1	0	0	0	1	2023	2	2	0	2
Paucimonas	1	2	0	0	35	1900	0	1	22	19
Phytobacter	1	0	0	4	44	1071	116	255	15	3
Streptococcus australis	64	109	8	125	36	896	11	9	61	108
A. graevenitzii	23	115	1	7	0	1254	2	4	0	0
Chelonobacter	278	612	2	163	143	17	43	89	8	7
Veillonella atypica	110	246	19	234	27	113	4	6	142	379
Aerococcus	244	162	8	219	149	138	21	31	69	201
Prevotella	44	304	5	105	114	150	15	76	57	301
Veillonella dispar	62	334	7	269	26	53	7	24	42	204
Pasteurellaceae	155	766	0	0	26	30	19	7	0	0
Shigella	0	0	1	15	89	1	532	342	0	0
Veillonella	38	118	6	83	54	309	1	7	65	293
Xylanibacter	71	164	9	115	118	185	19	54	57	176
V. atypica/dispar	5	21	0	12	2	739	0	0	24	131
Klebsiella pneumoniae	0	0	0	0	0	0	250	650	0	0
N. flavescens/subflava	35	573	0	0	11	212	16	12	0	0
G. paraadiacens	0	2	0	2	1	759	0	1	2	2
Prevotella oris	0	1	7	163	109	11	0	0	183	278
Fusobacterium	0	0	1	11	13	684	0	1	11	11
Leptotrichia buccalis	1	9	0	0	18	666	0	1	1	1
E. asburiae/hormaechei	0	0	0	0	1	5	255	351	0	0
Prevotella pallens	3	20	0	0	59	468	1	0	0	0
Campylobacter concisus	53	43	20	33	43	343	0	2	0	4
Streptococcus oralis	18	21	5	274	31	24	0	6	31	92
E.hormaechei/K. variicola	0	0	0	0	0	484	0	0	0	0
Streptococcus mutans	2	0	69	26	8	351	0	0	8	10
Moryella indoligenes	13	52	0	0	1	392	4	1	2	0
P. melaninogenica	23	184	1	4	53	152	4	21	4	2
Firmicutes	71	84	5	49	137	3	4	13	10	50

Table 2.3: OTUs detected in biological replicate samples

Species	P2 EB rep#1	P2 EB rep#2	P6 SA rep#1	P6 SA rep#2	P6 SC rep#1	P6 SC rep#2	P6 EB rep#1	P6 EB rep#2
Helicobacter pylori	0	0	841	735	6000	3002	208	0
S. mitis/oralis	1223	1451	79	24	2	0	63	0
Escherichia coli	0	0	657	1121	17	6	341	1
H. parainfluenzae	374	292	182	109	7	0	177	0
Streptococcus mitis	416	439	29	12	2	0	23	0
Rothia mucilaginosa	320	427	22	14	2	0	29	1
Neisseria subflava	2	0	145	46	0	0	561	0
Clostridium	0	0	360	178	12	2	158	0
Streptococcus	167	374	56	26	2	0	75	0
Veillonella rogosae	4	0	139	74	9	0	301	0
Veillonella atypica	143	47	86	37	2	2	172	0
Veillonella dispar	42	15	102	50	2	1	134	0
Veillonella	108	46	64	15	4	0	90	0
P. catoniae	0	0	34	11	1	1	273	0
P. melaninogenica	7	3	67	36	0	0	179	0
Gemella haemolysans	92	176	1	4	0	0	2	0
Chelonobacter	49	86	3	55	2	2	62	0
Neisseria flava	105	144	4	3	0	0	2	0
Aerococcus	55	163	2	5	0	0	30	0
Neisseria sicca	186	20	11	1	2	0	4	0
Gemella	162	8	12	2	0	0	5	0
C. perfringens	0	0	83	39	1	1	63	0
Shigella	0	0	51	91	0	0	32	0
S. parasanguinis	99	66	0	0	0	0	8	0
A. odontolyticus	4	0	38	30	2	0	98	1
S. australis	111	10	4	3	3	0	8	0
S. salivarius	25	25	18	5	2	1	59	0
Prevotellaceae	60	50	5	3	0	0	8	0
Neisseria flavescens	1	2	22	7	0	0	87	1
Sarcina	0	0	3	54	5	2	49	1
Gemella sanguinis	41	16	21	4	1	0	25	0
Neisseria flava/sicca	58	44	1	1	0	0	1	0
Firmicutes	43	10	11	6	0	0	30	0
Prevotella	30	24	6	8	0	0	30	0
Oribacterium sinus	0	1	14	8	6	0	61	0
Phytobacter	0	0	4	31	8	6	40	0
G.adiacens	35	12	20	0	1	0	21	0
Catonella morbi	0	0	15	4	0	0	68	0
Leptotrichia buccalis	2	0	7	9	1	0	64	0
Xylanibacter	7	20	0	8	1	0	45	0
N. flavescens/subflava	0	0	3	2	0	0	73	0
F. periodonticum	0	0	14	5	0	0	57	0
Barnesiella	1	1	2	4	0	0	54	0
Streptococcus oralis	50	4	3	0	0	0	5	0
C. concisus	14	7	4	6	0	0	27	0

Table 2.4: Change in OTU relative abundance over time

Site	Species	Participant	Relative abundance at 1st time point (t_1)	Relative abundance at 2nd time point (t_2)	%Δ (t_2-t_1)
Stomach antrum	*Streptococcus salivarius*	P9	38.9	0.9	-38.0
	Streptococcus	P9	15	1.6	-13.4
	Streptococcus parasanguinis	P9	7.1	0.8	-6.2
	Klebsiella singaporensis	P9	2.2	11	+8.8
	Klebsiella	P9	1.3	10.8	+9.5
	Escherichia coli	P9	2.7	13.7	+11.0
	Klebsiella pneumoniae/variicola	P9	3.5	18.5	+14.9
	Rothia mucilaginosa	P2	14.1	2.7	-11.5
	Prevotellaceae	P2	9.6	1.7	-7.9
	Veillonella dispar	P2	7.1	0.3	-6.8
	Prevotella melaninogenica	P2	5.5	0.1	-5.4
	Haemophilus parainfluenzae	P2	0.8	6.3	+5.5
	Streptococcus mitis	P2	3.4	16.9	+13.5
	Streptococcus mitis/oralis	P2	6.8	49.6	+42.8
	Haemophilus	P7	4.3	9.3	+5.0
Stomach corpus	*Actinomyces odontolyticus*	P9	7.1	0.1	-7.0
	Bifidobacterium	P9	7.8	0.1	-7.7
	Streptococcus	P9	7.8	0.6	-7.2
	Escherichia coli	P9	0	5.6	+5.6
	Klebsiella variicola	P9	0	7	+7.0
	Klebsiella	P9	3.5	14.5	+10.9
	Klebsiella pneumoniae/variicola	P9	1.4	28.3	+26.9
	Lactobacillus reuteri	P2	23.8	0	-23.8
	Paralactobacillus	P2	13.9	0	-13.9
	Streptococcus mitis	P2	2.3	23	+20.7
	Streptococcus mitis/oralis	P2	5	50.2	+45.1
	Rothia mucilaginosa	P7	20.3	1	-19.3
	Prevotellaceae	P7	3.6	9.7	+6.1
	Streptococcus mitis/oralis	P7	6.4	19.7	+13.4
Barrett's esophagus	*Streptococcus salivarius*	P9	38	0.4	-37.6
	Streptococcus	P9	10.9	0.3	-10.6
	Streptococcus parasanguinis	P9	5.7	0.2	-5.6
	Klebsiella variicola	P9	0.1	8.4	+8.3
	Escherichia coli	P9	0.1	10.7	+10.6
	Klebsiella	P9	1.1	14.2	+13.1
	Klebsiella pneumoniae/variicola	P9	7.4	37.1	+29.7
	Neisseria flavescens/subflava	P2	0	5.5	+5.5
	Pasteurellaceae	P2	0.5	5.9	+5.4
	Prevotellaceae	P2	1.4	9.1	+7.7
	Prevotella	P7	10.1	3.8	-6.2
	Streptococcus mitis/oralis	P7	8.6	13.7	+5.1
	Haemophilus	P7	5.4	13.5	+8.1
Squamous esophagus	*Streptococcus salivarius*	P9	43.8	1.4	-42.3
	Streptococcus	P9	12.3	0.5	-11.8
	Streptococcus mitis/oralis	P9	8.7	0.1	-8.6
	Streptococcus parasanguinis	P9	7.7	0.2	-7.5
	Shigella	P9	0	9.6	+9.6
	Escherichia coli	P9	0.2	60	59.8
	Rothia mucilaginosa	P2	29.2	8.9	-20.3
	Streptococcus parasanguinis	P2	12.6	1.3	-11.3
	Streptococcus salivarius	P2	12.1	3	-9.1
	Chelonobacter	P2	0.2	4.9	+4.8
	Haemophilus parainfluenzae	P2	1.9	15.4	+13.6
	Streptococcus mitis/oralis	P2	8.6	23.7	+15.1
	Prevotellaceae	P7	10.1	3.4	-6.6
	Haemophilus	P7	4.9	9.9	+5.0
	Streptococcus mitis/oralis	P7	7.6	25.9	+18.3

* Only OTUs that exhibited an increase of decrease of ≥ 5% between the two time points sampled are represented

CHAPTER 3: TIFA signaling in gastric epithelial cells initiates the *cag* Type 4 Secretion System-dependent innate immune response to *Helicobacter pylori* infection

PREFACE

The data presented in this chapter has been previously published in Gall *et al. mBio* 2017 (*144*). Tho Tran (Fred Hutch Summer Undergraduate Research Program) assisted in generating the *TIFA* KO AGS cells. We are especially grateful to Dr. Elizabeth Gray and Dr. Daniel Stetson (Department of Immunology, University of Washington) for providing the lentiCRISPR plasmid backbone and helpful discussions. We are also grateful to Itunuoluwa Adekoya and Xinyi Guo (Department of Molecular Genetics, University of Toronto) for their generous assistance with supplying critical reagents and protocols.

INTRODUCTION

Helicobacter pylori is a Gram-negative bacterium that colonizes greater than 50% of the world's population. *H. pylori's* only known niche is the human stomach, where the bacterium resides in intimate contact with gastric epithelial cells causing inflammation that, in a subset of infected individuals, progresses to gastric and duodenal ulcers and cancer (*145*). It has been estimated that *H. pylori* has resided with its human host for at least 100,000 years, predating modern human migration out of Africa, making it the oldest known and one of the most successful human pathogens (*33*, *34*).

H. pylori is able to achieve chronic colonization, in part, due to its ability to evade host immune responses. A number of *H. pylori* pathogen-associated molecular patterns (PAMPs) avoid stimulation of their cognate pattern recognition receptors (PRRs). *H. pylori*'s LPS is tetra-

acetylated, making it a poor ligand for TLR4 (*76*) and divergent flagellin monomer sequences abrogate its interaction with TLR5 (*77*, *78*). The O-antigen of *H. pylori* LPS contains Lewis antigens which mimic host receptors and facilitate immune escape (*146*). Furthermore, the unique dephosphorylated lipid A structure in *H. pylori* confers resistance to host antimicrobial peptides, as well as antibiotic polymyxin B (*147*). Despite sophisticated evasion strategies, several virulence factors induce a robust immune response. *H. pylori*-mediated gastritis is initiated by proinflammatory cytokines released by gastric epithelial cells, as well as neutrophils and macrophages that are recruited to the site of infection (*59*). Cytotoxin-associated gene A (CagA) has been extensively characterized as a major contributor to epithelial cell transformation that can result in gastric cancer. Infection with *cagA*+ strains is associated with increased inflammation and subsequent development of peptic ulcers and gastric adenocarcinoma (*45*, *46*). CagA is encoded within a region of the chromosome known as the *cag* pathogenicity island (*cag*-PAI). Along with *cagA*, *cag*-PAI contains genes required for assembly of a type IV secretion system (T4SS). CagA is injected directly into epithelial cells via the *cag*-T4SS, which acts as a molecular syringe. Once CagA is delivered into the host cytosol, it is phosphorylated by host kinases leading to aberrant host cell signaling. After several months of experimental infection with a single *H. pylori* strain, mice and rhesus macaques accumulated bacterial strain variants that contained mutations in the *cagY* gene, which renders the *cag*-T4SS non-functional. Interestingly, strains with functional *cag*-T4SS were also recovered from the same animals (*48*, *49*) suggesting that the ability to switch the *cag*-T4SS "on" or "off" is advantageous for the bacteria.

Along with CagA, the *cag*-T4SS delivers bacterial factors that are known to activate the global transcription factor NF-κB, leading to the upregulation of proinflammatory genes and

production of cytokines such as IL-8 (*52*). IL-8 is a major chemokine for neutrophil recruitment to the site of infection and has been extensively used as a physiologically relevant readout of the NF-κB inflammatory pathway. Active *H. pylori* infection is characterized by extensive neutrophil infiltration of the gastric mucosa where these cells not only recruit lymphocytes, which establish chronic inflammation, but also contribute to tissue damage through production of reactive oxygen species (*148*). Prior to this study, most of the *cag*-T4SS-dependent IL-8 response in gastric epithelial cells has been attributed to NOD1 activation based on a foundational study demonstrating that NOD1 activation by *H. pylori* peptidoglycan leads to NF-κB activation and IL-8 production, and that *Nod1*-deficient mice are more susceptible to *H. pylori* infection (*57*). Although several groups have challenged the notion that NOD1-dependent responses predominate in *H. pylori* infected gastric epithelial cells (*149-151*), a comprehensive understanding of the relevant pathogen recognition pathways has remained elusive. Interestingly, recent work has suggested that additional bacterial products may be delivered by the *cag-T4SS*. TLR9-dependent inhibition of IL-8 induction in reporter cell lines and suppression of *H. pylori* load in *Tlr9-/-* mice suggests that bacterial DNA containing inhibitory CpG motifs can also transit the *cag*-T4SS, though in this case dampening NF-κB signaling (*79*, *80*).

In this study, we identify **T**RAF-**I**nteracting Protein With **F**orkhead-**A**ssociated Domain (TIFA) as a critical innate signaling component downstream of *cag*-T4SS-induced inflammation. TIFA has been extensively studied in the context of its interaction with TRAF6 and ability to activate NF-κB (*152-154*). Recent work has revealed that TIFA is specifically activated by the cytosolic presence of the bacterial metabolite heptose-1,7-bisphosphate (HBP), a metabolic intermediate in LPS biosynthesis (*155*, *156*). HBP is highly conserved among Gram-negative bacteria, but is absent from eukaryotic cells. Thus, TIFA-dependent detection of HBP represents

a novel innate immune sensing pathway that is distinct from classical TLR- or NOD-family pattern recognition receptor-driven signaling cascades. HBP is detected in the host cytosol, and has been proposed to gain access to this compartment through dynamin-dependent endocytosis of extracellularly released HBP (*Neisseria, Salmonella typhimurium*), phagolysosomal degradation of engulfed bacteria within macrophages (*E. coli*), as well as through intracellular bacterial replication (*S. flexneri*) (*155-158*). Here, we reveal an additional mechanism whereby HBP is presented to the TIFA-signaling pathway: type IV secretion system translocation. In the context of *H. pylori* infection, HBP is delivered to the host cytoplasm through the *cag*-T4SS system, where it activates an acute TIFA-mediated innate immune response in gastric epithelial cells. Furthermore, we show that host NOD1 and the bacterial CagA toxin are sequentially responsible for the *H. pylori*-induced inflammation that follows the early TIFA response.

RESULTS

NOD1 gene targeting does not eliminate *cag*-T4SS-dependent IL-8 response in gastric epithelial cells.

To determine whether NOD1 was solely responsible for the IL-8 response in gastric epithelial cells, we used CRISPR/Cas9 gene editing tools to target *NOD1* in a human gastric epithelial cell line (AGS cells). We designed a guide RNA targeting the N-terminal caspase recruitment domain (CARD) of NOD1, which is required for interaction with its downstream signaling partner RIP2 (*159*). We clonally selected two *NOD1* KO cell lines and characterized the deletions on both alleles of *NOD1*. *NOD1* KO#1 cell line contained identical 2 bp deletions adjacent to the PAM motif, while *NOD1* KO#2 cell line contained a 112 bp deletion on one allele and a 2 bp deletion on the second allele (Fig. 3.1A). To assess functional loss of NOD1, we treated control or *NOD1*-targeted cells with a NOD1-specific ligand (C12-iE-DAP). We found

that the response to NOD1-specific ligand was completely abrogated in *NOD1* KO cells when compared to control targeted cells, yet all cell lines retained IL-8 response to IL1β, a NOD1-independent stimulus (Fig. 3.1B). When we co-cultured control-targeted AGS cells with G27, a wild type clinical isolate of *H. pylori*, we found that the cells produced IL-8 in response to infection and that, consistent with published data, the IL-8 response was completely dependent on an intact *cag*-T4SS. Surprisingly, *NOD1* KO attenuated but did not abolish IL-8 production in response to infection with wild type *H. pylori* (Fig. 3.1C), suggesting additional host pathway(s) are activated by bacterial factors delivered through the *cag*-T4SS.

TIFA gene targeting in epithelial cells suppresses the IL-8 response to _H. pylori_ infection.

Given the recent discovery of TIFA as a critical innate immune signaling component in response to Gram-negative bacteria, we hypothesized that TIFA may be playing a role in *H. pylori* detection by gastric epithelial cells. Using CRISPR, we targeted TIFA in wild type or *NOD1* KO AGS cells and assessed IL-8 responses following exposure to strain G27, a clinical isolate of *H. pylori*. We determined that in response to *H. pylori* infection, IL-8 responses were significantly attenuated in *TIFA* KO cells; particularly at the early time point (6 hours) compared to the control targeted cells (Fig. 3.2A). To address reproducibility of NOD1 and TIFA-dependent IL-8 signaling in AGS cells infected with *H. pylori*, we analyzed our data in aggregate across three independent experiments. We found that *H. pylori* induced NOD1-dependent IL-8 production was attenuated at 24 hours. However, IL-8 levels at 6 and 12 hours in *NOD1* KO cells varied across experiments and when analyzed across biological replicates was not statistically significantly different from control AGS cells (Fig. 3.3A). *TIFA* KO AGS cells infected with *H. pylori* consistently showed significantly reduced IL-8 levels at 6, 12 and 24

hours, both in analysis of a representative experiment (Fig. 3.2A) and across three independent experiments (Fig. 3.3A). Because we observed some differences in analyzing representative experiments versus combined data from three independent experiments, we include statistical analysis of biological replicates in Figure 3.3. To assess whether TIFA-dependent IL-8 induction was unique to the G27 strain, we co-cultured *TIFA* KO or *TIFA/NOD1* DKO AGS cells with different *H. pylori* strains (G27, PMSS1, J99 and 26695). We found that, although the overall IL-8 levels varied across strains, all of the strains tested induced TIFA-dependent IL-8 production in AGS cells (Fig. 3.4A). In addition, we found that the effect of targeting both *NOD1* and *TIFA* was additive, since the *NOD1*/*TIFA* DKO cells showed a more dramatic decrease in IL-8 responses than targeting either *NOD1* or *TIFA* alone (Fig. 3.2A, 3.3A, 3.4A). This indicates that both of these pathogen recognition pathways contribute to *H. pylori* detection, yet are functionally independent. Interestingly, we observed residual IL-8 signal at the later time points, suggesting that in addition to peptidoglycan and HBP, at least one other bacterially-derived factor delivered through the *cag*-T4SS is driving an immune response in gastric epithelial cells. To ensure that the effect on IL-8 production was TIFA-dependent and did not result from CRISPR off-target effects, we transduced CRISPR-targeted AGS cells with lentivirus containing the complete TIFA coding sequence and showed that the IL-8 produced in response to *H. pylori* infection in TIFA complemented cells was restored. We found that at the 6 hour time point, IL-8 induced in *TIFA* complemented cells was statistically significantly higher than in control targeted cells ($p = 0.001$), which may be due to *TIFA* overexpression since in the complemented cells, *TIFA* expression is driven by the lentiviral MND promoter (Fig. 3.2B, 3.3B). Furthermore, since TIFA signaling relies on oligomerization, which can be caused by protein overexpression, we confirmed that no IL-8 was produced in mock treated TIFA complemented cells (Fig. 3.2B).

Activation of TIFA-mediated inflammatory response to *H. pylori* is *cag*-T4SS dependent.

The IL-8 response in AGS cells to *H. pylori* is dependent on a functional *cag*-T4SS, since infection with a *cag*-T4SS mutant (*ΔcagE*) results in complete loss of IL-8 production (Fig. 3.1C). Similar to wild type AGS cells, *TIFA* KO AGS cells do not produce IL-8 in response to *ΔcagE* mutant *H. pylori* (data not shown). Importantly, our data indicate that without a functional *cag*-T4SS, the TIFA-dependent immune response to *H. pylori* is completely abrogated. To confirm that *H. pylori* activates a TIFA-mediated inflammatory response and that it is dependent on the *cag*-T4SS, we co-cultured *H. pylori* with HCT116 cells, a colorectal adenocarcinoma cell line that, like AGS cells, also expresses α5β1 integrin required for *cag*-T4SS attachment and CagA translocation (*160*, *161*) and has a functional TIFA signaling pathway (*158*). When we infected control or TIFA-targeted HCT116 cells with *H. pylori*, we found that in the absence of TIFA, the IL-8 response is completely abrogated, while the IL-8 response to a TIFA-independent ligand, IL1β, is intact in both control and TIFA-targeted cells. Consistent with our data in AGS cells, we found that IL-8 produced by colon epithelial cells in response to *H. pylori* is completely *cag*-T4SS-dependent, since no IL-8 is produced when we co-culture with a *ΔcagE* mutant (Fig. 3.2C, 3.3C). However, in contrast to AGS cells, IL-8 induced following *H. pylori* detection in the context of this colon epithelial cell line appears to be completely TIFA-dependent and does not rely on NOD1 activation or sensing of the NOD1- and TIFA-independent bacterially-derived factor.

Gastric epithelial cells robustly respond to bacterially-derived HBP.

To assess whether AGS cells are able to produce IL-8 in response to HBP stimulation, we reversibly permeabilized control or *TIFA* KO AGS with digitonin and treated them with *Neisseria* lysates containing HBP (*ΔgmhB*) or heptose-7-monophosphate (HMP; *ΔhldA*) (*156*). Control AGS cells treated with HBP showed an accumulation of IL-8 over a 24-hour time period, whereas, HMP treated cells showed substantially lower IL-8 responses. Notably, when we assessed *TIFA* KO AGS cells treated with HBP, we found the same reduction in IL-8 responses in control targeted AGS cells treated with HMP (Fig. 3.2D, 3.3D). These data suggest that AGS cells recognize HBP and activate TIFA to drive the NF-κB-dependent IL-8 response. Published reports have demonstrated that HBP-inducible phosphorylation of TIFA at the T9 amino acid drives intermolecular oligomerization, which recruits and activates its downstream signaling partner TRAF6 (*155*, *157*, *158*). Therefore, we assessed whether the T9 residue is essential for TIFA activation in AGS cells during *H. pylori* infection. We stably complemented *TIFA* KO cells with either wild type N-terminally tagged TIFA or a T9A substitution containing TIFA. We found that, similar to *TIFA* KO AGS cells, IL-8 responses were reduced in the T9A complemented cells. *H. pylori* infection of both N and C-terminally tagged wild type complemented cells resulted in control levels of IL-8 (Fig. 3.2E, 3.3E). These data are consistent with previous studies and suggest that in AGS cells, *H. pylori*-induced inflammation requires phosphorylation of TIFA at T9 in order to activate TRAF6 and propagate the NF-κB driven immune response.

To determine whether *H. pylori* cell lysates containing HBP could activate NF-κB in a TIFA-dependent manner, we treated NF-κB-luciferase reporter human embryonic kidney (293T) cells with various ligands and measured luciferase reporter activity. 293T cells have a high transfection efficiency and lack endogenous TLR and some nucleic acid sensing pathways (*162*,

163), allowing for dissection of the TIFA-dependent response with little contribution of other PAMP sensing pathways. Consistent with published data (*155*, *158*), we found that wild type reporter cells robustly responded to HBP, but not the upstream monophosphorylated derivative HMP and the induction of NF-κB-luciferase activity was largely dependent on TIFA. When we treated the reporter cells with G27 *H. pylori* cell lysates (Fig. 3.2F, 3.3F) or lysates from different *H. pylori* strain backgrounds (Fig. 3.4B), only the wild type 293T cells and not *TIFA* KO cells responded, showing greater than 100-fold induction of NF-κB-luciferase. Both wild type and *TIFA* KO cells responded to a TIFA-independent stimulus, TNFα (Fig. 3.2F, 3.3F). Together these data confirm that *cag*-T4SS-dependent delivery of *H. pylori* HBP into host epithelial cells triggers the activation of TIFA leading to NF-κB activation and subsequent production of IL-8.

***H. pylori* heptose biosynthesis mutants are filamentous and have delayed growth.**

In Gram-negative bacteria, the biosynthesis of ^{D,D}Heptose and ^{L,D}Heptose, which are incorporated into the core oligosaccharide of LPS, occurs in the bacterial cytosol by highly conserved enzymes. In *E. coli*, the reaction begins with the conversion of sedoheptulose-7-P to ^{D,D}Heptose-7-P by isomerase GmhA, followed by heptokinase activity of bifunctional HldE to generate ^{D,D}Heptose-1,7-PP (HBP, the molecule that activates TIFA). HBP is then converted to ^{D,D}Heptose-1-P (HMP) by phosphatase GmhB, which is further modified by the ADP-transferase activity of HldE to form ADP-^{D,D}Heptose. ADP-^{D,D}Heptose is then converted to ADP-^{L,D}Heptose by epimerase HldD. WaaC then transfers the first ^{L,D}Heptose to Kdo for ongoing lipopolysaccharide synthesis (*164*). Sequenced *H. pylori* strains contain conserved homologues of the four *E. coli* enzymes involved in ADP-heptose biosynthesis (Fig. 3.5A). Using a

phosphate release assay, Yu *et al*. showed that when recombinant *H. pylori* enzymes GmhA, HldE and GmhB are combined with a sedoheptulose-7-P substrate significantly more phosphate is released than the enzymes alone or an enzyme mixture that is missing HldE, supporting the hypothesis that these proteins function similarly to the ADP-heptose biosynthesis pathway described for other Gram-negative bacteria (*165*). Furthermore, the crystal structure of *H. pylori* HldD revealed that the substrate binding site, as well as the overall structure, were highly similar to *E. coli*'s HldD, suggesting conserved enzymatic function (*166*). It has also been shown that deletion of several enzymes involved in assembly of the highly conserved LPS core in *H. pylori* results in mutants that are unable to colonize mice, typifying the essential nature of most PAMPs (*167*, *168*). Furthermore, despite the fact that *waaC* was the first LPS biosynthesis gene identified in *H. pylori*, attempts to generate deletion mutants proved unsuccessful (*169*).

In our study, using the *H. pylori* G27 strain, we attempted to generate deletion mutants for all four predicted heptose biosynthesis genes, but were unable to delete *gmhA* or *hldE*. HPG27_814 is annotated as a hypothetical protein in the fully sequenced G27 genome (*170*). Using the web-based Phyre2 protein structure prediction tool (*171*), we found that HPG27_814 contained 35% sequence identity and mapped with 100% confidence as a homolog of *E. coli* GmhB (data not shown). Deletion of *hldD* and putative *gmhB* in G27 resulted in highly filamentous mutants that had a pronounced growth defect. Complementation of *hldD* and *gmhB* at the neutral *rdxA* locus restored wild type shape and growth rates (Fig. 3.5B & C). Our observations are consistent with a previous report showing that deletion of *hldD* in 26695 strain resulted in bacteria with truncated LPS (deep-rough phenotype), decreased growth rate, increased susceptibility to novobiocin and decreased adherence to AGS cells (*172*). To our knowledge analysis of *gmhB* mutants has not been undertaken in *H. pylori*. However, in our

study, deletion of *gmhB* in G27 resulted in an even more pronounced growth defect than deletion of *hldD*. This suggests that, although the heptose biosynthesis enzymes are part of the same pathway, deletion of individual enzymes has differing effects on *H. pylori*. Furthermore, another recent study characterized a *gmhA* deletion mutant in the strain 26695 (*165*). Similar to the *hldD* mutant, they showed that *ΔgmhA* bacteria displayed truncated LPS, decreased growth rate, increased susceptibility to novobiocin and detergents and were less able to adhere to AGS cells. Our inability to generate a *ΔgmhA* mutant may reflect strain specific differences between G27 and 26695. It is also possible that *ΔgmhA* 26695 mutant generated by Yu *et al.* contains a suppressor mutation that partially alleviates the lethality of deleting *gmhA* and thus results in viable, albeit sickly, bacteria.

***H. pylori* HldE drives HBP synthesis and TIFA-dependent NF-κB activation.**

In order to determine whether *H. pylori* HBP is driving the TIFA-dependent NF-κB activation, we used an *E. coli* overexpression system where we put *H. pylori hldE*, which encodes the enzyme that produces HBP, under an IPTG-inducible promoter. We collected uninduced and IPTG-induced cell lysates and used them to treat NF-κB-luciferase reporter cells. We found that only *E. coli* cells that expressed *H. pylori* HldE potently activated NF-κB, a response that was further enhanced by IPTG treatment. In contrast, *E. coli* expressing *H. pylori* GmhB, which converts HBP to HMP, showed background levels of NF-κB activation that were equivalent to vector only expressing bacteria in a representative experiment (Fig. 3.5D) and across three independent experiments (Fig. 3.6A). To confirm that the enhanced NF-κB activation by lysates from *H. pylori* HldE-expressing *E. coli* was TIFA-dependent, we treated wild type or *TIFA* KO reporter cells with a dilution series of lysates from IPTG-induced GmhB

or HldE expressing bacteria. We standardized our input based on total protein measured by a BCA protein assay and found that across the dilution series, lysates from HldE expressing *E. coli* consistently showed increased NF-κB activation relative to GmhB expressing bacteria and that the NF-κB signal was completely TIFA dependent (Fig. 3.6B). Since the ADP-heptose biosynthesis enzymes appear to function similarly in *H. pylori* as in other Gram-negative bacteria and HldE, the enzyme that synthesizes HBP, appears essential, we focused our analysis on enzymes downstream of HBP. We hypothesized that targeting *gmhB* might result in HBP accumulation within the bacteria and, thereby, increased TIFA-dependent NF-κB activation. Using the NF-κB-luciferase reporter cells, we treated wild type or *TIFA* KO cells with lysates generated from wild type, *ΔgmhB,* or *ΔhldD* (encoding an enzyme downstream of GmhB) bacteria. We normalized our input based on total protein estimation using a BCA protein assay, since optical density is not an accurate reflection of total cell number when working with filamentous mutants. We found that lysates from *ΔhldD* mutants induced statistically significantly more NF-κB ($p = 0.05$) than wild type *H. pylori* (Fig. 3.5E). However, when we assessed data across three independently conducted experiments, we found no significant difference between NF-κB activation induced by wild type, *ΔgmhB*, *ΔhldD* and their respective complemented strain lysates (Fig. 3.6C). It is possible that *H. pylori* controls metabolic pathways to prevent excess cytosolic HBP accumulation in the absence of GmhB. Nevertheless, our overexpression data in *E. coli* suggests that *H. pylori* HldE generates HBP, which signals through TIFA leading to NF-κB activation.

CagA contributes to the late NF-κB-dependent IL-8 response in gastric epithelial cells.

When we assessed *NOD1/TIFA* DKO AGS cells for IL-8 production in response to *H. pylori* infection, we found that IL-8 levels were substantially reduced at the earlier time points. However, in the absence of both NOD1 and TIFA signaling we found residual IL-8 that accumulated over time, being especially evident at the 24-hour time point (Fig. 3.2A). We hypothesized that CagA may be driving this residual IL-8 signal since the N-terminal domain (amino acids 24-221) of CagA has been proposed to activate NF-κB (*149*, *173*, *174*). Indeed, when we co-cultured wild type or *TIFA* KO AGS cells with *ΔcagA* mutant *H. pylori*, we found a significant decrease in the IL-8 response at the 24-hour time point (Fig. 3.7A, 3.8), which was restored to wild type levels when cells were co-cultured with *ΔcagA* complemented *H. pylori* (Fig. 3.8). The reduced IL-8 was particularly evident in *TIFA* KO AGS cells, confirming that both TIFA activation and CagA detection contribute to the IL-8 response in AGS cells. We also showed that CagA is present and becomes phosphorylated within AGS cells co-cultured with wild type or *ΔcagA* complemented *H. pylori* (Fig. 3.7B). When we examined HCT116 colon epithelial cells, where the IL-8 response to *H. pylori* appears to be almost entirely TIFA-dependent, we did not observe a significant difference in IL-8 levels in cells treated with wild type or isogenic *ΔcagA* mutant (Fig. 3.7C). We also observed that, while in AGS cells wild type *H. pylori* delivers CagA into the host cell where it is phosphorylated by host kinases, CagA was not phosphorylated in HCT116 cells, suggesting that CagA is either not delivered into these cells or that HCT116 cells are unable to phosphorylate translocated CagA (Fig. 3.7D).

DISCUSSION

Using CRISPR/Cas9 gene targeting of specific pathogen recognition pathways, we reveal that TIFA is involved in the human cellular response to *H. pylori*, and were able to dissect the relative contribution of *H. pylori*-derived factors that contribute to the NF-κB-mediated immune

response in gastric epithelial cells. While it was previously accepted that NOD1 activation following *H. pylori* cell wall fragment (PG) detection is the main proinflammatory signal that leads to IL-8 production, here we show that *H. pylori* HBP-dependent TIFA activation also plays a critical role in the early immune response to *H. pylori* (Fig. 3.9). Furthermore, we reveal a previously unrecognized manner by which HBP gains access to the cytosolic TIFA pathway, since *H. pylori* HBP is delivered directly to the host cell cytosol through the *cag*-T4SS. It remains an open question of whether HBP delivery to the host is an inadvertent consequence of forming the *cag*-T4SS that connects the bacterial and host cytosol, or whether *H. pylori* HBP delivery to the host instigates an inflammatory response that benefits the bacteria, such as by the recruitment of regulatory T cells and activation of other tolerogenic mechanisms that prevent bacterial clearance and support chronic colonization (*52*, *61*).

It was recently demonstrated that TIFA activation fine-tunes the downstream inflammatory response based upon the rates of cytosolic replication by invasive bacteria (*158*). That study suggested that TIFA signaling is one mechanism by which intestinal epithelial cells can potentially distinguish commensal bacteria from pathogenic invaders. Interestingly, in the context of invasive *Shigella* infection the temporal pattern of NOD1 and TIFA activation is the inverse of what we observe during *H. pylori* infection: NOD1 constitutes the initial response to *Shigella* and TIFA is activated later (*158*), while with *H. pylori* the HBP response occurs earlier. This difference may be attributable to the very different lifestyles of these bacteria. While HBP slowly accumulates within the mammalian cell as *Shigella* grows, a bolus of the cytosolic HBP present within *H. pylori* can presumably be rapidly delivered as the *cag*-T4SS penetrates the host cell, rapidly activating the TIFA pathway.

The impact of the CagA toxin on *H. pylori*-induced inflammation is somewhat controversial. Because *ΔcagA H. pylori* strains induce a robust inflammatory response, a number of studies concluded that CagA is dispensable for the *cag*-T4SS-dependent NF-κB-driven immune response (*175-177*). However, a recent consensus has emerged that suggests CagA itself can activate the NF-κB inflammatory pathway since transfection with CagA expression constructs leads to NF-κB activation (*149*), and that CagA physically binds immune signaling component TAK1 to promote NF-κB activation (*173*, *178*). Our data support the latter studies showing that CagA can drive an NF-κB-mediated immune response. However, we find that CagA likely activates this pathway later than TIFA and NOD1. Because both the TIFA and NOD1 pathways converge on TRAF6 activation, it is possible that initial activation of these pathways potentiates CagA interaction with TAK1 (Fig. 3.9) and that CagA then further amplifies and/or sustains NF-κB activation. Further work is needed to fully elucidate the mechanism by which CagA activates NF-κB.

Several groups have recently provided insight into the LPS structure of various commonly studied *H. pylori* strains (*167*, *179-182*). Li *et al.* proposed a redefinition of the *H. pylori* LPS structure to contain Lipid A, a short, highly conserved core hexa-saccharide domain composed of Glucose-Galactose-^{D,D}Heptose-^{L,D}Heptose-^{L,D}Heptose-KDO and the direct attachment of the variable O-antigen to the ^{D,D}Heptose molecule (*167*). This is in contrast to the LPS structure of other Gram-negative bacteria, which contain an inner core resembling the hexa-saccharide domain of *H. pylori* and an outer core to which the O-antigen is attached. Studies have shown that deletion of enzymes involved in the assembly of the highly conserved LPS core in *H. pylori* results in bacteria that are unable to colonize mice (*52*, *61*, *167*, *168*). Our own data suggests that *hldE* and *gmhA*, at least in the G27 strain background, appear to be essential in *H.*

pylori and deletion of *hldD* and *gmhB* results in highly filamentous and slow growing bacteria. The enzymes involved in the biosynthesis of ADP-heptose and assembly of the core LPS oligosaccharide present bacterial pathways that can potentially be therapeutically targeted.

Our data suggest that TIFA, NOD1 and CagA all contribute to the NF-κB-driven inflammatory response in gastric epithelial cells, however, how much each of these pathways contributes to natural infection remains an open question. Although AGS cells are a useful and tractable model system to study *H. pylori* interaction with gastric epithelial cells, they do not fully recapitulate the complexity of primary gastric epithelial cells. Interestingly, gene expression analysis of primary human stomach tissue validates that *TIFA* and *NOD1* are both expressed, supporting their physiological relevance to *H. pylori* infection observed in our study. Furthermore, primary stomach tissue has much higher *TIFA* expression levels than *NOD1*, which may reflect the relative contribution of both pathways to *H. pylori* detection (*158*). Future studies will focus on assessing NOD1 and TIFA innate immune signaling pathways in primary gastric organoids and animal models of infection to further elucidate their respective contributions to *H. pylori* detection.

How *H. pylori* is able to maintain a chronic infection despite a robust host immune response has remained a mystery. To help answer that question, we must first understand the underlying host inflammatory pathways that *H. pylori* activates and subverts. Our study reveals a previously unappreciated role of TIFA in the innate immune response initiated in *H. pylori* infected gastric epithelial cells. Furthermore, we demonstrate, for the first time, that HBP can be directly delivered to host cells through a bacterial secretion system where it potently activates TIFA and drives the downstream NF-κB-mediated inflammatory response. Gaining a comprehensive view of the early signaling events that take place at the interface of *H. pylori* and

gastric epithelial cells is ultimately required to determine how this host-pathogen interaction can be manipulated in the host's favor. Our study adds a critical piece to our understanding of the host immune response to an important human pathogen.

EXPERIMENTAL PROCEDURES

CRISPR/Cas9 Gene Targeting and Complementation

CRISPR/Cas9 gene targeting of AGS cells was performed as described by Gray *et al* (*183*). Briefly, we used a single lentiviral plasmid that expresses the gene targeting guide RNA under a U6 promoter, as well as an MND promoter-driven Cas9-T2A-puromycin or – blasticidin resistance cassette (pRRL lentiviral vector). 293T cells were transfected with 1.5 μg pVSV-G, 3 μg psPAX-2, and 6 μg pRRL lentiviral vector. Lentiviral supernatants were collected 48 hours later and used to transduce AGS cells. AGS cells were then selected with puromycin (0.5 μg/mL) or blasticidin (12.5 μg/mL) for 7-10 days. As a control, cells were transduced with pRRL expressing Cas9 only or a human non-targeting control guide RNA, as described by Sanjana *et al* (*184*). *NOD1*-targeted cells were clonally selected and gene targeting verified by TOPO cloning and Sanger sequencing. *TIFA* targeting was verified using an *in vitro* RGEN-RFLP assay, as previously described (*185*). The following guide RNA sequences were used: *NOD1* 5'-gTTTTCAGTAATTGAATGTGG-3' and *TIFA* 5'-cagatgacggtttaccatcc-3'. To restore TIFA in targeted cells, the TIFA coding DNA sequence (CDS) was cloned into the pRRL lentiviral backbone to generate an MND promoter-driven TIFA-T2A-zeocin plasmid. *TIFA* targeted cells were subsequently transduced with pRRL-MND-TIFA-T2A-zeocin plasmid, as described above, and selected with 250 μg/mL zeocin for 10-14 days. To ensure that the complementation construct was CRISPR resistant, we introduced SNPs into the guide RNA targeted genomic sequence that resulted in synonymous mutations, which maintain the TIFA amino acid sequence

but prevent guide RNA binding and Cas9 cutting. The following single oligonucleotide was used in a site-directed mutagenesis reaction to alter the TIFA CDS: 5'-GAGACAGTAACTTGTCTCCAaATGACaGTcTAtCAcCCaGGCCAGTTGCAGTGTGGAAT A-3' (guide RNA sequence is underlined and introduced SNPs are in lowercase). In addition, C-terminal 6X-His and V5 tags were added to TIFA CDS to allow downstream protein expression analysis.

Bacterial strains

G27, a clinical isolate of *H. pylori* that contains the *cag* pathogenicity island (*186*), or isogenic mutants were grown at 37°C in a trigas incubator equilibrated with 10% oxygen, 10% carbon dioxide, and 80% nitrogen on solid media containing horse blood agar or in liquid culture containing Brucella broth (BD Biosciences) with 10% heat-inactivated FBS (Gemini – Benchmark), as previously described (*187*). Isogenic knock-out mutants were constructed using a vector-free allelic replacement strategy, where >60% of the CDS was replaced by a chloramphenicol resistance cassette and selected with 15 μg/mL chloramphenicol, as previously described (*188*). To generate complementation mutants, we integrated a wild type copy of the deleted gene at a neutral locus, either *rdxA* with metronidazole selection (*189*) or an intragenic region between HPG27_186 and HPG27_187 (McGee locus) with kanamycin selection (*190*). The primers used for generating *H. pylori* mutants are listed in Table 3.1. *E. coli* DH5α, HST08 or BL21 were grown and transformed according to standard methods (*191*). For induced protein overexpression experiments, *H. pylori gmhB* and *hldE* genes were amplified and cloned into pET15b vector (Novagen). *E. coli* BL21 cells were transformed, selected with 100 μg/mL ampicillin and grown to OD_{600} = 0.6. Cells were then induced with 1 mM IPTG for 4 hours and

harvested by centrifugation. Cell pellets were then processed to obtain cell lysates, as described above for NF-κB-luciferase assays, or resuspended in Laemmli buffer with β-mercaptoethanol and protein expression analyzed by Western blot.

Cell Treatments and analysis

AGS cells, a human gastric adenocarcinoma cell line (ATCC CRL-1739), were grown in DMEM (Gibco) supplemented with 10% heat-inactivated FBS (Gemini – Benchmark). HCT116 cells, a human colon adenocarcinoma cell line (ATCC CCL-247), were grown in McCoy's 5A Media (ATCC) supplemented with 10% FBS. *TIFA* KO HCT116 cells were generated using CRISPR/Cas9 gene targeting, as previously described (*158*). For co-culture with *H. pylori*, AGS or HCT116 cells were seeded at 1 x 10^5 cells/well in 24-well plates 16 hours prior to infection. The day of infection, media was removed from human cells and mid-log *H. pylori* was added at multiplicity of infection 10:1 resuspended in either DMEM + 10% FBS + 20% Brucella broth for AGS cells or McCoy's 5A + 10% FBS + 20% Brucella broth for HCT116 cells. Supernatants from three individual wells per each experimental condition were collected at indicated time points and assayed for IL-8 concentration using a human IL-8 ELISA kit according to manufacturer's instructions (Biolegend). As indicated, cells were also treated with C12-iE-DAP (Invivogen), IL1β (Biolegend) or TNFα (Peprotech). NF–κB-luciferase assays were performed as previously described (*155*) using the Dual-Glo Luciferase Assay system (Promega). Wild type or *TIFA* KO human embryonic kidney (HEK) 293T cells were plated in triplicate and co-transfected with 90 ng NF-κB-luciferase and 10 ng *Renilla* luciferase plasmids then treated the following day with *Neisseria* lysates containing HBP, HMP or cell lysates from *H. pylori* or isogenic mutants in 5 μg/mL digitonin-containing permeabilization buffer (*192*). To obtain cell

lysates, a volume equivalent to 1 OD_{600} of mid-log phase *H. pylori* culture was pelleted by centrifugation, washed once with PBS, resuspended in 100 μl of water, boiled for 10 min, centrifuged to remove cell debris and supernatant passed through a 0.22 μm syringe filter. Input for luciferase assays was normalized using a BCA protein assay kit (Pierce) and 1 μl of normalized lysate was used to stimulate 293T reporter cells.

Immunoblotting

After 24 hours of co-culture with *H. pylori*, AGS cells were washed with ice-cold PBS and lysed in Laemmli buffer with β-mercaptoethanol and boiled for 5 minutes. For CagA translocation and phosphorylation analysis, cell lysates were separated on Mini-protean TGX polyacrylamide gels (Bio-rad) and blotted for anti-phosphotyrosine (4G10 EMD Millipore) and beta-actin (Cell Signaling Technology) overnight at 4°C. Membranes were then blocked for several hours in 5% non-fat milk in TBST then incubated with anti-CagA antibody (Santa Cruz; sc-28368) overnight at 4°C.

Statistical Analysis

Statistical significance of difference between groups was assessed using one-way analysis of variance (ANOVA) with Bonferroni correction for multiple comparisons. Statistical differences were assessed within individual experiments based on mean values from 3 independent samples per experimental condition, as well as across at least two independently performed experiments. *P*-values greater than or equal to 0.05 were considered statistically significant. All analyses were performed using Prism v7.0 software (GraphPad).

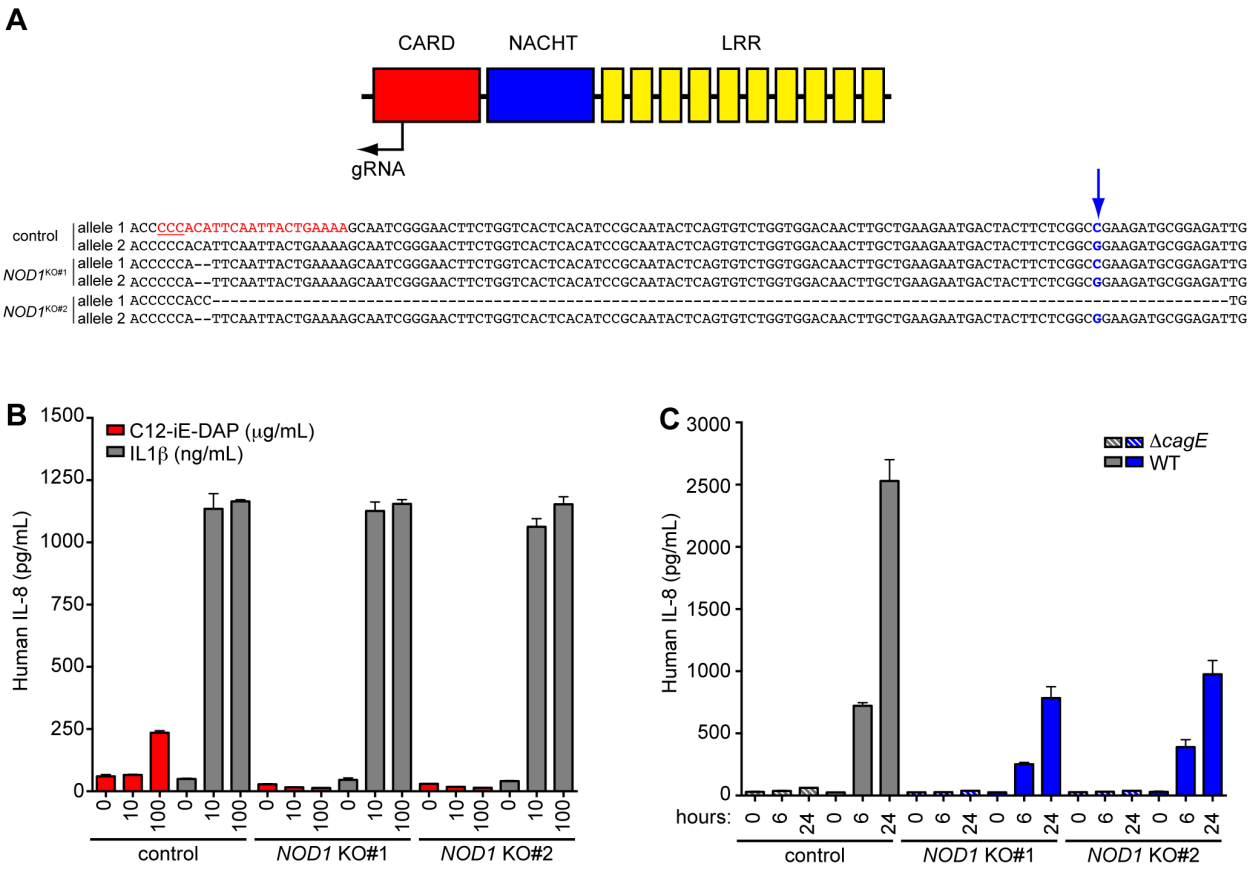

Figure 3.1. NOD1 only partially contributes to *H. pylori* detection
(A) Schematic representation of NOD1 structural domains and location of the guide RNA used to generate CRISPR targeted, clonally selected *NOD1* KO cell lines. A portion of the sequence of each allele in control targeted cells is shown with the guide RNA sequence highlighted in red and the protospacer adjacent motif (PAM) underlined. The SNP used to distinguish allele 1 and 2 is shown in blue with arrow. The deletions generated in *NOD1* KO#1 and #2 cell lines are represented by dashes. (B) IL-8 ELISA assay performed on control targeted, *NOD1* KO#1 and #2 AGS cells treated with IL1β or C12-iE-DAP. Each condition was tested in triplicate with bars showing the mean with standard deviation. (C) Control or *NOD1* targeted cells were co-cultured with wild type G27 *H. pylori* or *ΔcagE* isogenic mutant at MOI = 10 and IL-8 concentration in supernatant measured by ELISA. Each condition was tested in triplicate with bars showing the mean with standard deviation. Data shown in (B) and (C) is representative of at least three independent experiments.

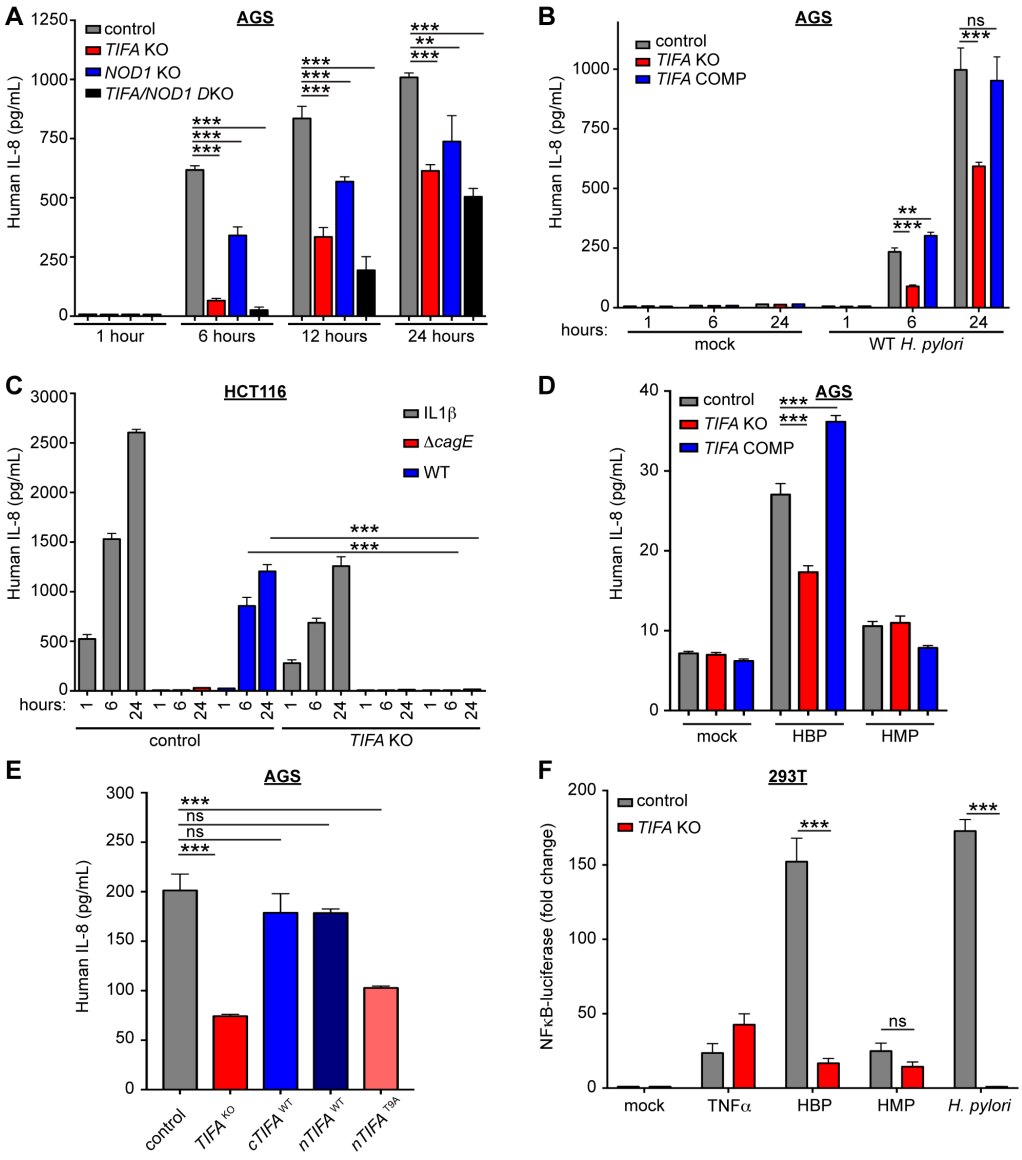

Figure 3.2. TIFA is required for early *cag*-T4SS-dependent NF-κB-driven immune response in gastric epithelial cells

(A) Control, *TIFA*-targeted, *NOD1* KO#1 or *TIFA*-targeted *NOD1* KO#1 AGS cells (DKO) were co-cultured with wild type G27 *H. pylori* and IL-8 concentration in the supernatant measured by ELISA. (B) Control, *TIFA*-targeted or *TIFA*-targeted and stably complemented with full length TIFA AGS cells were mock treated or co-cultured with wild type *H. pylori* and IL-8 concentration in the supernatant measured by ELISA. (C) Control or *TIFA* targeted colorectal adenocarcinoma cells (HCT116) were treated with IL1β, wild type or *ΔcagE* isogenic mutant *H. pylori* and IL-8 concentration measured in the supernatant. (D) Control or *TIFA* KO AGS cells were reversibly permeabilized with digitonin for 15 min and mock treated or stimulated with HBP (*ΔgmhB*) or HMP (*ΔhldA*) containing *Neisseria* lysates. Supernatants were collected after 6 hours and IL-8 measured by ELISA. (E) Control, *TIFA* KO, C-terminally tagged wild type TIFA, N-terminally tagged wild type or T9A TIFA complmented AGS cells were co-cultured with *H.*

pylori and IL-8 measured in culture supernatants after 6 hours of infection. For co-culture experiments (A-C and E), *H. pylori* was added at MOI = 10, supernatant collected at indicated time points and each condition tested in triplicate with bars showing the mean with standard deviation. (F) NF-κB-luciferase activity in wild type or *TIFA*-targeted 293T cells treated with TNFα (5 ng/mL), *N. meningitidis* derived HBP and HMP or wild type *H. pylori* lysate. Data was normalized to signal from co-transfected Renilla-luciferase plasmid and represented as normalized fold change from mock treated samples. Each condition was tested in triplicate with bars showing the mean with standard deviation. Data shown in A-F is representative of at least two independent experiments. Statistical significance was determined using ANOVA with Bonferroni correction for multiple comparisons; ns, not significant ($p > 0.05$), **$p < 0.01$, ***$p < 0.001$.

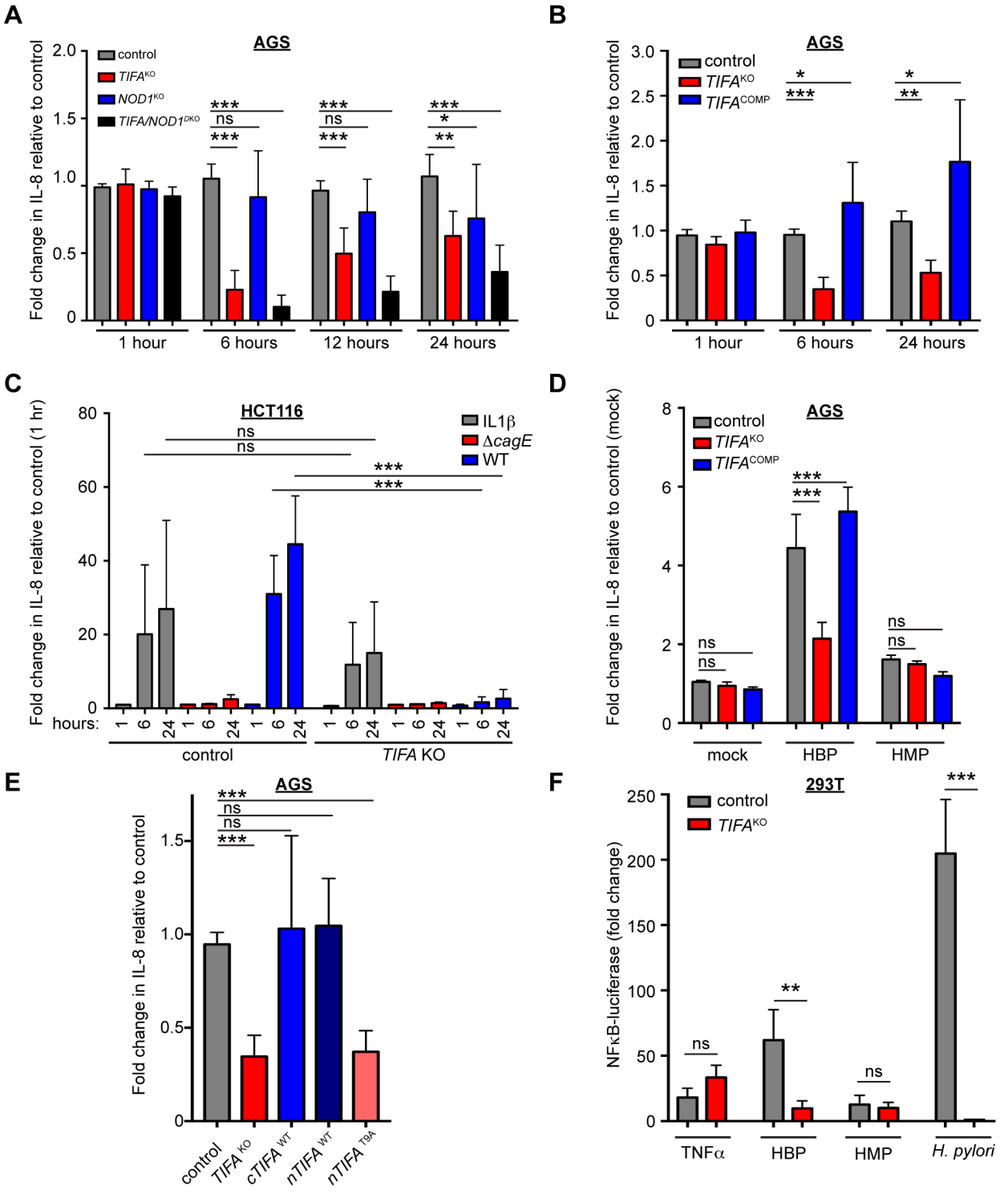

Figure 3.3. TIFA is required for early *cag*-T4SS-dependent NF-κB-driven immune response in gastric epithelial cells

(A) Control, *TIFA*-targeted, *NOD1* KO#1 or *TIFA*-targeted *NOD1* KO#1 AGS cells (DKO) were co-cultured with wild type *H. pylori* and IL-8 concentration in the supernatant measured by ELISA. (B) Control, *TIFA*-targeted or *TIFA*-targeted and stably complemented with full length

TIFA AGS cells were co-cultured with wild type *H. pylori* and IL-8 concentration in the supernatant measured by ELISA. (C) Control or *TIFA* targeted colorectal adenocarcinoma cells (HCT116) were treated with IL1β, wild type or *ΔcagE* isogenic mutant *H. pylori* and IL-8 concentration measured in the supernatant. Data in A-C was combined from three independent experiments and represented as fold change in IL-8 concentration relative to control targeted AGS (A-B) or HCT116 (C) cells. (D) Control or *TIFA* KO AGS cells were reversibly permeabilized with digitonin for 15 min and mock treated or stimulated with HBP (*ΔgmhB*) or HMP (*ΔhldA*) containing *Neisseria* lysates. Supernatants were collected after 6 hours and IL-8 measured by ELISA. Data is shown from two independent experiments and represented as fold change in IL-8 concentration relative to control targeted AGS cells. (E) Control, *TIFA* KO, C-terminally tagged wild type TIFA, N-terminally tagged wild type or T9A TIFA complmented AGS cells were co-cultured with *H. pylori* and IL-8 measured in culture supernatants after 6 hours of infection. Data is shown from two independent experiments and represented as fold change in IL-8 concentration relative to control targeted AGS cells. (F) NF-κB-luciferase activity in wild type or *TIFA*-targeted 293T cells treated with TNFα (5 ng/mL), *N. meningitidis* derived HBP and HMP or wild type *H. pylori* lysate. Data is shown from three independent experiments in which NF-κB-luciferase signal was normalized to signal from co-transfected Renilla-luciferase plasmid and represented as normalized fold change from mock treated samples. In A-F, the bars indicate the mean with standard deviation of data from 2-3 independent experiments. Statistical significance was determined using ANOVA with Bonferroni correction for multiple comparisons; ns, not significant ($p > 0.05$), *$p < 0.05$, **$p < 0.01$, ***$p < 0.001$.

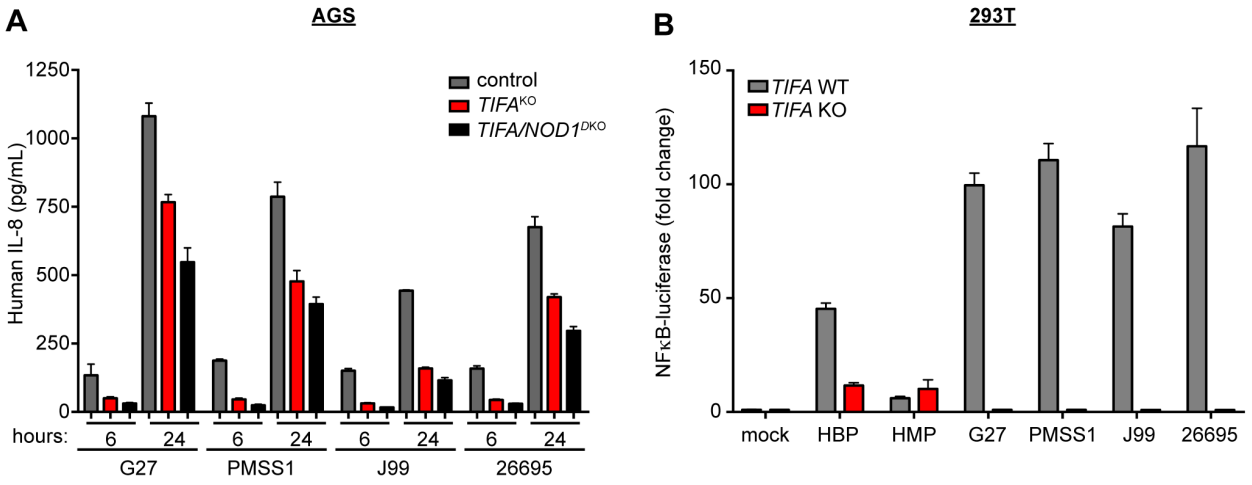

Figure 3.4. Multiple *H. pylori* strains induce TIFA-dependent signaling in epithelial cells
(A) Control, *TIFA*-targeted or *TIFA*-targeted *NOD1* KO#1 AGS cells (DKO) were co-cultured with indicated *H. pylori* strains (MOI = 10) and IL-8 concentration in the supernatant measured by ELISA at 6 and 24 hours. (B) NF-κB-luciferase activity in wild type or *TIFA*-targeted 293T cells mock treated or stimulated with *N. meningitidis* derived HBP and HMP or bacterial lysates from indicated *H. pylori* strains (lysate normalized using OD_{600} measurements). NF-κB-luciferase signal was normalized to signal from co-transfected Renilla-luciferase plasmid and represented as normalized fold change from mock treated samples. (A and B) data is representative of two independent experiments in which each strain was tested in triplicate with bars showing the mean with standard deviation.

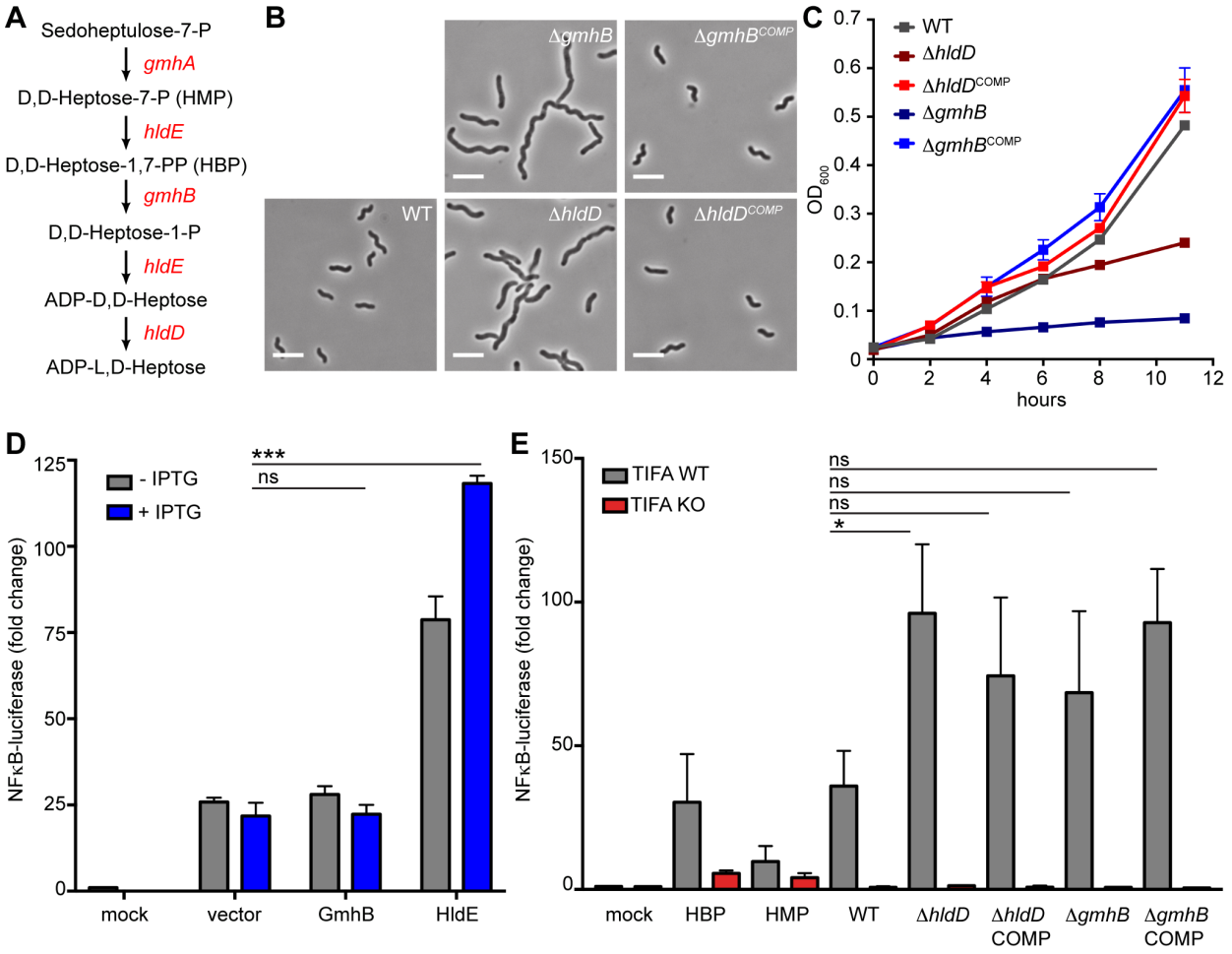

Figure 3.5. *H. pylori* ADP-heptose synthesis mutants are filamentous and have pronounced growth defects

(A) ADP-heptose biosynthesis pathway in *H. pylori*. (B) Phase contrast images of wild type or *H. pylori* mutants lacking the indicated genes and their respective complemented strains. Scale bars = 5 μm. (C) Growth curve analysis of wild type, mutant and complemented strains as measured by OD_{600} over 12 hours. Each strain was grown in triplicate and data represented as mean with standard deviation. Data is representative of two independent experiments. (D) NF-κB-luciferase activity in 293T cells treated with *E. coli* lysates from cells expressing indicated *H. pylori* enzymes with or without the addition of 1 mM isopropyl-b-D-thiogalactopyranoside (IPTG). (E) NF-κB-luciferase activity in wild type or *TIFA*-targeted 293T cells treated with *N. meningitidis* derived HBP (*ΔgmhB*), HMP (*ΔhldA*) or *H. pylori* cell lysates from strains of indicated genotype. Data in D and E was normalized to signal from co-transfected Renilla-luciferase plasmid and represented as normalized fold change from mock treated samples. Each condition was tested in triplicate with bars showing the mean with standard deviation and representative of at least two independent experiments. Statistical significance was determined using ANOVA with Bonferroni correction for multiple comparisons; ns, not significant ($p > 0.05$), *$p < 0.05$, ***$p < 0.001$.

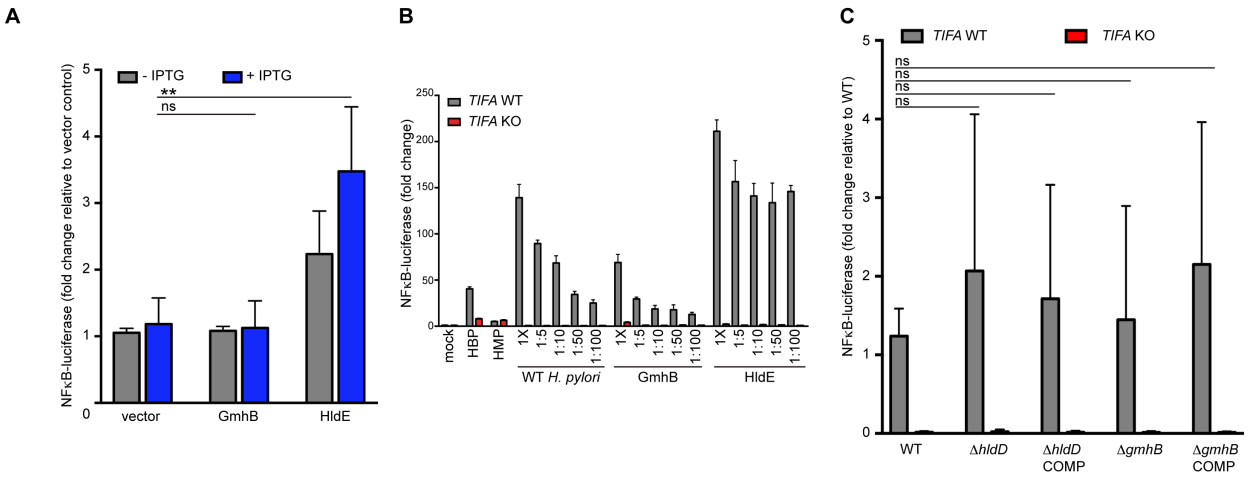

Figure 3.6. *H. pylori* HldE drives TIFA-dependent NF-κB activation
(A) NF-κB-luciferase activity in 293T cells treated with *E. coli* lysates from cells expressing indicated *H. pylori* enzymes with or without the addition of 1 mM isopropyl-b-D-thiogalactopyranoside (IPTG). Data was combined from three independent experiments and represented as mean and standard deviation of fold change relative to NF-κB activity in 293T cells treated with *E. coli* lystes expressing vector only without the addition of IPTG. (B) NF-κB-luciferase activity in wild type or *TIFA*-targeted 293T cells treated with indicated dilutions of wildtype *H. pylori* or *E. coli* lysates from cells expressing *H. pylori* GmhB or HldE and treated with IPTG. Cell lysate input was normalized based on total protein estimated using a BCA protein assay. (C) NF-κB-luciferase activity in wild type or *TIFA*-targeted 293T cells treated with *H. pylori* cell lysates from strains of indicated genotype. Data was combined from three independent experiments and represented as mean and standard deviation of fold change relative to NF-κB activity in wild type 293T cells stimulated with wild type *H. pylori* lysate. Statistical significance was determined using ANOVA with Bonferroni correction for multiple comparisons; ns, not significant ($p > 0.05$), **$p < 0.01$.

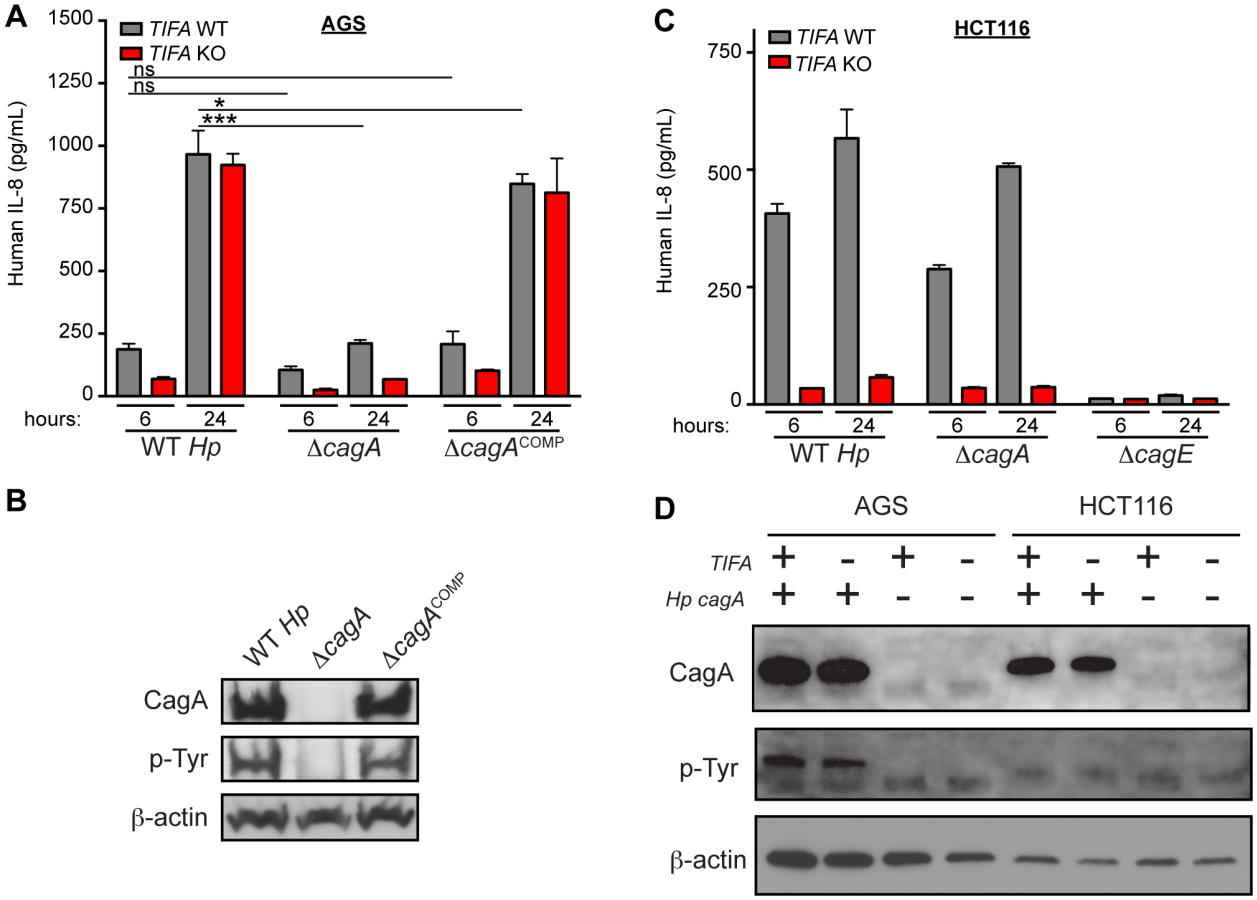

Figure 3.7. CagA contributes to the late NF-κB-driven immune response in gastric epithelial cells

(A) Control or *TIFA*-targeted AGS cells were co-cultured with wild type, *ΔcagA* or *ΔcagA* complemented isogenic *H. pylori* mutants at MOI = 10 and IL-8 concentration in supernatant assayed by ELISA at indicated timepoints. (B) Western blot analysis of cell lysates from control or *TIFA*-targeted AGS cells collected 24 hours after co-culture (MOI = 10) with wild type, *ΔcagA* or *ΔcagA* complemented isogenic mutants. (C) Control or *TIFA*-targeted HCT116 cells co-cultured with wild type, *ΔcagA or ΔcagE* isogenic mutants at MOI = 10 and IL-8 concentration in supernatant measured by ELISA at indicated time points. For experiments show in A and C, each condition was tested in triplicate with bars showing the mean with standard deviation. Data is representative of at least 2 indpendent experiments. Statistical significance was determined using ANOVA with Bonferroni correction for multiple comparisons; ns, not significant ($p > 0.05$), *$p < 0.05$, ***$p < 0.001$. (D) Western blot analysis of cell lysates from control or *TIFA*-targeted AGS or HCT116 cells collected 24 hours after co-culture (MOI = 10) with wild type or *ΔcagA* isogenic *H. pylori* mutants. For Western blots shown in B and D, the phospho-tyrosine (p-Tyr) blot indicates a band consistent with CagA size (~130 kD) and represents CagA that is translocated and phosphorylated inside the host cell.

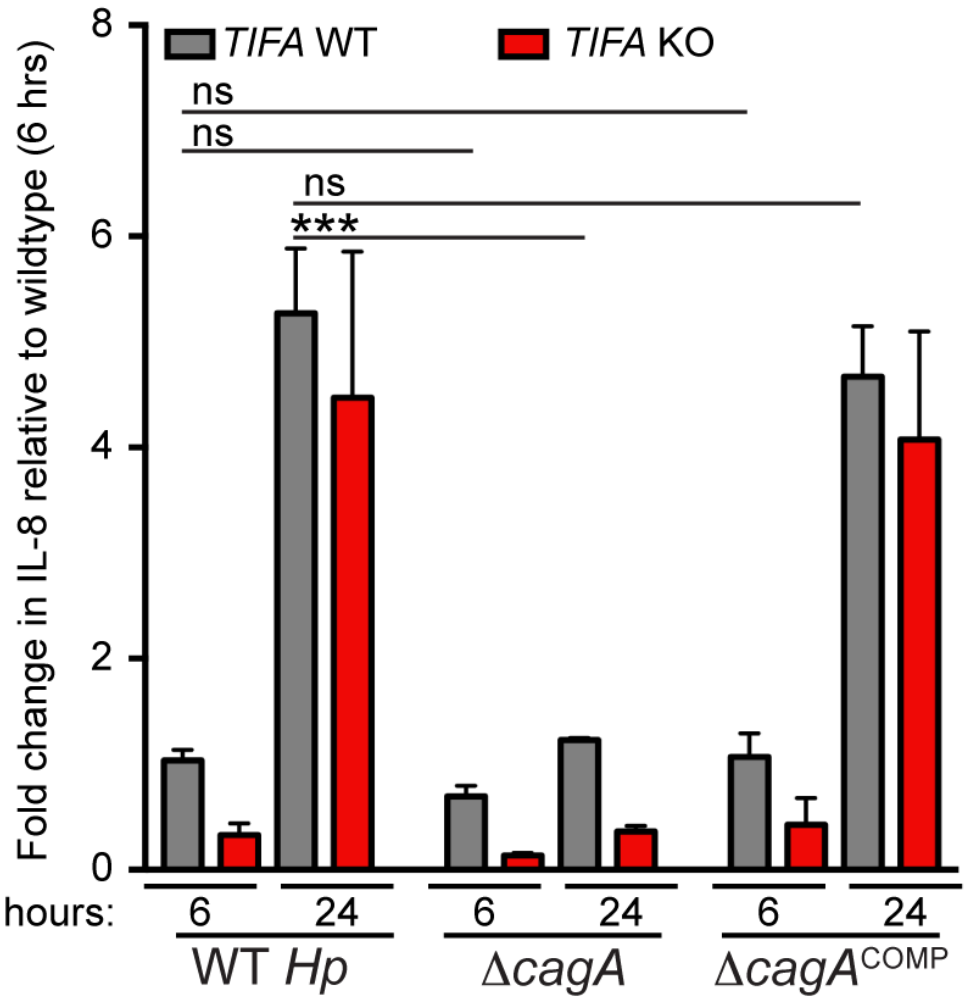

Figure 3.8. CagA contributes to the late NF–κB-driven immune response in gastric epithelial cells

Control or *TIFA*-targeted AGS cells were co-cultured with wild type, *ΔcagA* or *ΔcagA* complemented isogenic *H. pylori* mutants at MOI = 10 and IL-8 concentration in supernatant assayed by ELISA at indicated timepoints. Data was combined from two independent experiments and represented as mean and standard deviation of fold change in IL-8 concentration relative to control targeted AGS cells co-cultured with wild type *H. pylori* for 6 hours. Statistical significance was determined using ANOVA with Bonferroni correction for multiple comparisons; ns, not significant ($p > 0.05$), ***$p < 0.001$.

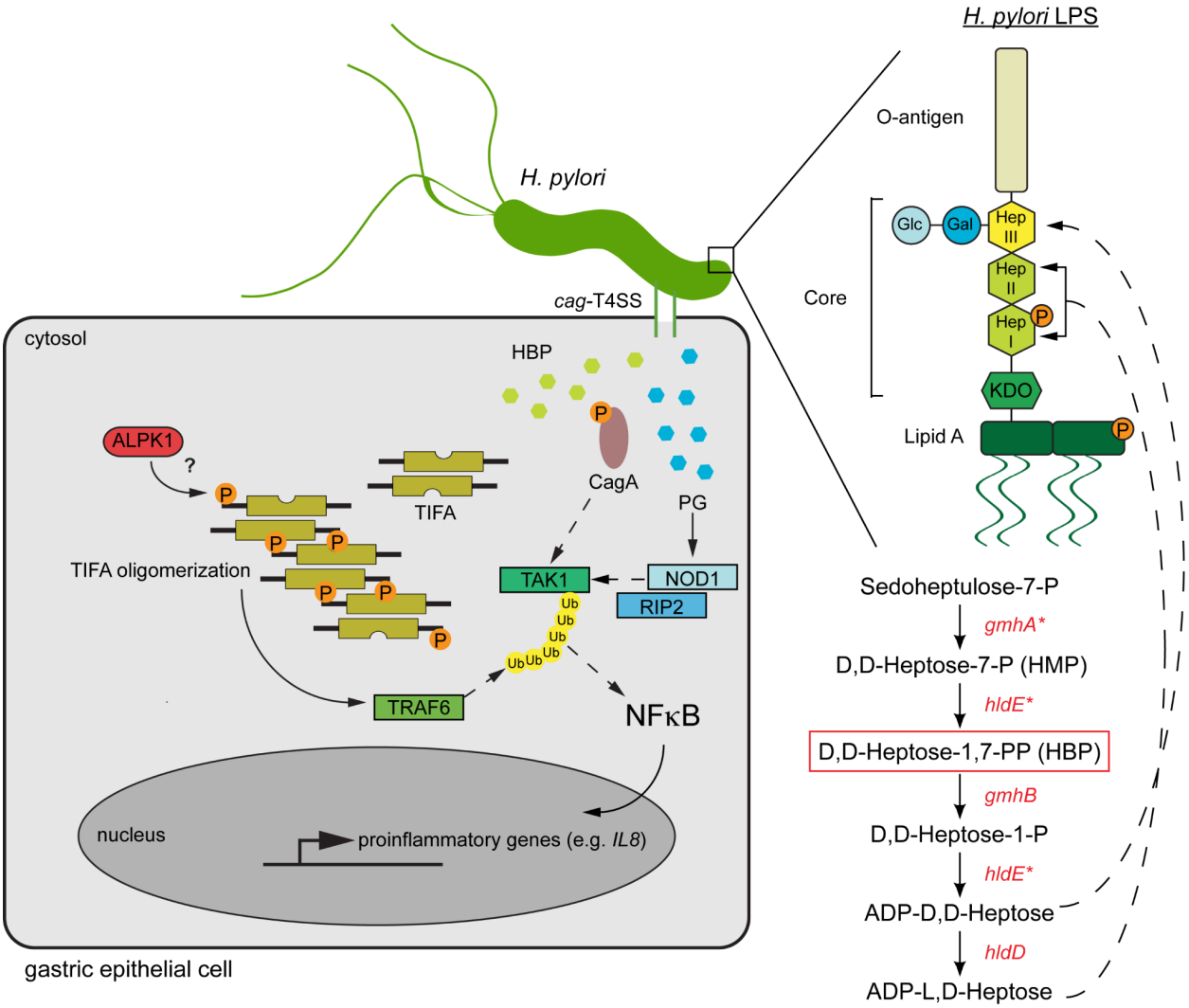

Figure 3.9. Model of *H. pylori cag*-T4SS-dependent, NF-κB-driven innate immune response in gastric epithelial cells

Schematic representation of *H. pylori* factors that are delivered through the *cag*-T4SS into gastric epithelial cells to initiate the NF-κB-mediated inflammatory response. The response is initiated by cytosolic delivery of HBP where it is detected by TIFA, which may be phosphorylated at the Thr9 residue by kinase ALPK1 (*157*). Phosphorylated TIFA forms oligomers that act as a scaffold to recruit and activate TRAF6, which in turn activates transcription factor NF-κB that translocates into the nucleus and upregulates a suite of proinflammatory genes, including *IL8*. Following TIFA activation, peptidoglycan (PG) delivered through the *cag*-T4SS activates NOD1 which ultimately amplifies NF-κB activation. Finally, CagA associates with host TAK1 and enhances its polyubiquitination, which is mediated by E3 ligase activity of TRAF6. Polyubiquitinated TAK1 then activates NF-κB, further amplifying the proinflammatory cascade

(*173*, *178*). HBP that is delivered through the *cag*-T4SS to activate TIFA is generated through the ADP-heptose biosynthesis pathway in the bacterial cytosol. Four *H. pylori* enzymes are involved in converting sedoheptulose-7-P into ADP-L,D-Heptose. Two of these enzymes (marked with an asterisk), GmhA and HldE appear to be essential in the G27 *H. pylori* strain. ADP-L,D-Heptose and ADP-D,D-Heptose are incorporated into the highly conserved core structure of *H. pylori* LPS that consists of a hexa-saccharide (Glucose – Galactose -D,D-Heptose [Hep III] - L,D-Heptose [Hep II] - L,D-Heptose [Hep I] – KDO). The variable O-antigen is directly attached to the Hep III molecule (*167*). The LPS molecule is assembled in the bacterial cytosol, transported across the periplasm and flipped across the outer bacterial membrane.

Table 3.1. Primers used to construct *H. pylori* mutants

Strain name	G27 gene number	Selection	Primer name	Primer sequence (5' → 3')
Δ*cagE*	503	CM	Δ*cagE* primer 1	CTTTCTGTCATTGCGCGGAG
			Δ*cagE* primer 2	GTTCAGTGATTTCGCCTTCCA
			Δ*cagE* primer 3	tccacttttcaatctatatccTATGATTAGCTTTTTTTGT
			Δ*cagE* primer 4	ccagtttctcgcactgataaACTGTATTTGTCAAAGAAAT
Δ*hldD*	813	CM	Δ*hldD* primer 1	GCGACATGTTAGCTGGCTTG
			Δ*hldD* primer 2	CGCTCCGCCTAAATTCTTGC
			Δ*hldD* primer 3	tccacttttcaatctatatccGATTAAATTCTTAAAATGC
			Δ*hldD* primer 4	ccagtttctcgcactgataaTAGCATTTTAAAAGAGCATT
Δ*gmhB*	814	CM	Δ*gmhB* primer 1	GGCCTTTCTTTTGGGCTTGG
			Δ*gmhB* primer 2	ATGCCCTAAAGAACTGGGGC
			Δ*gmhB* primer 3	tccacttttcaatctatatccTCGCATGGTTTAGTAATTCA
			Δ*gmhB* primer 4	ccagtttctcgcactgataaCATGTTAGCTGGCTTGAACG
Δ*cagA*	507	CM	Δ*cagA* primer 1	CTAGCCTTTAGACGCCTGCA
			Δ*cagA* primer 2	AGCGCGATCGATTTGCTCTA
			Δ*cagA* primer 3	tccacttttcaatctatatccATCAACTTTAAGAAAAGCCA
			Δ*cagA* primer 4	ccagtttctcgcactgataaCGAGTTGAACAATGCTGTAA
Δ*hldD* comp	813	Mtz	*rdxA*::*hldD* primer 1	agcgttaatggtggtatgctcCAATGCAAAGATCTTAAAG
			rdxA::*hldD* primer 2	CTTTAAGATCTTTGCATTGGAGCATACCACCATTAACGCT
			rdxA::*hldD* primer 3	AAAAATCCTAGTCGTAGGCGCATGGGCGTGAGCTTAATGG
			rdxA::*hldD* primer 4	ccattaagctcacgcccatgcGCCTACGACTAGGATTTTT
Δ*gmhB* comp	814	Mtz	*rdxA*::*gmhB* primer 1	agcgttaatggtggtatgctcGCATGATCATAAAGGAGCG
			rdxA::*gmhB* primer 2	CGCTCCTTTATGATCATGCGAGCATACCACCATTAACGCT
			rdxA::*gmhB* primer 3	GATAAGAATGCGTTATATTGCATGGGCGTGAGCTTAATGG
			rdxA::*gmhB* primer 4	ccattaagctcacgcccatgcAATATAACGCATTCTTATC
Δ*cagA* comp	507	Kan	McGee:*cagA* primer 1	tcgataccgtcgacctcgagcGCAACTCCATAGACCAC
			McGee:*cagA* primer 2	agagtaattctgtgggtaccTTAGCAAGGGGTGGT

*Note: primer sequence homologous to antibiotic resistance cassette or integration locus is represented by lowercase lettering

CM – chloramphenicol

Mtz – metronidazole

Kan – kanamycin

CHAPTER 4: Development of primary gastric epithelial organoid cell culture system to study *H. pylori* interactions with host cells

PREFACE

Christina Leverich, a technician in the Salama lab, contributed to the data presented in this chapter. Members of Dr. Thaddeus Stappenbeck's lab at Washington University in St. Louis, particularly Dr. Christina Hickey, provided invaluable training in organoid culture methods. Mayumi Holly, a graduate student in the Department of Microbiology at University of Washington, provided important reagents, protocols and suggestions that helped establish this culture method in our lab. I am also grateful for the University of Washington Falkow Graduate Student Award, which provided the funding that allowed me to visit the Stappenbeck lab and learn how to culture gastrointestinal organoids.

INTRODUCTION

Data presented in chapter 3 showed that the sequential activation of host TIFA and NOD1 by *H. pylori* drives the initial inflammatory response in a human gastric adenocarcinoma cell line (*144*). Cancer cell lines do not fully recapitulate the complexity of human gastric epithelial cells. How much TIFA and NOD1 signaling contribute to the inflammatory response in natural infection remains an open question.

The stomach epithelium is composed of diverse cell types that differ in topology and number depending on the anatomical site where they reside (Fig. 4.1). For example, the stomach corpus contains surface mucus producing pit cells, which overlay the gastric glands. The stomach corpus, the largest part of the stomach, contains parietal cells that secrete stomach acid and chief cells that secrete various enzymes that aid in food digestion. The stomach antrum

contains shorter glands and lacks parietal and chief cells. Both stomach corpus and antrum contain Leucin-rich repeat containing G-protein coupled receptor 5 (LGR5+) stem cells that are self-renewing progenitor cells for all of the diverse cell types found in the gastric epithelium (*193*). *H. pylori* typically infects the stomach antrum where it can trigger development of duodenal ulcers, however, this pattern of infection is associated with a lower risk of cancer progression. Individuals who are predominantly infected in the stomach corpus or have inflammation throughout the stomach are at a greater risk of developing gastric cancer (*12*). Although it is well established that *H. pylori* induces inflammation in gastric epithelial cells, the anatomical site from which those cells are derived is consequential for subsequent disease progression. Therefore, enhanced tools are needed in order to study *H. pylori* – gastric epithelial cell interactions in a physiologically more relevant context.

Over the last several years, significant advances have been made in the ability to isolate and propagate gastrointestinal stem cells and differentiate them into primary-like epithelial cells. There are two main strategies for establishing gastrointestinal organoid cultures. One involves isolating LGR5+ cells from adult mucosal tissue (*194*, *195*), while the other is based on differentiating an induced pluripotent stem cell (*196*). Embedding LGR5+ cells in matrigel, a substance that mimics extracellular matrix in the gastrointestinal tract, and culturing the cells with media containing stem cell growth factors Wnt3a, R-spondin and Noggin (WRN) allows for expansion and passaging of stem cells. Withdrawing WRN factors from the media leads to differentiation of the cells into the tissue types from which the cells were derived. Matrigel-embedded LGR5+ cells from the gastrointestinal tract form three-dimensional mini organs that are termed organoids (*197*). The Stappenbeck lab developed an immortalized cell line that secretes mouse Wnt-3A, R-spondin and Noggin, which can be used as the base conditioned

media that maintains organoids in their undifferentiated state (*195*). Using a single protocol they were also able to establish organoid cell lines from a variety of sites along the gastrointestinal tract derived from human biopsy samples and show that the cell lines underwent region-specific differentiation (*198*).

This chapter focuses on determining the *in vivo* relevance of Nod1 signaling using a mouse model of infection, as well as establishing the organoid culture method developed by the Stappenbeck group in our lab. Using gastric organoids from genetically modified mice (*i.e.* *Nod1*$^{-/-}$ and *Tifa*$^{-/-}$) will enable us to investigate *H. pylori* – gastric epithelial cell interactions in an experimentally more tractable and at the same time physiologically more relevant tissue culture system.

RESULTS

Nod1-deficient mice are more susceptible to *H. pylori* infection

We previously showed that NOD1 contributes modestly to *H. pylori* detection in an *in vitro* co-culture model (*144*). We, therefore, wanted to determine whether Nod1 plays a role in controlling *H. pylori in vivo* using a mouse model of infection. Consistent with published reports (*57*, *199*), we observed that *Nod1*-deficient mice are more susceptible to our mouse adapted *H. pylori* strain, NSH57, which is derived from clinical isolate G27 and contains the *cag*-T4SS (*200*). We observed an increased bacterial burden (median CFU 6.5 x 10^4) in *Nod1*$^{-/-}$ mice after 1 week of infection when compared to wild-type mice (median CFU 1.8 x 10^3). Furthermore, 9 out of 10 *Nod1*$^{-/-}$ mice were infected to above the level of detection in our CFU enumeration assay, as compared to 4 out of 10 wild-type mice suggesting that Nod1 is important for restricting *H. pylori* infection *in vivo* (Fig. 4.2A).

NF-κB-dependent genes *Il6* and *Il17a* are induced in *H. pylori* infection

To determine if differences in the NF-κB driven immune response may explain the heightened susceptibility of *Nod1*$^{-/-}$ mice to *H. pylori* infection, we analyzed NF-κB-dependent gene expression profiles in stomach tissue of *Nod1*$^{-/-}$ versus wild-type *H. pylori* infected and uninfected mice. Expression of *Ccl5*, *Mip2*, *Kc* and *Tnfa* did not differ in *Nod1*$^{-/-}$ versus wild-type mice 1-week post infection. *Il6* and *Il17a* expression was 4.7 and 3-fold higher, respectively, in wild-type infected mice, as compared to uninfected controls. However, baseline expression of *Il6* and *Il17a* was higher in uninfected *Nod1*$^{-/-}$ mice than their wild-type counterparts. We did not find a clear difference in *Il6* and *Il17a* gene expression levels in *Nod1*$^{-/-}$ versus wild-type infected mice (Fig. 4.2B).

Beta defensin genes are not differentially expressed in wild type versus *Nod1*$^{-/-}$ mice following *H. pylori* infection

Intact Nod1 signaling may lead to restricted bacterial growth through induction of beta defensins, antimicrobial peptides secreted by gastrointestinal epithelial cells. To test this hypothesis, we analyzed expression of four beta defensin genes in wild type and *Nod1*$^{-/-}$ mice infected with *H. pylori*. Mouse β-defensin 1 is constitutively expressed and is a functional homolog of human β-defensin 1 (*201*). Mouse β-defensin 2 is induced in response to inflammation at mucosal surfaces (*202*). Mouse β-defensin 3 is a homolog to human β-defensin 2, is expressed by lung and intestinal epithelial cells and is inducible by bacterial infection (*203*). Mouse β-defensin 4 is an ortholog to human β-defensin 2 and has been shown to act as a chemoattractant for dendritic cells, macrophages and neutrophils (*204*). We did not see any difference in gene expression levels of mouse β-defensin 1 – 4 in wild type versus *Nod1*$^{-/-}$ mice

infected with *H. pylori*. Furthermore, after 1 week of infection we did not observe induction of any of the β-defensin genes by *H. pylori* infection (Fig. 4.2C).

Previous studies in our lab determined that wild-type *H. pylori* strain PMSS1 preferentially colonizes the stomach antrum after 1 week of infection (*205*). Looking at whole stomach tissue in order to detect gene expression differences caused by *H. pylori* infection is limited to detecting large fold changes across the entire stomach. It is likely that gene expression differences occurring mainly in the antrum would be diluted when looking at the whole stomach. Furthermore, it is possible that major gene expression differences occur specifically in gastric epithelial cells early after infection and are not sustained throughout the 1 week time course. These limitations provide the rationale for pursuing better methods for modeling *H. pylori* – gastric epithelial cell interactions in tissue culture.

Differentiated mouse and human gastric organoids express markers of mature primary gastric epithelial cells

In order to more thoroughly assess the contribution of Nod1 signaling in the gastric epithelium on the *H. pylori*-mediated immune response, we sought to establish and validate gastric organoids as an alternative tissue culture system to study *H. pylori* – gastric epithelial cell interactions. We isolated and propagated mouse stomach organoids using a protocol developed by the Stappenbeck lab (*195*). We performed qPCR analysis to determine whether gastric organoids (GOs) show differential gene expression patterns depending on whether the cells are in the differentiated or undifferentiated state. We found that mouse differentiated organoids show nearly 3 log higher expression of *Muc5ac*, a marker of surface mucus secreting epithelial cells, than undifferentiated cells. Others have reported that differentiated gastric organoids show

reduced expression of *MUC6*, a marker of mucus-producing gastric neck cells and pepsinogen (*PGC*), a marker of chief cells, relative to undifferentiated gastric organoids (*206*). Consistent with published reports, we observed reduced expression of *Muc6* and *Pgc* in differentiated cells. Conversely, undifferentiated cells expressed 2-3 log higher levels of stem cell markers *Lgr5* and *Troy* than differentiated cells. Both differentiated and undifferentiated cells did not express *Cdx2*, a marker of intestinal epithelial cells, suggesting maintenance of tissue specificity (Fig. 4.3A). Furthermore, histological comparison of differentiated versus undifferentiated GOs showed a thickening of the epithelial cell layer and large basal nuclei in differentiated organoids consistent with their maturation into primary gastric epithelial cells (Fig. 4.3B). Similar to mouse GOs, human gastric organoids (hGOs), expressed higher levels of *MUC5AC* in the differentiated state and low levels of *LGR5*, *TROY, MUC6 and PGC* when compared to undifferentiated cells (Fig. 4.4).

Gastric organoids grow in a polarized monolayer on permeable membranes

Previous studies have used a microinjection technique to deliver *H. pylori* into the lumen of 3D gastric organoids then analyzed gene and protein expression differences to model changes induced by *H. pylori* infection (*207*, *208*). This approach is technically challenging and the large number of cells required limits options for downstream analysis. We sought to develop a more tractable gastric organoid co-culture system. When we seed undifferentiated mGOs onto permeable transwell inserts they form an epithelial cell monolayer. Withdrawing WRN factors from the culture media causes the cells to stop proliferating and differentiate into primary-like epithelial cells that maintain transepithelial resistance measurements of ≥900 Ωm^2 (Fig. 4.5). We can then co-culture these differentiated cell monolayers with *H. pylori* on the apical side and

measure cytokine secretion into the basal compartment, as well as analyze expression of specific genes and proteins of interest in gastric epithelial cells.

DISCUSSION

Here we show that *Nod1* deficient mice are colonized to a greater extent than wild-type mice with a mouse adapted strain of *H. pylori*. It is not fully clear how intact Nod1 signaling restricts *H. pylori* colonization. The well-accepted explanation in the field is that *H. pylori* mediated Nod1 activation in gastric epithelial cells leads to NF-κB activation and production of chemokines such as IL-8 (or the functional mouse homologs Mip-2 and Kc), which recruit neutrophils to the site of infection, where they, presumably, dispose of the bacteria. Neutrophils have been shown to clear *Helicobacter* infection in mice in the absence of IL-10 production (*60*). After 1 week of infection, we did not observe significant differences in *Mip2* and *Kc* expression in stomach tissue of *Nod1*$^{-/-}$ versus wild-type mice. We also did not find any differences in beta defensin expression in wild type or *Nod1*$^{-/-}$ mice following *H. pylori* infection. This could be because the gene expression differences are not sustained over that period of time or they are localized to specific niches within the stomach (*i.e.* stomach antrum) and looking at whole stomach tissue does not allow for those differences to be detected.

We also found that the basal expression levels of *Il6* and *Il17a* were higher in *Nod1*$^{-/-}$ mice compared to wild-type. Additional experiments with increased number of animals are needed to determine the reproducibility of this finding. However, it is plausible that in the absence of Nod1 signaling induced by commensal microbiota, basal levels of pro-inflammatory cytokines would be affected. Commensal microbiota have been suggested to establish and maintain a proper balance of pro-inflammatory Th17 cells and anti-inflammatory regulatory T cells in the gut. Disturbance of this balance in germ-free animals or induced with antibiotic

treatment has been shown to exacerbate inflammatory diseases such as inflammatory bowel disease (*209*). Nod1 stimulation by commensal microbiota has also been suggested to regulate myeloid cell persistence through IL-17A-dependent mechanisms (*210*).

Despite inconclusive results from our gene expression studies, our *in vivo* infection data suggests that Nod1 signaling contributes to controlling *H. pylori* infection in the mouse model system. Future studies will focus on determining whether Nod1 signaling in gastric epithelial cells or the myeloid compartment plays a predominant role in mediating the protective effect against *H. pylori* infection. Furthermore, given our previous data demonstrating the dominant role of TIFA signaling in gastric epithelial cells in response to *H. pylori* infection (*144*), we will determine if *Tifa*$^{-/-}$ mice are more susceptible to *H. pylori*.

Commonly used tissue culture systems for the study of *H. pylori* pathogenesis have many limitations. Most of these systems rely on using tumor derived immortalized epithelial cells lines that are not comprised of the diverse cell types found in the gastric epithelium (Fig. 4.1). Immortalized cell lines often have some non-functional PRRs limiting their utility in studying immune responses to pathogens. Few of the gastric epithelial cell lines used are capable of growing in a polarized monolayer that more accurately represents *H. pylori* and gastric epithelial cell surface interactions that occur *in vivo*. Mouse and human stomach tissue derived organoids represent a novel *ex vivo* tissue culture system that overcomes some of the limitations of using conventional cell lines. Furthermore, culturing gastric organoids on permeable transwell inserts enables us to easily infect cells with *H. pylori*, overcoming technical challenges of microinjecting 3D matrigel-embedded organoid cultures (*208*).

In this chapter, we present data showing the successful isolation, propagation and differentiation of mouse and human gastric organoids into primary-like gastric epithelial cells

based on phenotypic changes, gene and protein expression profiles. We also show that gastric organoids form polarized monolayers on transwell inserts, which are amenable to *H. pylori* infection. Future studies will focus on characterizing immune responses in human gastric organoids, including evaluation of *cag*-T4SS dependent and independent immune responses, donor-to-donor immune response variation, as well as genetic manipulation using CRISPR/Cas9. We will also compare immune responses in gastric organoids derived from *Nod1* and *Tifa* deficient mice to determine the functional relevance of these pathogen recognition pathways to *H. pylori* infection.

EXPERIMENTAL PROCEDURES

Mouse infections

Mice were housed in an Association for the Assessment and Accreditation of Laboratory Animal Care-accredited facility and all procedures were approved by Fred Hutch Institutional Animal Care and Use Committee. *Nod1*$^{-/-}$ mice were a generous gift form Takeda Pharmaceuticals, LLC. Mice were inoculated with 5 x 10^7 *H. pylori* CFU in 100 ul of Brucella Broth plus 10% FBS by oral gavage, as previously described (*211*). Stomachs were harvested after 1 week of infection and divided into 3 sections for 1) CFU enumeration 2) preserved in RNA later for qPCR analysis 3) Paraffin embedded for histology. For CFU counts, stomachs homogenates were plated on horse blood agar plates and colonies counted then normalized to weight of stomach tissue.

Culturing gastric organoids from mouse stomach tissue

Mouse gastric organoids were isolated from wild-type C57BL/6J mice (Jackson), cultured and maintained according to published protocols (*195*). Briefly, mouse stomachs were

resected and two 0.5-1 cm^2 pieces were cut from the stomach corpus and antrum. Tissue was dissociated in collagenase solution (2 mg/mL collagenase type 1 [Invitrogen], 50 ug/mL gentamicin [Sigma] in primary culture media [Advanced DMEM/F12 + 10% FBS]), embedded in 20 μl of matrigel (Corning) and plated in 24-well plates. Each well was supplemented with 50% conditioned media containing mouse Wnt-3A, R-sponding and Noggin growth factors (media was obtained as supernatant collected from L-WRN cells, which were a generous gift from the Stappenbeck lab) and 10 μM ROCK (Y-27632) inhibitor (BD Biosciences). Media was changed every 2 days and cells passaged on the third day at a 1:2 – 1:5 dilution, depending on cell density.

Culturing gastric organoids from human stomach tissue

Human gastric organoids were isolated from human discarded stomach antrum or corpus tissue obtained through NWBioTrust. Organoids were isolated, cultured and maintained as described above for mouse organoids. The conditioned medium was additionally supplemented with 10 μM TGFβ receptor inhibitor (SB-431542).

Quantitative PCR

RNA was isolated from mouse stomach tissue preserved in RNAlater. Stomachs were homogenized in lysis buffer and RNA isolated using an RNeasy RNA isolation kit (Qiagen). Complementary DNA was generated using High Capacity RNA to cDNA Kit (Applied Biosystems). Gene expression was quantified using PowerUp SYBR Green MasterMix (Applied Biosystems) and primers listed in Table 4.1 (mouse) and Table 4.2 (human). Gene expression was normalized to *Hprt* (mouse) or *ACTB* (human) housekeeping genes.

Transwell gastric organoid monolayer co-culture with *H. pylori*

Gastric organoids were grown as polarized monolayers on transwell permeable inserts as previously described (*212*). Briefly, 3-day old cultures were dissociated and 200,000 – 400,000 cells seeded Transwell inserts (Corning – 3470) in 24-well plates. Prior to seeding, transwell inserts were coated with 100 μl of a 1:40 dilution of matrigel in sterile PBS. Fifty-percent conditioned media with 10 μM ROCK inhibitor was added to the bottom and top of the transwell insert. The following day, conditioned media was replaced with primary cell culture media (Advanced DMEM/F12 + 10% FBS) to induce primary cell differentiation and media changed daily, thereafter. Transepithelial resistance was measured one day after seeding organoids on transwell insert using an EVOM2 voltmeter (World Precision Instruments). For immunostaining, transwells were washed with PBS, fixed in 4% paraformaldehyde in PBS for 20 min at room temperature then permeabilized with 70% ethanol (three washes, 5 minutes each). Nuclei were stained with DAPI (1 μg/mL). Transwell membranes were then cut out from the insert and mounted on a clean microscope slide with Prolong Diamond Anti-Fade (Molecular Probes).

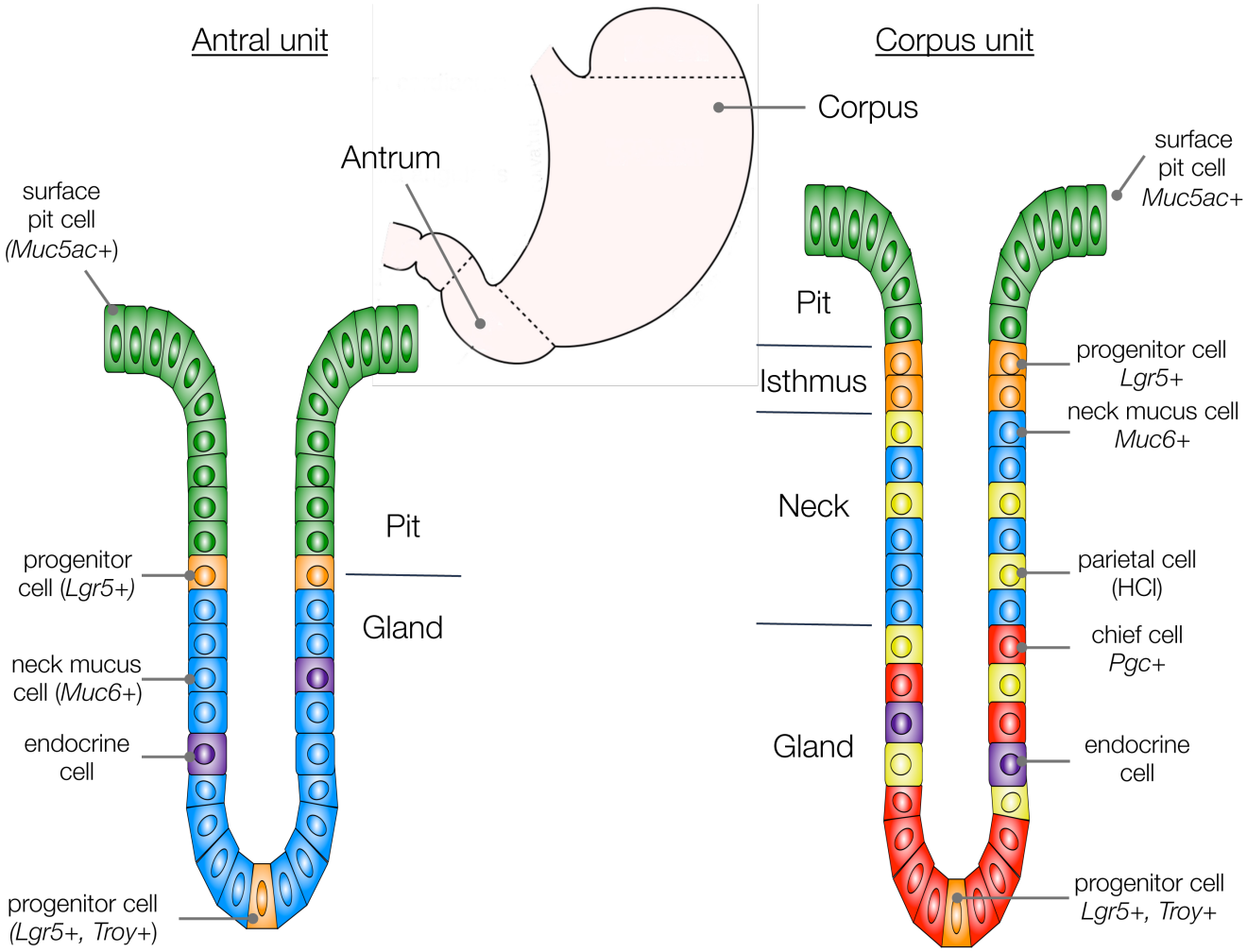

Figure 4.1. Schematic representation of cell types present in the gastric epithelium
Shown is the arrangement of cell types present in the human gastric antral and corpus units, highlighting the specific genes expressed by each cell type. Figure adapted from (*193*).

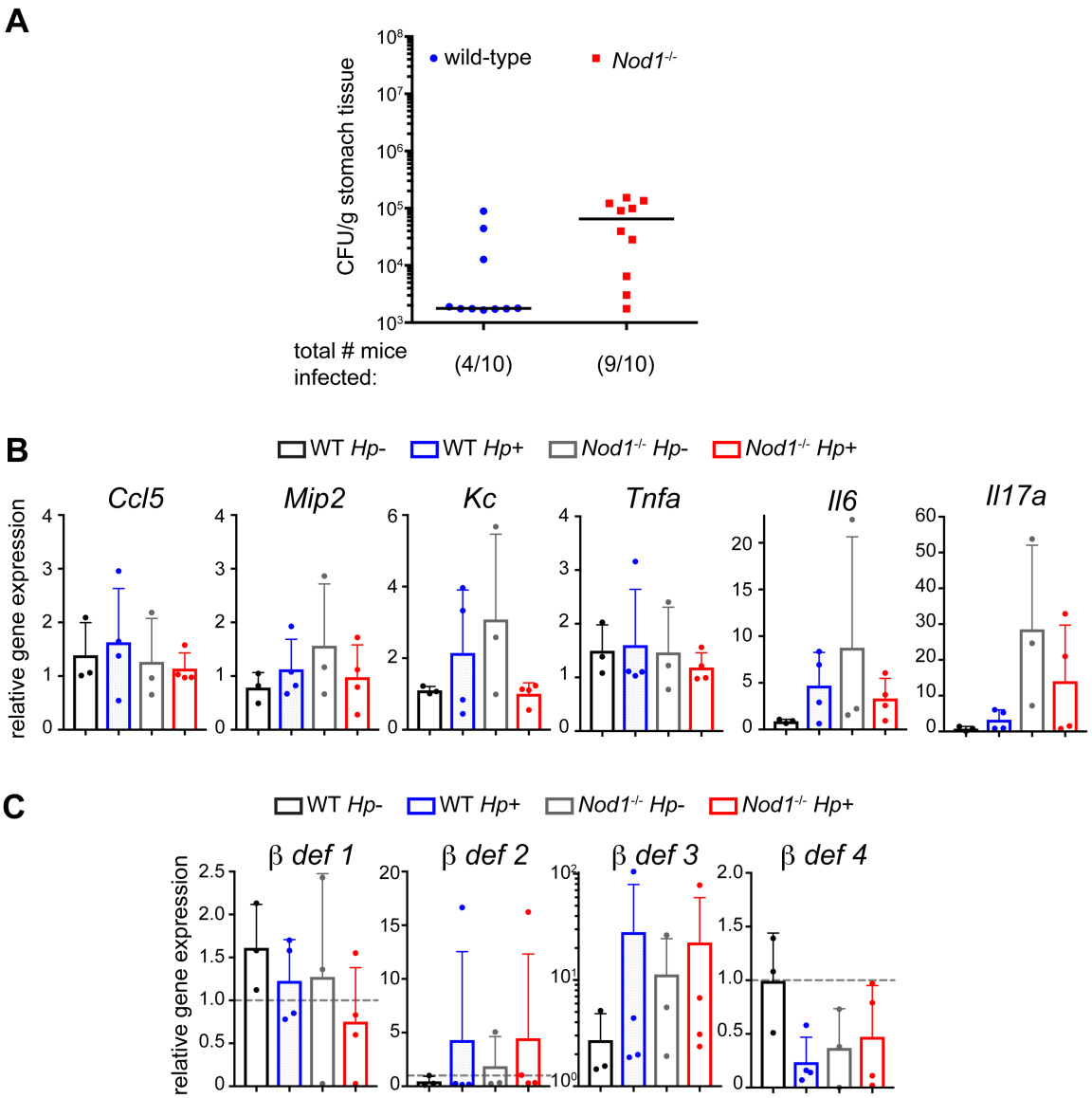

Figure 4.2. *Nod1*$^{-/-}$ mice are more susceptible to *H. pylori* infection
(A) WT or *Nod1-/-* mice were infected with 5 x 10^7 *H. pylori* colony forming units (CFU) via oral gavage and stomach tissue harvested after 1 week of infection. NSH57, a mouse adapted derivative of clinical isolate G27, strain was tested. Data is displayed as CFU per gram stomach tissue with the median indicated by the horizontal lines. (B) Stomach tissue gene expression of NF-κB dependent genes normalized to *Hprt* in WT or *Nod1-/-* mice, uninfected or infected with *H. pylori* strain NSH57 for 1 week. (C) Stomach tissue gene expression of beta defensins normalized to *Hprt* in WT or *Nod1-/-* mice, uninfected or infected with *H. pylori* strain NSH57 for 1 week.

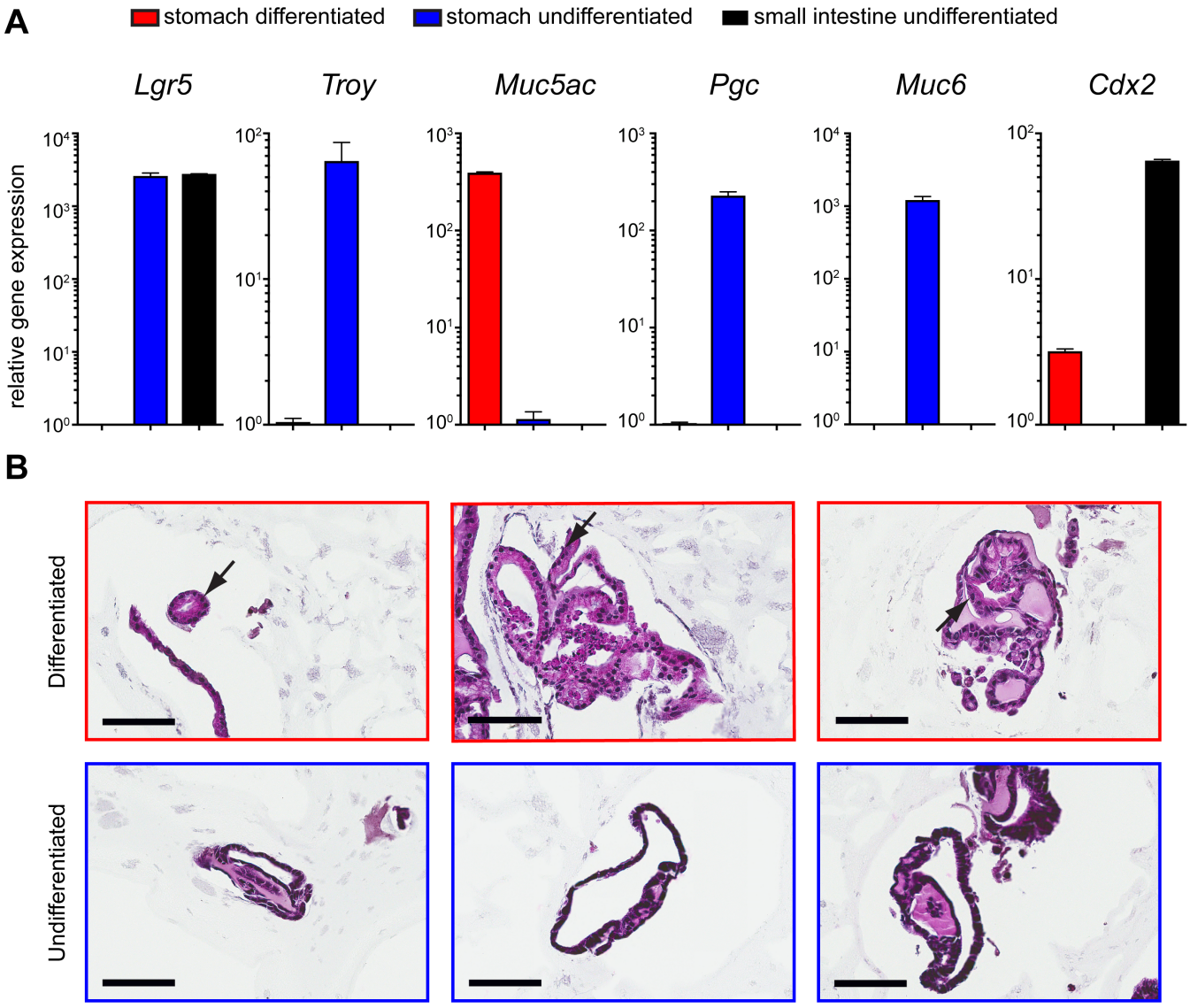

Figure 4.3. Differentiated mouse gastric organoids (mGOs) resemble primary-like gastric epithelial cells

(A) Indicated gene expression (normalized to *Hprt*) in differentiated vs. undifferentiated mGOs. Differentiated mGOs were cultured in the absence of WRN growth factors for three days. (B) Representative H&E stained differentiated vs. undifferentiated mouse GOs. Arrow indicates basally located nucleus in differentiated GOs. Scale bar = 80 μm.

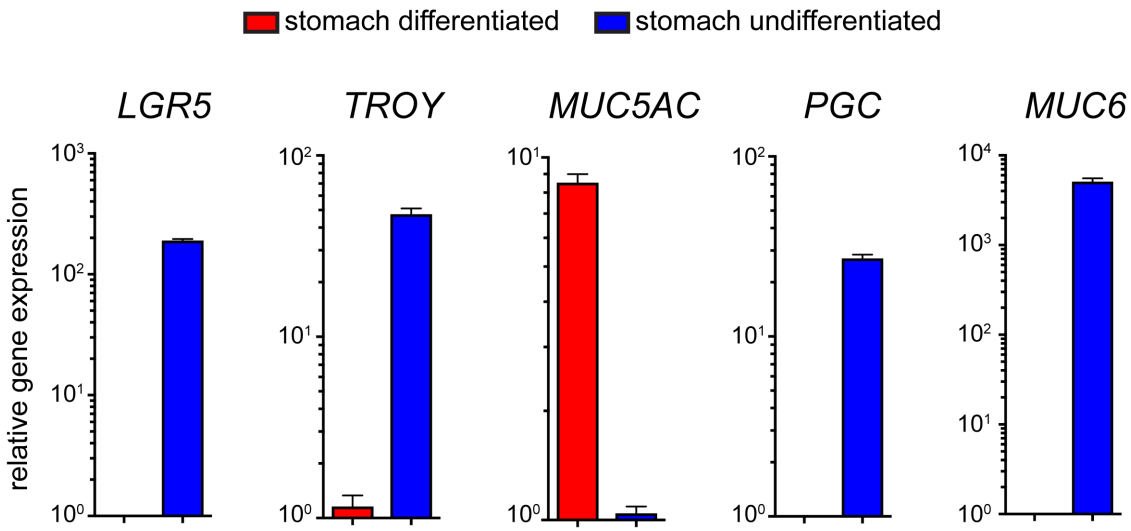

Figure 4.4. Gene expression in differentiated human gastric organoids (hGOs) consistent with surface pit cell phenotype

Indicated gene expression (normalized to *ACTB*) in differentiated vs. undifferentiated hGOs. Differentiated hGOs were cultured in the absence of WRN growth factors for three days. Organoids were derived from a stomach antrum sample provided by a 73-year old female donor (NS024)

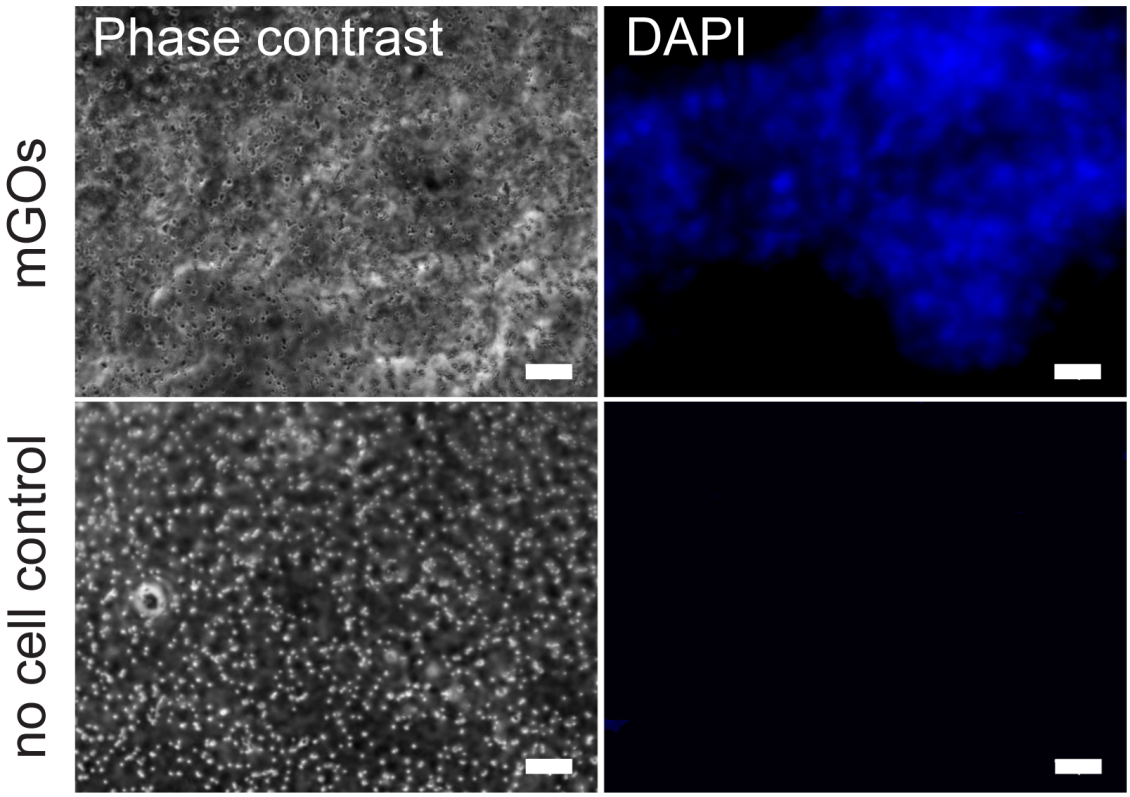

Figure 4.5. Gastric organoids form monolayer on transwell membrane inserts
WT mGOs form a monolayer when grown and differentiated on transwell inserts. Scale bar = 20 μm

Table 4.1. Mouse primers used for RT-qPCR

Species	Gene	Primer name	Primer sequence (5' → 3')
mouse	*Lgr5*	ms_Lgr5_fwd	TCCAACCTCAGCGTCTTC
		ms_Lrg5_rev	TGGGAATGTGTGTCAAAG
mouse	*Troy*	ms_Troy_fwd	TTCTGTGGGGGACACGATG
		ms_Troy_rev	AGAAAATTCAGCGCAGATGGAA
mouse	*Muc5ac*	ms_Muc5ac_fwd	CCATGAAGTGGGAGTGTGTG
		ms_Muc5ac_rev	TTGGGATAGCATCCTTCCAG
mouse	*Pgc*	ms_Pgc_fwd	CCAACCTGTGGGTGTCTTCT
		ms_Pgc_rev	TTAGGGACCTGGATGCTTTG
mouse	*Muc6*	ms_Muc6_fwd	TGCATGCTCAATGGTATGGT
		ms_Muc6_rev	TGTGGGCTCTGGAGAAGAGT
mouse	*Muc2*	ms_Muc2_fwd	GAACGGGGCCATGGTCAGCA
		ms_Muc2_rev	CATAATTGGTCTTGCATGCC
mouse	*Cdx2*	ms_Cdx2_fwd	CTTGCTGCAGACGCTCAAC
		ms_Cdx2_rev	TCTGTGTACACCACCCGGTA
mouse	*Hprt*	ms_Hprt_fwd	AAGTTTGTTGTTGGATATGC
		ms_Hprt_rev	CATCTTAGGCTTTGTATTTGG
mouse	*Ccl5*	ms_ccl5_qPCR_fwd	ATCTCCCACAGCCTCTGCC
		ms_ccl5_qPCR_rev	CAGCGCGAGGGAGAGGTA
mouse	*Mip2*	ms_mip2_qPCR_fwd	CCAAGGGTTGACTTCAAGAAC
		ms_mip2_qPCR_rev	AGCGAGGCACATCAGGTACG
mouse	*Kc*	ms_kc_qPCR_fwd	CAATGAGCTGCGCTGTCAGTG
		ms_kc_qPCR_rev	CTTGGGGACACCTTTTAGCATC
mouse	*Tnfa*	ms_tnf_qPCR_fwd	TCTGTCTACTGAACTTCGGGGTG
		ms_tnf_qPCR_rev	ACTTGGTGGTTTGCTACGACG
mouse	*Il6*	ms_il6_qPCR_fwd	CCGGAGAGGAGACTTCACAG
		ms_il6_qPCR_rev	GGAAATTGGGGTAGGAAGGA
mouse	*Il17a*	ms_il17a_qPCR_fwd	TCCAGAAGGCCCTCAGACTA
		ms_il17a_qPCR_rev	ACACCCACCAGCATCTTCTC
mouse	*Defb1*	ms_beta_defensin1_fwd	CCAGATGGAGCCAGGTGTTG
		ms_beta_defensin1_rev	AGCTGGAGCGGAGACAGAATCC
mouse	*Defb2*	ms_beta_defensin2_fwd	AAGTATTGGATACGAAGCAG
		ms_beta_defensin2_rev	TGGCAGAAGGAGGACAAATG
mouse	*Defb3*	ms_beta_defensin3_fwd	GCATTGGCAACACTCGTCAGA
		ms_beta_defensin3_rev	CGGGATCTTGGTCTTCTCTA
mouse	*Defb4*	ms_beta_defensin4_fwd	GCAGCCTTTACCCAAATTATC
		ms_beta_defensin4_rev	ACAATTGCCAATCTGTCGAA

Table 4.2. Human primers used for RT-qPCR

Species	Gene	Primer name	Primer sequence (5' → 3')
human	*LGR5*	hu_LGR5_fwd	AGTTTATCCTTCTGGTGGTAGTCC
		hu_LGR5_rev	CAAGATGTAGAGAAGGGGATTGA
human	*TROY*	hu_TROY_fwd	CTGCTCATCCTCTGTGTCATCTATTG
		hu_TROY_rev	CCGTTGTACTGAATGTCCTGTG
human	*MUC5AC*	hu_MUC5AC_fwd	CCAAGGAGAACCTCCCATAT
		hu_MUC5AC_rev	CCAAGCGTCATTCCTGAG
human	*PGC*	hu_PGC_fwd	TTCCCTCTGCCACCTTCCT
		hu_PGC_rev	CGACTCCCACGGTGCAGTA
human	*MUC6*	hu_MUC6_fwd	CAGCAGGAGGAGATCACGTTCAAG
		hu_MUC6_rev	GTGGGTGTTTTCCTGTCTGTCATC
human	*MUC2*	hu_MUC2_fwd	TGTAGGCATCGCTCTTCTCA
		hu_MUC2_rev	GACACCATCTACCTCACCCG
human	*CDX2*	hu_CDX2_fwd	CTGGAGCTGGAGAAGGAGTTTC
		hu_CDX2_rev	ATTTTAACCTGCCTCTCAGAGAGC
human	*ACTB*	β-actin fwd	AGCGAGCATCCCCCAAAGTT
		β-actin rev	AGGGCACGAAGGCTCATCATT

CHAPTER 5: Detection and response of myeloid-derived cells to *H. pylori* infection

PREFACE

Ami Yamamoto, a graduate student in the Molecular and Cellular Biology Program at University of Washington, contributed to the data presented in this chapter. I am also grateful to Dr. Julia Kargl and Dr. McGarry Houghton for providing the *MPO*$^{-/-}$ and NE$^{-/-}$ mice, as well as helpful suggestions. A special thank you to members of Dr. Daniel Stetson's lab at University of Washington, particularly Dr. Elizabeth Gray and Dr. Hannah Volkman for providing THP1 cells, other valuable reagents and helpful suggestions for assessing the type I IFN response in THP1 cells.

INTRODUCTION

During *H. pylori* infection, the majority of bacteria remain in the mucus layer overlying the gastric epithelium. A small proportion of bacteria will attach to gastric epithelial cells and will induce a proinflammatory response via mechanisms described in Chapter 3 and 4. Inflammatory signals from gastric epithelial cells recruit macrophages and neutrophils to the site of infection. Additionally, *H. pylori* utilizes a secreted serine protease, HtrA, which cleaves apical-junctional complexes between adjoining epithelial cells to gain access to the basolateral compartment. Once there, *H. pylori* can interact with α5β1 integrins, which are required for *cag*-T4SS assembly and CagA translocation (*11*). However, this localization also makes the bacteria vulnerable to detection by myeloid-derived cells, such as macrophages and neutrophils.

Infection with *H. pylori* is characterized by rapid infiltration of the gastric mucosa with macrophages and neutrophils and bacterial eradication through antibiotic treatment coincides

with neutrophil disappearance. It has been shown that persistence of even a small amount of neutrophils in the gastric mucosa after antibiotic treatment indicates therapeutic failure and persistence of *H. pylori* infection (*213*). How effective are neutrophils at clearing infection and by which mechanisms does clearance occur remain open questions. The two main mechanisms by which neutrophils restrict bacterial growth are through the production of myeloperoxidase (MPO) and neutrophil elastase (NE). MPO is an enzyme that converts hydrogen peroxide into hypchlorous acid, which readily kills bacteria. It is stored in granules within neutrophils and released into the extracellular space during degranulation. NE is a serine protease secreted by activated neutrophils and macrophages that destroys bacterial (and host) proteins. MPO and NE are also localized to neutrophil extracellular traps, which are formed via extrusion of neutrophil nuclear components (DNA & histones) that trap and degrade pathogens (*214*). Evidence that *Helicobacter* is susceptible to neutrophil-mediated clearance comes from studies using *Il10*$^{-/-}$ mice infected with *H. felis*, which demonstrated that in the *Il10*$^{-/-}$ background, infection led to more severe gastritis and rapid bacterial clearance by day 8 post-infection. Depleting neutrophils from these mice prevented bacterial clearance (*60*).

Myeloid-derived cells engage a number of pathogen recognition receptors in response to *H. pylori* and the downstream immune response can be pro or anti-inflammatory depending on the cellular context. *H. pylori* urease, heat shock protein 60 and neutrophil activating protein are detected by TLR2 on monocytes and induce pro-inflammatory cytokine production (*63-65*). TLR9 expression is induced in *H. pylori* infected gastric mucosa and is mainly localized to infiltrating macrophages, dendritic cells and T cells. *H. pylori* DNA detection by TLR9 leads to an overall anti-inflammatory response in a mouse model of infection (*215*). *H. pylori* RNA is detected by TLR8, with possible contribution from TLR7, in dendritic cells and leads to the

production of pro-inflammatory cytokines (*71*). Macrophages and dendritic cells also express DC-SIGN a C-type lectin receptor, which recognizes mannosylated or fucosylated pathogen-derived ligands. *H. pylori* Lewis Y antigen recognition by DC-SIGN leads to production of IL-10 and dampening of the NF-κB-driven proinflammatory immune response (*81*).

Although the majority of published studies have focused on the NF-κB-mediated inflammatory response, it is known that *H. pylori* can also induce a type I interferon (IFN) response. Type I IFN responses are typically induced in response to viral pathogens and are important in mediating viral clearance. Intracellular bacteria have also been shown to induce type I IFN responses mainly through recognition of bacterially derived nucleic acids. Type I IFN responses to bacteria can be protective or harmful for the host, depending on the bacterial pathogen, specific virulence factors and the site of infection (*216*). Evidence suggests that *H. pylori* can initiate a type I IFN response through activation of endosomal TLRs, cytosolic receptor RIG-I and NOD1 activation (*71*, *199*). Furthermore, infection of IFN α and β receptor deficient mice with a CagA+ strain of *H. pylori* results in enhanced bacterial colonization suggesting that type I IFN signaling is protective in the context of *H. pylori* infection (*199*). What is the *H. pylori* ligand that induces the type I IFN response in host cells, is delivery of the ligand *cag*-T4SS dependent and is induction of the type I IFN response advantageous for the bacteria, remain open questions.

Some pathogen recognition receptors that are triggered by *H. pylori* in gastric epithelial cells versus myeloid derived cells are the same, while others differ depending on the cell type. The downstream consequences of recognition can be pro or anti-inflammatory. It is not clear to what extent the epithelial versus myeloid compartments contribute to the overall immune response, such that an overall tolerogenic environment is established that favors bacterial

persistence. This chapter focuses on the contribution of myeloid-derived cells to *H. pylori* detection and the subsequent innate immune response elicited.

RESULTS

Myeloperoxidase and neutrophil elastase are not required for restricting bacterial colonization *in vivo*

Since neutrophils are rapidly recruited to *H. pylori* infected stomach mucosa and are thought to mediate bacterial clearance, we wanted to assess whether MPO and/or NE, the main bactericidal neutrophil effectors, are protective during *H. pylori* infection. We infected wild-type, MPO or NE-deficient mice with a mouse adapted *H. pylori* strain MSD132 (*217*), which lacks a functional *cag*-T4SS or a clinical isolate of *H. pylori* PMSS1, which naturally infects mice to high levels and maintains a functional *cag*-T4SS (*218*). Surprisingly, we did not observe a difference in bacterial load after 1-week infection with either *H. pylori* strain or mouse genotype when compared to wild type (Figure 5.1). This suggests that in the mouse model of infection, MPO and NE are dispensable for restricting bacterial growth, at least at the early stages of infection.

Human monocytes activate pathogen recognition pathways in response to *H. pylori* that are distinct from gastric epithelial cells

In AGS cells, a gastric epithelial cell line commonly used to study *H. pylori* interactions with the human host, almost the entire IL-8 response, which is used as a proxy for NF-κB-mediated inflammation, is dependent on the *cag*-T4SS. THP1 cells, a human monocytic cell line, co-cultured with *cag*-T4SS deficient (*ΔcagE*) *H. pylori* induce less IL-8 at 6 hours post-infection. However, after 24 hours, IL-8 production by THP1 cells is nearly the same in *ΔcagE* versus wild

type infected cells, suggesting that *cag*-T4SS dependent detection of *H. pylori* occurs at early time points (Fig. 5.2A). The IL-8 response in THP1 cells is also dose dependent, as increasing MOI yields increased IL-8 induction after 24 hours of infection. At higher MOIs of 25 and 50, the assay saturation limit is reached (Fig. 5.2B), therefore using lower MOIs of 10 or below are necessary when studying THP1 immune response to *H. pylori*. Pre-treating THP1 cells with phorbol 12-myristate 13-acetate (PMA), induces cell differentiation from monocytes into macrophage-like cells. However, PMA-stimulation also triggers an NF-κB-dependent immune response since THP1 cells produce IL-8 in the absence of bacterial stimulation (Fig. 5.2A). Hence, for further studies we used undifferentiated THP1s for co-culture with *H. pylori* in order to avoid confounding by the PMA-driven immune response.

H. pylori initiates a type I interferon response in human monocytes

Since *H. pylori* has been reported to induce a type I IFN response in dendritic cells (*71*) and IFNα/β receptor deficient mice are more susceptible to *H. pylori* infection (*199*), we wanted to determine if THP1 cells induce a type I IFN in response to *H. pylori*. As a positive control for induction of IFN-stimulated genes (ISGs), we stimulated THP1 cells with 3',3'- cyclic guanosine monophosphate–adenosine monophosphate (cGAMP), a bacterially derived cyclic dinucleotide that binds stimulator of interferon genes (STING) and induces TBK1-IRF3-dependent type I IFN production (*219*). THP1 cells infected with *H. pylori* induced higher expression of *IFNB*, *IFIT1* and *ISG15*, known ISGs, relative to uninfected control THP1 cells. Levels of gene expression modestly increased with increased *H. pylori* MOI, but did not reach the high levels of cGAMP stimulation (Fig. 5.3). These data suggest that a bacterial ligand from *H. pylori* is capable of inducing a type I IFN response in host monocytes.

H. pylori type I interferon response is partially dependent on *cag*-T4SS

Having shown that *H. pylori* can induce a type I IFN response in THP1 cells, we next wanted to determine if that response is dependent on the *cag*-T4SS. We found that *ΔcagE* mutants, which lack a functional *cag*-T4SS, induced *IFNB* in THP1 cells, although the response was weaker than the response induced by wild-type bacteria (Fig. 5.4). Interestingly, *ΔcagE* mutants did not induce expression of *IFIT1* or *ISG15*. This experiment needs to be repeated in order to establish the reproducibility of this finding. However, this preliminary data suggests that, analogous to the IL-8 response in THP1 cells (Fig. 5.2 A), *H. pylori* may induce a type I IFN response in a *cag*-T4SS dependent and independent manner.

DISCUSSION

It has long been postulated that *H. pylori* induces an NF-κB-dependent inflammatory response in gastric epithelial cells, which then secrete chemokines that recruit neutrophils to the site of infection where they, at least partially, contribute to bacterial clearance. Here, we present data showing that two major mechanisms, by which neutrophils combat bacterial infection, production of myeloperoxidase and neutrophil elastase, are dispensable in the context of *H. pylori*. It is possible that MPO and NE serve redundant functions to restrict *H. pylori* growth. Infecting MPO and NE double knockout mice would help address that possibility. Additionally, infecting neutrophil-deficient mice with *H. pylori* will help determine to what extent neutrophils are able to restrict *H. pylori* growth *in vivo*. Published studies suggest that neutrophils are not effective in clearing the infection in the tolerogenic environment that *H. pylori* induces via dendritic cell and Treg dependent production of anti-inflammatory cytokines (*60*, *61*). In order to see the potential effect of MPO and NE on restricting *H. pylori* infection *in vivo*, it may be

necessary to conduct the infection experiments in an *IL10*$^{-/-}$ background or to deplete Tregs in infected mice.

In contrast to AGS cells, a model gastric epithelial cell line, THP1 monocytes recognize *H. pylori* in a *cag*-T4SS dependent and independent manner. In addition to inducing an NF-κB-dependent immune response in THP1 cell, *H. pylori* also induces a type I IFN response that seems to be partially dependent on the *cag*-T4SS. Which bacterial ligand(s) induce the type I IFN response remains to be determined. The *cag*-T4SS dependent response is likely driven by a bacterial nucleic acid ligand that is delivered to the host cell cytosol. Two host signaling pathways that may be involved in *H. pylori* nucleic acid sensing are mediated through mitochondrial antiviral signaling (MAVS) and/or STING adapter proteins. RNA derivatives stimulate MAVS-dependent signaling, whereas STING-dependent signaling is activated by DNA species. Infecting STING and MAVS deficient THP1 cells with *H. pylori* will help determine if these host signaling pathways are relevant to *H. pylori* detection. MAVS and STING deficient mice are also available to further test the *in vivo* relevance of these signaling pathways. Alternatively, limited published data suggests that NOD1 sensing of *H. pylori* peptidoglycan not only activates NF-κB dependent inflammatory responses, but leads to type I IFN production via TRAF3-IRF7 dependent signaling (*199*). We did not see a difference in ISG expression in stomachs of wild type versus *Nod1*$^{-/-}$ mice after 1 week of infection (data not shown). However, as discussed in Chapter 4, this could be because ISGs are induced in a specific niche of the stomach or primarily in myeloid-derived cells that are recruited to the site of infection, thus the signal-to-noise ratio in whole stomach tissue may preclude seeing relevant gene expression differences. Further work is necessary to determine if NOD1-dependent type I IFN responses are relevant for cytosolic sensing of *H. pylori* by myeloid derived cells.

The *cag*-T4SS independent type I IFN response may be driven by endosomal TLR detection of *H. pylori* nucleic acids. Microbial nucleic acids can be localized to the endosome through pathogen phagocytosis where specific endosomal TLRs are activated based on the nucleic acid species present. TLR3 recognizes double-stranded RNA, TLR 7 and 8 recognize single-stranded RNA and TLR9 recognizes DNA (*220*). Activation of these TLRs and signaling through MYD88 or TRIF (in the case of TLR3) adapter proteins leads to production of type I IFN. MYD88 and TRIF deficient THP cells can be co-cultured with *cag*-T4SS mutant bacteria to determine if the *cag*-T4SS independent type I IFN response is dependent on endosomal TLR signaling.

The data presented in this chapter suggest that *H. pylori* activates pathogen recognition pathways in myeloid-derived cells that are distinct from those activated in gastric epithelial cells. Whether induction of type I IFNs in response to *H. pylori* infection is beneficial or detrimental to the host remains an open question. IFNα/β receptor deficient mice are more susceptible to *H. pylori* infection suggesting that type I IFN signaling may be protective (*199*). On the other hand, TLR9 activation by *H. pylori* DNA, which induces NF-κB and type I IFN, has been shown to result in a sum anti-inflammatory response that presumably favors bacterial persistence (*24*, *79*, *80*). Using the gastric organoid transwell co-culture system described in Chapter 4, it is now possible to dissect the cross talk between *H. pylori*, gastric epithelial cells and myeloid derived cells (Fig. 5.5). Future studies will focus on dissecting the functional relevance of simultaneous NF-κB and ISG induction on bacterial persistence. A comprehensive picture of how *H. pylori* initiates an immune response in gastric epithelial cells versus myeloid-derived cells is ultimately required to understand how the host-pathogen interaction can be manipulated in the host's favor.

EXPERIMENTAL PROCEDURES

Cell treatments and analysis

THP1 cells (ATCC), which are a human monocytic cell line derived from acute monocytic leukemia, were cultured in RPMI plus 10 % FBS and 0.05 mM β-mercaptoethanol. To induce differentiation into macrophage-like cells, THP1 cells were pretreated with 100 nM phorbol 12-myristate 13-acetate (PMA), after 24 hours PMA was removed and cells cultured with fresh media without PMA for an additional 24 hours. PMA-differentiated or undifferentiated THP1 cells were co-cultured with *H. pylori* in RPMI plus 10% FBS, 0.05 mM beta-mercaptoethanol and 20% BB10. Supernatants were collected and assayed for IL-8 concentration using ELISA (Biolegend) or cells were lysed with RLT buffer (RNeasy kit - Qiagen) and RNA isolated according to manufacturer's instructions for qPCR analysis. 3',3'-cGAMP (Invivogen) was used as a positive control for ISG induction in THP1 cells. Ninety-two μl of Opti-MEM (Gibco) was mixed with 8 μl of Lipofectamine 2000 (Invitrogen) transfection reagent and incubated for 5 min at room temperature. Ninety-two μl of Opti-MEM was mixed with 8 μl (500 μM stock) of cGAMP, then combined with Opti-MEM/Lipofectamine mixture and incubated for an additional 5 min at room temperature. A total of 200 μl of cGAMP-containing (20 μM final concentration) transfection mixture was added dropwise to each well of a 6-well plate containing 1 x 10^6 THP1 cells. At indicated time points cells were collected for RNA isolation, as described above.

Mouse infections

Mice were housed in an Association for the Assessment and Accreditation of Laboratory Animal Care-accredited facility and all procedures were approved by Fred Hutch Institutional Animal Care and Use Committee. Myeloperoxidase and neutrophil elastase deficient mice were a

generous gift form Dr. McGarry Houghton. Mice were inoculated with 5 x 10^7 *H. pylori* CFU in 100 μl of Brucella Broth plus 10% FBS by oral gavage, as previously described (*211*). Mouse adapted strain MSD132 (*217*) or clinical isolate strain PMSS1 (*218*) were used for the experiments. For CFU enumeration, stomachs were harvested after 1 week of infection and dilutions of tissue homogenates were plated on horse blood agar plates and colonies counted then normalized to weight of stomach tissue.

Quantitative PCR

THP1 cells were plated at a concentration of 1 x 10^6 cells per well in 6-well plates in a total volume of 5 mL. After treatment and at designated time points, cells were scraped, pelleted and resuspended in lysis buffer, then centrifuged through a QIAshredder column (Qiagen). RNA was isolated using an RNeasy RNA isolation kit (Qiagen). Complementary DNA was generated using High Capacity RNA to cDNA Kit (Applied Biosystems). Gene expression was quantified using primers listed in Table 5.1 and PowerUp SYBR Green MasterMix (Applied Biosystems). Gene expression was normalized to human *GAPDH* housekeeping gene.

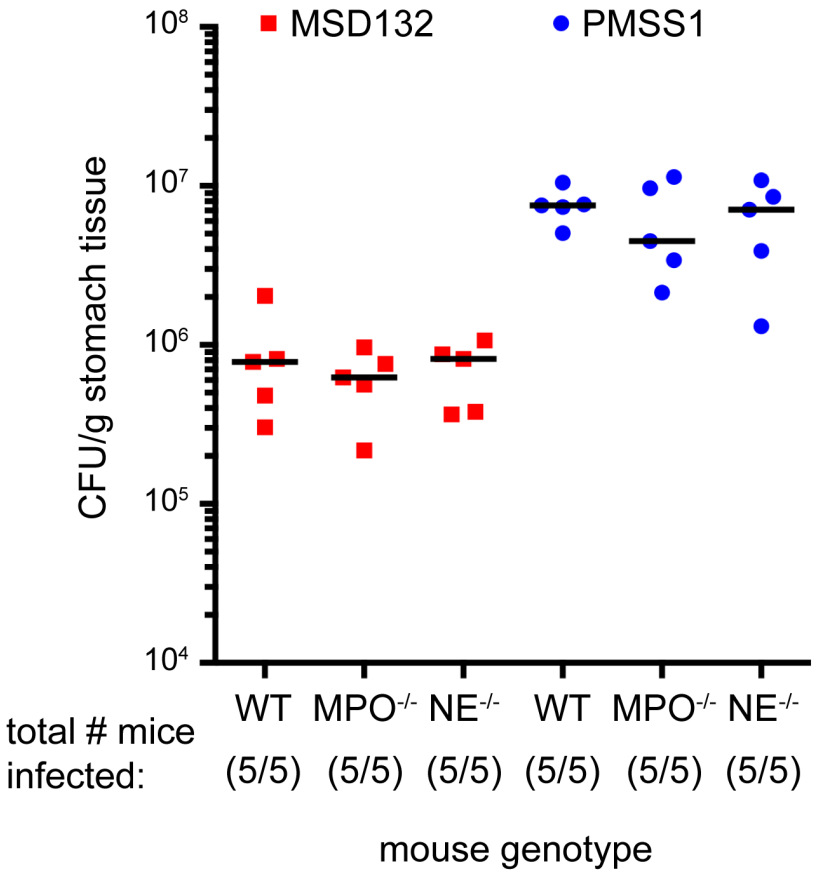

Figure 5.1. MPO and neutrophil elastase deficient mice are colonized to wild-type levels with *H. pylori* after 1 week of infection
Myeloperoxidase $(MPO)^{-/-}$ and neutrophil elastase $(NE)^{-/-}$ mice were infected with 5 x 10^7 *H. pylori* colony forming units (CFU) via oral gavage and stomach tissue harvested after 1 week of infection. MSD132, a mouse adapted derivative of clinical isolate G27 (*217*), and PMSS1, a clinical isolate that naturally colonizes mice to high levels (*218*), strains were tested. Data is displayed as CFU per gram stomach tissue with the median indicated by the horizontal lines.

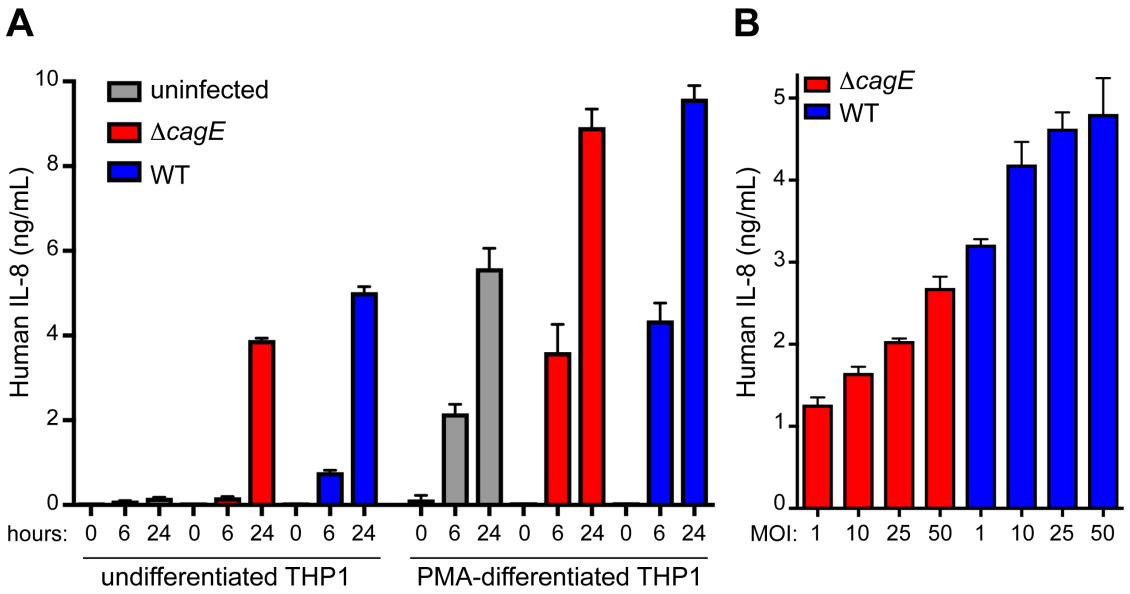

Figure 5.2. *H. pylori* induces *cag*-T4SS-dependent and independent NF-κB activation in THP1 cells

(A) Undifferentiated or PMA-differentiated THP1 cells were co-cultured with wild-type G27 *H. pylori* or *ΔcagE* isogenic mutant at MOI = 10 and IL-8 concentration in supernatant measured by ELISA. (B) Undifferentiated THP1 cells were co-cultured with indicated MOIs of wild-type G27 *H. pylori* or *ΔcagE* isogenic mutant for 24 hours and and IL-8 concentration in supernatant measured by ELISA. (A and B) Each condition was tested in triplicate with bars showing the mean with standard deviation.

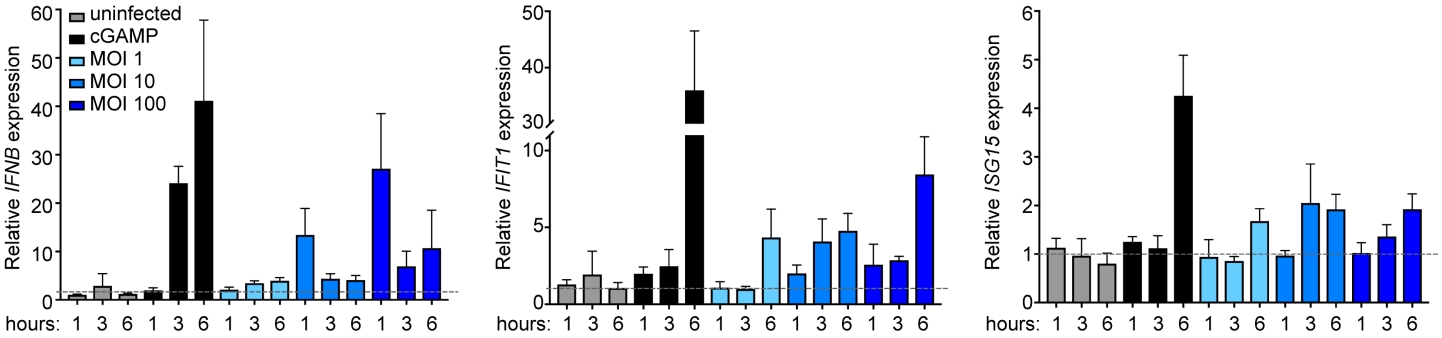

Figure 5.3. *H. pylori* induces a type I IFN response in THP1 cells
Undifferentiated THP1 cells were co-cultured with wild-type G27 *H. pylori* strain at MOI = 1, 10 or 100. As a positive control, cells were stimulated with 20 μM 3',3' cGAMP, a potent inducer of ISGs. At 1, 3 and 6 hours post-infection, cells were collected and RNA harvested. Gene expression relative to human *GAPDH* of interferon stimulated genes *IFNB*, *IFIT1* and *ISG15* is shown as mean with standard deviation. Biological duplicates in technical triplicates were tested for each condition.

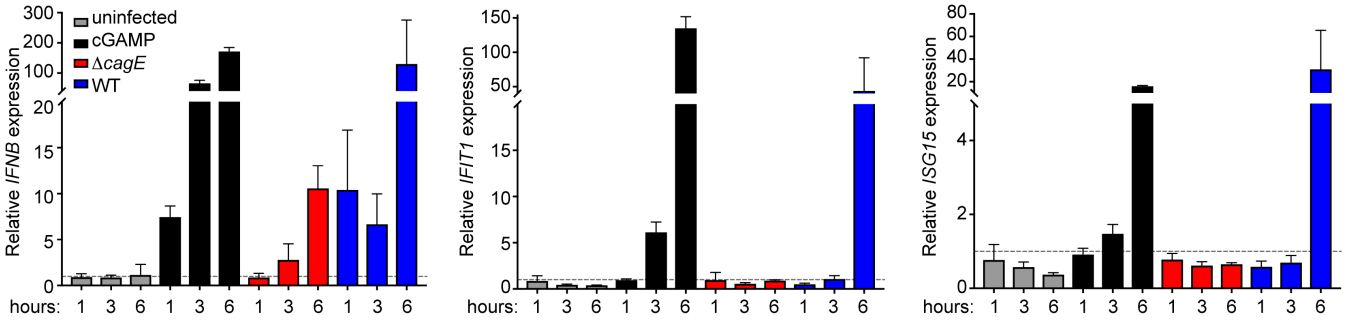

Figure 5.4. *H. pylori* induced ISGs in THP1 cells is *cag*-T4SS-dependent
Undifferentiated THP1 cells were co-cultured with wild-type G27 *H. pylori* strain or *ΔcagE* isogenic mutant at MOI = 10. As a positive control, cells were stimulated with 20 μM 3',3' cGAMP, a potent inducer of ISGs. At 1, 3 and 6 hours post-infection, cells were collected and RNA harvested. Gene expression relative to human *GAPDH* of interferon stimulated genes *IFNB*, *IFIT1* and *ISG15* is shown as mean with standard deviation. Biological duplicates in technical triplicates were tested for each condition.

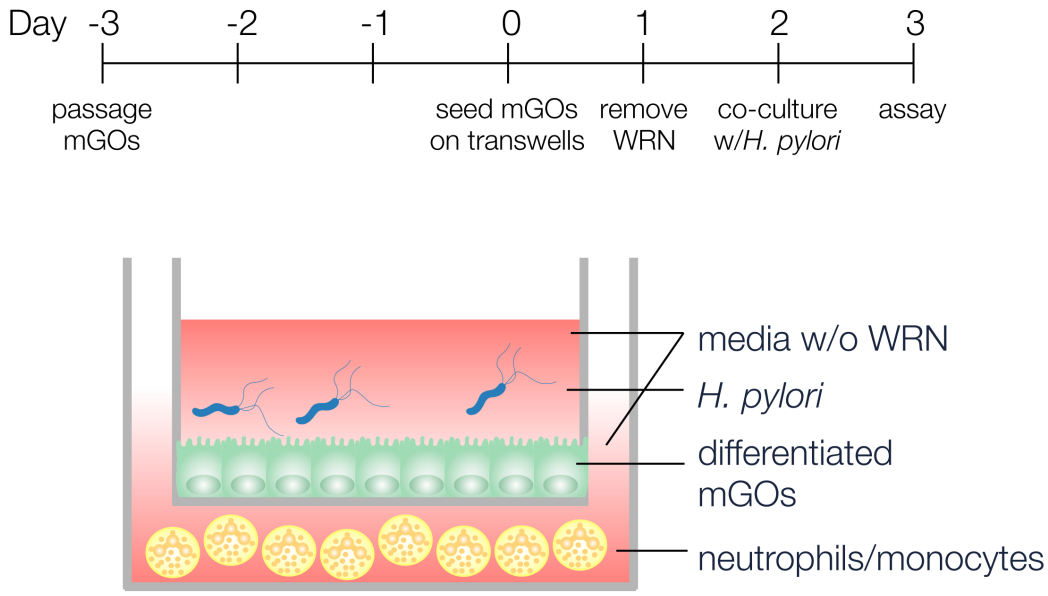

Figure 5.5. Transwell co-culture experimental set up to study *H. pylori* – gastric epithelial – myeloid-derived cell interactions
Experimental time course and schematic of proposed mGO transwell co-culture system.

Table 5.1. Primers used for RT-qPCR

Species	Gene	Primer name	Primer sequence (5' → 3')
human	*IFNB*	IFNB_qPCR_#2_fwd	ACGCCGCATTGACCATCTATG
		IFNB_qPCR_#2_rev	CGGAGGTAACCTGTAAGTCTGT
human	*IFI27*	IFI27_qPCR_fwd	TGCTCTCACCTCATCAGCAGT
		IFI27_qPCR_rev	CACAACTCCTCCAATCACAACT
human	*IFIT1*	IFIT1_qPCR_fwd	TCAGGTCAAGGATAGTCTGGAG
		IFIT1_qPCR_rev	AGGTTGTGTATTCCCACACTGTA
human	*ISG15*	ISG15_qPCR_fwd	TCCTGGTGAGGAATAACAAGGG
		ISG15_qPCR_rev	GTCAGCCAGAACAGGTCGTC
human	*GAPDH*	GAPDH_qPCR_fwd	AACAGCCTCAAGATCATCAGC
		GAPDH_qPCR_rev	CACCACCTTCTTGATGTCATC

CHAPTER 6: Conclusions and Future Directions

H. pylori causes inflammation in the gastric mucosa of virtually all infected individuals. How *H. pylori* manages to chronically persist in the host, despite eliciting a strong immune response remains an open question. In order to begin answering that question, a comprehensive understanding of the mechanisms underlying *H. pylori* detection by the host and the nature of the subsequent immune response (*i.e.* pro or anti-inflammatory) is needed. The goals of this dissertation research were to:

1) Define how presence of *H. pylori* shapes microbial communities in the upper gastrointestinal tract
2) Identify mechanisms by which *H. pylori* triggers an innate immune response in gastric epithelial cells
3) Identify mechanisms by which *H. pylori* triggers an innate immune response in myeloid-derived cells

Chapter 2 addressed the first goal by presenting data characterizing microbial communities present in the upper gastrointestinal tract of individuals with Barrett's esophagus. Samples from normal squamous esophagus, Barrett's esophagus, stomach corpus and stomach antrum from the same individuals revealed that microbial communities in the upper gastrointestinal tract were more similar within individuals rather than the same site in a different individual. When *H. pylori* was present, it numerically dominated all other bacterial species (99% percent of reads in stomach corpus and 28% of reads in stomach antrum), which is consistent with published reports comparing the stomach microbial composition in *H. pylori* positive versus negative individuals (*28*, *30*, *32*). *H. pylori* infection is inversely associated with

development of esophageal adenocarcinoma (*93-95*). We found that in the Seattle Barrett's Esophagus Cohort infection with *H. pylori* was associated with decreased incidence of aneuploidy, a measure of genomic instability that predicts progression to esophageal adenocarcinoma (*107*). Due to our study's limitations (*i.e.* insufficient number of *H. pylori* positive participants), we were unable to assess whether *H. pylori* stably colonizes the esophagus. Future studies will focus on *H. pylori* interactions with esophageal epithelial cells and *H. pylori* interactions with members of the esophageal microbial community to determine if dynamics of those relationships contribute to protection against esophageal adenocarcinoma development.

Chapter 3 investigated the innate immune sensing pathways triggered in gastric epithelial cells upon contact with *H. pylori*. Specifically, we focused on delineating the immune response downstream of bacterial factors delivered to the gastric epithelial cell cytosol through *H. pylori*'s *cag*-T4SS. Prior to our study, the entire *cag*-T4SS-dependent IL-8 response in gastric epithelial cells was attributed to NOD1 detection of *H. pylori* cell wall fragments, which leads to NF-κB activation and IL-8 production (*57*). We found that an LPS metabolic precursor, HBP enters the host cell cytosol via the *cag*-T4SS, activates host TIFA and culminates in NF-κB activation triggering a proinflammatory immune response. The TIFA mediated response precedes NOD1 activation and occurs within minutes of contact with *H. pylori* (*221*). NOD-1 mediated NF-κB activation only modestly contributed to the overall response to *H. pylori* infection. This raises questions regarding the contribution of TIFA versus NOD1-mediated signaling during *H. pylori* infection *in vivo*. Using *Tifa*-deficient mice, we can assess the relevance of Tifa signaling *in vivo*. If Tifa activation plays a central role in the immune response to *H. pylori*, then we expect *Tifa*$^{-/-}$ mice to be more susceptible to *H. pylori* infection.

AGS cells have some non-functional pathogen recognition pathways, namely Toll-like receptors, which may contribute significantly to *H. pylori* detection *in vivo*. Although this limitation was advantageous for identifying the TIFA-mediated immune response to *H. pylori*, this model gastric epithelial cell line does not reflect the complexity of the human gastric epithelium. Indeed, data presented in Chapter 4 revealed that infection of *Nod1*$^{-/-}$ mice with *cag*-T4SS expressing mouse adapted *H. pylori* results in higher bacterial loads when compared to wild-type mice. Despite the modest contribution of NOD1 signaling in AGS cells, Nod1 appears to be important in restricting bacterial growth in a mouse model of infection. The discrepancy between our *in vitro* and *in vivo* findings suggests that a better gastric epithelial cell model is needed to further our understanding of innate immune signaling pathways involved in *H. pylori* detection. In chapter 4, we introduce mouse and human gastric organoids as a novel *ex vivo* model for studying *H. pylori*-gastric epithelial cell interactions. Lgr5-experssing cells can be selected, expanded and propagated in the presence of stem cell growth factors Wnt, R-spondin and Noggin. When those factors are withdrawn, gastric organoids differentiate into primary-like gastric epithelial cells. Seeding gastric organoids on a permeable support induces the formation of a polarized gastric epithelial monolayer which can be used for infection studies where bacteria are added to the apical side and myeloid-derived cells such as neutrophils or macrophages added to the basal side. The transwell system will allow for host-pathogen interaction studies in a physiologically more relevant *ex vivo* setting.

Chapter 5 begins to address the third goal of this dissertation by exploring the contribution of myeloid-derived immune cells to detection and response to *H. pylori* infection. The longstanding dogma in the field of *H. pylori* pathogenesis states that NF-κB-driven immune responses initiated by gastric epithelial cells lead to release of IL-8, a chemokine that recruits

neutrophils and macrophages to infected stomach tissue. Neutrophils are presumed to contribute, at least partially, to clearance of *H. pylori*. When we infected myeloperoxidase and neutrophil elastase deficient mice with *H. pylori*, we did not observe a difference in bacterial burden as compared to wild-type mice suggesting that the two main mechanisms by which neutrophils kill bacteria are dispensable in the context of *H. pylori* infection. It is possible that the actions of MPO and NE are redundant, thus infecting mice deficient in one of these enzymes would not show any effects. *H. pylori* may also be resistant to oxidative damage-mediated killing since it expresses a suite of enzymes designed to deal with oxidative stress, such as superoxide dismutase, catalase and a family of peroxiredoxins (*222*). Infecting neutrophil deficient mice with *H. pylori* will help address the question of whether neutrophils help restrict bacterial growth *in vivo*.

Chapter 5 also presented data suggesting that *H. pylori* initiates a type I IFN response in monocytes. Published data suggests that the net effect of type I IFN signaling in the context of *H. pylori* infection is protective, since IFNα/β receptor deficient mice are colonized to a greater extent with *H. pylori* than their wild-type counterparts (*199*). However, many questions remain regarding this response. For example, what are the bacterial ligand(s) driving the type I IFN response in *H. pylori*? Is the type I IFN response restricted to myeloid-derived cells or do gastric epithelial cells also produce type I IFNs in response to *H. pylori* infection? What is the consequence of the crosstalk between the NF-κB-dependent and IFN-dependent signaling on the overall immune response to *H. pylori*?

One possible mechanism by which *H. pylori* establishes a persistent infection may involve eliciting a pro-inflammatory response in gastric epithelial cells through activation of specific pathogen recognition pathways (*e.g.* TIFA or NOD1-mediated) and an anti-

inflammatory response in myeloid-derived cells through activation of a distinct set of PRRs. A robust inflammatory response initiated by gastric epithelial cells ensures the recruitment of large numbers of myeloid-derived cells. Once the myeloid-derived cells arrive, *H. pylori* may selectively activate a combination of PRRs that culminate in an anti-inflammatory response favoring bacterial persistence. Additionally, this strategy may help protect *H. pylori*'s replicative niche by ensuring that all other bacterial competitors are unable to survive in the inflamed gastric mucosa, but *H. pylori* is protected by the anti-inflammatory, *H. pylori*-specific adaptive immune response. We can begin testing this hypothesis by performing adoptive transfer experiments in which *Nod1* or *Tifa*-deficient mice are reconstituted with bone marrow cells from wild-type mice then infect with *H. pylori*. If Nod1 and Tifa activation in gastric epithelial cells is required for limiting bacterial colonization, then we expect *Nod1*$^{-/-}$ and *Tifa*$^{-/-}$ mice with a wild-type hematopoietic compartment would be more susceptible to *H. pylori* infection. Furthermore, if Nod1 and Tifa signaling is dispensable in the hematopoietic compartment, then reconstituting wild-type mice with bone marrow from *Nod1*$^{-/-}$ and *Tifa*$^{-/-}$ mice would be predicted not to have an effect on bacterial colonization. Transwell co-culture experiments with *H. pylori* and gastric organoids derived from *Nod1*$^{-/-}$ and *Tifa*$^{-/-}$ mice will help further clarify the contribution of these pathogen recognition pathways on activating myeloid-derived cells.

Defining which innate immune pathways are triggered by *H. pylori* in gastric epithelial cells versus myeloid-derived cells and the functional relevance of those pathways to bacterial persistence is ultimately required to understand how the host-pathogen interaction can be manipulated in the host's favor. A comprehensive understanding of the relevant innate immune pathways will inform strategies for achieving bacterial clearance while limiting host-damaging inflammation.

BIBLIOGRAPHY

1. L. E. Wroblewski, R. M. Peek, K. T. Wilson, *Helicobacter pylori* and gastric cancer: factors that modulate disease risk. *Clin. Microbiol. Rev.* **23**, 713–739 (2010).

2. A. R. Sepulveda, *Helicobacter*, Inflammation, and Gastric Cancer. *Curr Pathobiol Rep*. **1**, 9–18 (2013).

3. D. B. Polk, R. M. Peek, *Helicobacter pylori*: gastric cancer and beyond. *Nat. Rev. Cancer*. **10**, 403–414 (2010).

4. L. M. Asenjo, J. P. Gisbert, [Prevalence of *Helicobacter pylori* infection in gastric MALT lymphoma: a systematic review]. *Rev Esp Enferm Dig*. **99**, 398–404 (2007).

5. W. Fischbach, MALT lymphoma: forget surgery? *Dig Dis*. **31**, 38–42 (2013).

6. S. Rosebeck, P. C. Lucas, L. M. McAllister-Lucas, Protease activity of the API2-MALT1 fusion oncoprotein in MALT lymphoma development and treatment. *Future Oncol*. **7**, 613–617 (2011).

7. S. Schreiber *et al.*, The spatial orientation of *Helicobacter pylori* in the gastric mucus. *Proc. Natl. Acad. Sci. U.S.A.* **101**, 5024–5029 (2004).

8. T. L. Cover, U. S. Krishna, D. A. Israel, R. M. Peek, Induction of gastric epithelial cell apoptosis by *Helicobacter pylori* vacuolating cytotoxin. *Cancer Res.* **63**, 951–957 (2003).

9. P. Jain, Z.-Q. Luo, S. R. Blanke, *Helicobacter pylori* vacuolating cytotoxin A (VacA) engages the mitochondrial fission machinery to induce host cell death. *Proc. Natl. Acad. Sci. U.S.A.* **108**, 16032–16037 (2011).

10. L. E. Wroblewski, R. M. Peek, "Targeted disruption of the epithelial-barrier by *Helicobacter pylori*". *Cell Commun. Signal*. **9**, 29 (2011).

11. N. Tegtmeyer *et al.*, *Helicobacter pylori* Employs a Unique Basolateral Type IV Secretion Mechanism for CagA Delivery. *Cell Host Microbe*. **22**, 552–560.e5 (2017).

12. N. Uemura *et al.*, *Helicobacter pylori* infection and the development of gastric cancer. *N. Engl. J. Med.* **345**, 784–789 (2001).

13. M. Miftahussurur, I. A. Nusi, D. Y. Graham, Y. Yamaoka, *Helicobacter*, Hygiene, Atopy, and Asthma. *Front Microbiol*. **8**, 1034 (2017).

14. J. L. Schneider, D. A. Corley, The Troublesome Epidemiology of Barrett's Esophagus and Esophageal Adenocarcinoma. *Gastrointest. Endosc. Clin. N. Am.* **27**,

353–364 (2017).

15. N. Castaño-Rodríguez, N. O. Kaakoush, W. S. Lee, H. M. Mitchell, Dual role of *Helicobacter* and *Campylobacter* species in IBD: a systematic review and meta-analysis. *Gut*. **66**, 235–249 (2017).

16. V. Jaruvongvanich, A. Sanguankeo, S. Jaruvongvanich, S. Upala, Association between *Helicobacter pylori* infection and multiple sclerosis: A systematic review and meta-analysis. *Mult Scler Relat Disord*. **7**, 92–97 (2016).

17. J. C. Atherton, M. J. Blaser, Coadaptation of *Helicobacter pylori* and humans: ancient history, modern implications. *J. Clin. Invest.* **119**, 2475–2487 (2009).

18. Y. Chen, M. J. Blaser, Inverse associations of *Helicobacter pylori* with asthma and allergy. *Arch. Intern. Med.* **167**, 821–827 (2007).

19. J. Reibman *et al.*, Asthma is inversely associated with *Helicobacter pylori* status in an urban population. *PLoS ONE*. **3**, e4060 (2008).

20. J. Luther, M. Dave, P. D. R. Higgins, J. Y. Kao, Association between *Helicobacter pylori* infection and inflammatory bowel disease: a meta-analysis and systematic review of the literature. *Inflamm. Bowel Dis.* **16**, 1077–1084 (2010).

21. I. C. Arnold *et al.*, Tolerance rather than immunity protects from *Helicobacter pylori*-induced gastric preneoplasia. *Gastroenterology*. **140**, 199–209 (2011).

22. P. D. R. Higgins *et al.*, Prior *Helicobacter pylori* infection ameliorates *Salmonella typhimurium*-induced colitis: mucosal crosstalk between stomach and distal intestine. *Inflamm. Bowel Dis.* **17**, 1398–1408 (2011).

23. K. Hussain *et al.*, *Helicobacter pylori*-Mediated Protection from Allergy Is Associated with IL-10-Secreting Peripheral Blood Regulatory T Cells. *Front Immunol*. **7**, 71 (2016).

24. J. Luther *et al.*, *Helicobacter pylori* DNA decreases pro-inflammatory cytokine production by dendritic cells and attenuates dextran sodium sulphate-induced colitis. *Gut*. **60**, 1479–1486 (2011).

25. Y. Onishi, Z. Fehervari, T. Yamaguchi, S. Sakaguchi, Foxp3+ natural regulatory T cells preferentially form aggregates on dendritic cells *in vitro* and actively inhibit their maturation. *Proc. Natl. Acad. Sci. U.S.A.* **105**, 10113–10118 (2008).

26. S. Delgado, R. Cabrera-Rubio, A. Mira, A. Suárez, B. Mayo, Microbiological survey of the human gastric ecosystem using culturing and pyrosequencing methods. *Microb. Ecol.* **65**, 763–772 (2013).

27. A. Mosca, M. Leclerc, J. P. Hugot, Gut Microbiota Diversity and Human Diseases: Should We Reintroduce Key Predators in Our Ecosystem? *Front Microbiol*. **7**, 455

(2016).

28. E. M. Bik *et al.*, Molecular analysis of the bacterial microbiota in the human stomach. *Proc. Natl. Acad. Sci. U.S.A.* **103**, 732–737 (2006).

29. A. F. Andersson *et al.*, Comparative analysis of human gut microbiota by barcoded pyrosequencing. *PLoS ONE*. **3**, e2836 (2008).

30. M. E. Martin *et al.*, The impact of *Helicobacter pylori* infection on the gastric microbiota of the rhesus macaque. *PLoS ONE*. **8**, e76375 (2013).

31. A. Gall *et al.*, Bacterial Composition of the Human Upper Gastrointestinal Tract Microbiome Is Dynamic and Associated with Genomic Instability in a Barrett's Esophagus Cohort. *PLoS ONE*. **10**, e0129055 (2015).

32. B. N. Parsons *et al.*, Comparison of the human gastric microbiota in hypochlorhydric states arising as a result of *Helicobacter pylori*-induced atrophic gastritis, autoimmune atrophic gastritis and proton pump inhibitor use. *PLoS Pathog.* **13**, e1006653 (2017).

33. B. Linz *et al.*, An African origin for the intimate association between humans and *Helicobacter pylori*. *Nature*. **445**, 915–918 (2007).

34. Y. Moodley *et al.*, Age of the association between *Helicobacter pylori* and man. *PLoS Pathog.* **8**, e1002693 (2012).

35. S. Nahar *et al.*, Evidence of intra-familial transmission of *Helicobacter pylori* by PCR-based RAPD fingerprinting in Bangladesh. *Eur. J. Clin. Microbiol. Infect. Dis.* **28**, 767–773 (2009).

36. S. Mamishi *et al.*, Intrafamilial transmission of *Helicobacter pylori*: genotyping of faecal samples. *Br. J. Biomed. Sci.* **73**, 38–43 (2016).

37. G. I. Pérez-Pérez *et al.*, Transient and persistent *Helicobacter pylori* colonization in Native American children. *J. Clin. Microbiol.* **41**, 2401–2407 (2003).

38. M. Granström, Y. Tindberg, M. Blennow, Seroepidemiology of *Helicobacter pylori* infection in a cohort of children monitored from 6 months to 11 years of age. *J. Clin. Microbiol.* **35**, 468–470 (1997).

39. G. I. Perez-Perez *et al.*, Evidence that cagA(+) *Helicobacter pylori* strains are disappearing more rapidly than cagA(-) strains. *Gut*. **50**, 295–298 (2002).

40. P. Santiago, Y. Moreno, M. A. Ferrús, Identification of Viable *Helicobacter pylori* in Drinking Water Supplies by Cultural and Molecular Techniques. *Helicobacter*. **20**, 252–259 (2015).

41. C. Kraft *et al.*, Genomic changes during chronic *Helicobacter pylori* infection. *J.*

Bacteriol. **188**, 249–254 (2006).

42. G. Morelli *et al.*, Microevolution of *Helicobacter pylori* during prolonged infection of single hosts and within families. *PLoS Genet.* **6**, e1001036 (2010).

43. D. Kersulyte, H. Chalkauskas, D. E. Berg, Emergence of recombinant strains of *Helicobacter pylori* during human infection. *Mol. Microbiol.* **31**, 31–43 (1999).

44. M. S. Dorer, S. Talarico, N. R. Salama, *Helicobacter pylori*'s unconventional role in health and disease. *PLoS Pathog.* **5**, e1000544 (2009).

45. M. J. Blaser *et al.*, Infection with *Helicobacter pylori* strains possessing cagA is associated with an increased risk of developing adenocarcinoma of the stomach. *Cancer Res.* **55**, 2111–2115 (1995).

46. A. M. Y. Nomura, G. I. Perez-Perez, J. Lee, G. Stemmermann, M. J. Blaser, Relation between *Helicobacter pylori* cagA status and risk of peptic ulcer disease. *Am. J. Epidemiol.* **155**, 1054–1059 (2002).

47. S. Odenbreit *et al.*, Translocation of *Helicobacter pylori* CagA into gastric epithelial cells by type IV secretion. *Science*. **287**, 1497–1500 (2000).

48. R. M. Barrozo *et al.*, Functional plasticity in the type IV secretion system of *Helicobacter pylori*. *PLoS Pathog.* **9**, e1003189 (2013).

49. R. M. Barrozo *et al.*, CagY Is an Immune-Sensitive Regulator of the *Helicobacter pylori* Type IV Secretion System. *Gastroenterology*. **151**, 1164–1175.e3 (2016).

50. S. Tan, L. S. Tompkins, M. R. Amieva, *Helicobacter pylori* usurps cell polarity to turn the cell surface into a replicative niche. *PLoS Pathog.* **5**, e1000407 (2009).

51. J. M. Noto *et al.*, Regulation of *Helicobacter pylori* Virulence Within the Context of Iron Deficiency. *J Infect Dis*. **211**, 1790–1794 (2015).

52. N. R. Salama, M. L. Hartung, A. Müller, Life in the human stomach: persistence strategies of the bacterial pathogen *Helicobacter pylori*. *Nat. Rev. Microbiol.* **11**, 385–399 (2013).

53. A. R. Lord *et al.*, Protective effects of *Helicobacter pylori* for IBD are related to the cagA-positive strain. *Gut*. **67**, 393–394 (2018).

54. C. Chen, P. Xun, C. Tsinovoi, K. He, Accumulated evidence on *Helicobacter pylori* infection and the risk of asthma: A meta-analysis. *Ann. Allergy Asthma Immunol.* **119**, 137–145.e2 (2017).

55. M. Unemo *et al.*, The sialic acid binding SabA adhesin of *Helicobacter pylori* is essential for nonopsonic activation of human neutrophils. *J. Biol. Chem.* **280**, 15390–15397 (2005).

56. M. Chamaillard *et al.*, An essential role for NOD1 in host recognition of bacterial peptidoglycan containing diaminopimelic acid. *Nat. Immunol.* **4**, 702–707 (2003).

57. J. Viala *et al.*, Nod1 responds to peptidoglycan delivered by the *Helicobacter pylori* cag pathogenicity island. *Nat. Immunol.* **5**, 1166–1174 (2004).

58. A. Grubman *et al.*, The innate immune molecule, NOD1, regulates direct killing of *Helicobacter pylori* by antimicrobial peptides. *Cell. Microbiol.* **12**, 626–639 (2010).

59. S. Keates, Y. S. Hitti, M. Upton, C. P. Kelly, *Helicobacter pylori* infection activates NF-kappa B in gastric epithelial cells. *Gastroenterology*. **113**, 1099–1109 (1997).

60. H. F. Ismail, P. Fick, J. Zhang, R. G. Lynch, D. J. Berg, Depletion of neutrophils in IL-10(-/-) mice delays clearance of gastric *Helicobacter* infection and decreases the Th1 immune response to *Helicobacter*. *J. Immunol.* **170**, 3782–3789 (2003).

61. J. Y. Kao *et al.*, *Helicobacter pylori* immune escape is mediated by dendritic cell-induced Treg skewing and Th17 suppression in mice. *Gastroenterology*. **138**, 1046–1054 (2010).

62. L. Mandell *et al.*, Intact gram-negative *Helicobacter pylori*, *Helicobacter felis*, and *Helicobacter hepaticus* bacteria activate innate immunity via toll-like receptor 2 but not toll-like receptor 4. *Infect. Immun.* **72**, 6446–6454 (2004).

63. A. Amedei *et al.*, The neutrophil-activating protein of *Helicobacter pylori* promotes Th1 immune responses. *J. Clin. Invest.* **116**, 1092–1101 (2006).

64. Y. Zhao *et al.*, *Helicobacter pylori* heat-shock protein 60 induces interleukin-8 via a Toll-like receptor (TLR)2 and mitogen-activated protein (MAP) kinase pathway in human monocytes. *J. Med. Microbiol.* **56**, 154–164 (2007).

65. K. N. Koch *et al.*, *Helicobacter* urease-induced activation of the TLR2/NLRP3/IL-18 axis protects against asthma. *J. Clin. Invest.* **125**, 3297–3302 (2015).

66. I. C. Arnold *et al.*, NLRP3 Controls the Development of Gastrointestinal CD11b+ Dendritic Cells in the Steady State and during Chronic Bacterial Infection. *Cell Rep*. **21**, 3860–3872 (2017).

67. I. Hitzler *et al.*, Caspase-1 has both proinflammatory and regulatory properties in *Helicobacter* infections, which are differentially mediated by its substrates IL-1β and IL-18. *J. Immunol.* **188**, 3594–3602 (2012).

68. P. Hofner *et al.*, Genetic polymorphisms of NOD1 and IL-8, but not polymorphisms of TLR4 genes, are associated with *Helicobacter pylori*-induced duodenal ulcer and gastritis. *Helicobacter*. **12**, 124–131 (2007).

69. P. Wang *et al.*, Association of NOD1 and NOD2 genes polymorphisms with *Helicobacter pylori* related gastric cancer in a Chinese population. *World J.*

Gastroenterol. **18**, 2112–2120 (2012).

70. E. M. El-Omar *et al.*, Interleukin-1 polymorphisms associated with increased risk of gastric cancer. *Nature*. **404**, 398–402 (2000).

71. R. Rad *et al.*, Extracellular and intracellular pattern recognition receptors cooperate in the recognition of *Helicobacter pylori*. *Gastroenterology*. **136**, 2247–2257 (2009).

72. P. Mitchell *et al.*, Chronic exposure to *Helicobacter pylori* impairs dendritic cell function and inhibits Th1 development. *Infect. Immun.* **75**, 810–819 (2007).

73. K. A. Eaton, S. R. Ringler, S. J. Danon, Murine splenocytes induce severe gastritis and delayed-type hypersensitivity and suppress bacterial colonization in *Helicobacter pylori*-infected SCID mice. *Infect. Immun.* **67**, 4594–4602 (1999).

74. S. Shiomi *et al.*, IL-17 is involved in *Helicobacter pylori*-induced gastric inflammatory responses in a mouse model. *Helicobacter*. **13**, 518–524 (2008).

75. A. A. Akhiani, K. Schön, L. E. Franzén, J. Pappo, N. Lycke, *Helicobacter pylori*-specific antibodies impair the development of gastritis, facilitate bacterial colonization, and counteract resistance against infection. *J. Immunol.* **172**, 5024–5033 (2004).

76. A. P. Moran, B. Lindner, E. J. Walsh, Structural characterization of the lipid A component of *Helicobacter pylori* rough- and smooth-form lipopolysaccharides. *J. Bacteriol.* **179**, 6453–6463 (1997).

77. A. T. Gewirtz *et al.*, *Helicobacter pylori* flagellin evades toll-like receptor 5-mediated innate immunity. *J. Infect. Dis.* **189**, 1914–1920 (2004).

78. E. Andersen-Nissen *et al.*, Cutting edge: *Tlr5*-/- mice are more susceptible to *Escherichia coli* urinary tract infection. *J. Immunol.* **178**, 4717–4720 (2007).

79. M. G. Varga *et al.*, Pathogenic *Helicobacter pylori* strains translocate DNA and activate TLR9 via the cancer-associated cag type IV secretion system. *Oncogene* (2016), doi:10.1038/onc.2016.158.

80. M. G. Varga *et al.*, TLR9 activation suppresses inflammation in response to *Helicobacter pylori* infection. *Am. J. Physiol. Gastrointest. Liver Physiol.* **311**, G852–G858 (2016).

81. S. I. Gringhuis, J. den Dunnen, M. Litjens, M. van der Vlist, T. B. H. Geijtenbeek, Carbohydrate-specific signaling through the DC-SIGN signalosome tailors immunity to *Mycobacterium tuberculosis*, HIV-1 and *Helicobacter pylori*. *Nat. Immunol.* **10**, 1081–1088 (2009).

82. M. M. Gerrits, A. H. M. van Vliet, E. J. Kuipers, J. G. Kusters, *Helicobacter pylori* and antimicrobial resistance: molecular mechanisms and clinical implications.

Lancet Infect Dis. **6**, 699–709 (2006).

83. P. Ruggiero, S. Peppoloni, R. Rappuoli, G. Del Giudice, The quest for a vaccine against *Helicobacter pylori*: how to move from mouse to man? *Microbes Infect.* **5**, 749–756 (2003).

84. T. Aebischer, A. Schmitt, A. K. Walduck, T. F. Meyer, *Helicobacter pylori* vaccine development: facing the challenge. *Int. J. Med. Microbiol.* **295**, 343–353 (2005).

85. P. Sutton, Y. T. Chionh, Why can't we make an effective vaccine against *Helicobacter pylori*? *Expert Rev Vaccines*. **12**, 433–441 (2013).

86. M. Zeng *et al.*, Efficacy, safety, and immunogenicity of an oral recombinant *Helicobacter pylori* vaccine in children in China: a randomised, double-blind, placebo-controlled, phase 3 trial. *Lancet*. **386**, 1457–1464 (2015).

87. C. Schmees *et al.*, Inhibition of T-cell proliferation by *Helicobacter pylori* gamma-glutamyl transpeptidase. *Gastroenterology*. **132**, 1820–1833 (2007).

88. P. Sutton, J. M. Boag, Status of vaccine research and development for *Helicobacter pylori*. *Vaccine* (2018), doi:10.1016/j.vaccine.2018.01.001.

89. D. M. Monack, A. Mueller, S. Falkow, Persistent bacterial infections: the interface of the pathogen and the host immune system. *Nat. Rev. Microbiol.* **2**, 747–765 (2004).

90. L. M. Brown, S. S. Devesa, W.-H. Chow, Incidence of adenocarcinoma of the esophagus among white Americans by sex, stage, and age. *J. Natl. Cancer Inst.* **100**, 1184–1187 (2008).

91. P. Lao-Sirieix *et al.*, Physiological and molecular analysis of acid loading mechanisms in squamous and columnar-lined esophagus. *Dis. Esophagus*. **21**, 529–538 (2008).

92. W. H. Chow *et al.*, An inverse relation between cagA+ strains of *Helicobacter pylori* infection and risk of esophageal and gastric cardia adenocarcinoma. *Cancer Res.* **58**, 588–590 (1998).

93. L. A. Anderson *et al.*, Relationship between *Helicobacter pylori* infection and gastric atrophy and the stages of the oesophageal inflammation, metaplasia, adenocarcinoma sequence: results from the FINBAR case-control study. *Gut*. **57**, 734–739 (2008).

94. D. K. Rex *et al.*, Screening for Barrett's esophagus in colonoscopy patients with and without heartburn. *Gastroenterology*. **125**, 1670–1677 (2003).

95. D. A. Corley *et al.*, *Helicobacter pylori* infection and the risk of Barrett's oesophagus: a community-based study. *Gut*. **57**, 727–733 (2008).

96. Epidemiology of, and risk factors for, *Helicobacter pylori* infection among 3194 asymptomatic subjects in 17 populations. The EUROGAST Study Group. *Gut*. **34**, 1672–1676 (1993).

97. M. Waghray *et al.*, Interleukin-1beta promotes gastric atrophy through suppression of Sonic Hedgehog. *Gastroenterology*. **138**, 562–72, 572.e1–2 (2010).

98. A. D. Jones *et al.*, *Helicobacter pylori* induces apoptosis in Barrett's-derived esophageal adenocarcinoma cells. *J. Gastrointest. Surg.* **7**, 68–76 (2003).

99. E. K. Costello *et al.*, Bacterial community variation in human body habitats across space and time. *Science*. **326**, 1694–1697 (2009).

100. Z. Pei *et al.*, Bacterial biota in the human distal esophagus. *Proc. Natl. Acad. Sci. U.S.A.* **101**, 4250–4255 (2004).

101. L. Yang *et al.*, Inflammation and intestinal metaplasia of the distal esophagus are associated with alterations in the microbiome. *Gastroenterology*. **137**, 588–597 (2009).

102. I. Amir, F. M. Konikoff, M. Oppenheim, U. Gophna, E. E. Half, Gastric microbiota is altered in oesophagitis and Barrett's oesophagus and further modified by proton pump inhibitors. *Environ. Microbiol.* (2013), doi:10.1111/1462-2920.12285.

103. S. Hardikar *et al.*, The role of tobacco, alcohol, and obesity in neoplastic progression to esophageal adenocarcinoma: a prospective study of Barrett's esophagus. *PLoS ONE*. **8**, e52192 (2013).

104. S. Singh *et al.*, Central adiposity is associated with increased risk of esophageal inflammation, metaplasia, and adenocarcinoma: a systematic review and meta-analysis. *Clin. Gastroenterol. Hepatol.* **11**, 1399–1412.e7 (2013).

105. J. Andrici, M. Tio, M. R. Cox, G. D. Eslick, Hiatal hernia and the risk of Barrett's esophagus. *J. Gastroenterol. Hepatol.* **28**, 415–431 (2013).

106. R. Anaparthy *et al.*, Association between length of Barrett's esophagus and risk of high-grade dysplasia or adenocarcinoma in patients without dysplasia. *Clin. Gastroenterol. Hepatol.* **11**, 1430–1436 (2013).

107. B. J. Reid *et al.*, Flow-cytometric and histological progression to malignancy in Barrett's esophagus: prospective endoscopic surveillance of a cohort. *Gastroenterology*. **102**, 1212–1219 (1992).

108. R. M. Peek, M. J. Blaser, *Helicobacter pylori* and gastrointestinal tract adenocarcinomas. *Nat. Rev. Cancer*. **2**, 28–37 (2002).

109. H. Higashi *et al.*, SHP-2 tyrosine phosphatase as an intracellular target of *Helicobacter pylori* CagA protein. *Science*. **295**, 683–686 (2002).

110. N. Liu *et al.*, Characterization of bacterial biota in the distal esophagus of Japanese patients with reflux esophagitis and Barrett's esophagus. *BMC Infect. Dis.* **13**, 130 (2013).

111. M. S. Leibowitz *et al.*, SHP2 is overexpressed and inhibits pSTAT1-mediated APM component expression, T-cell attracting chemokine secretion, and CTL recognition in head and neck cancer cells. *Clin. Cancer Res.* **19**, 798–808 (2013).

112. N. Segata *et al.*, Composition of the adult digestive tract bacterial microbiome based on seven mouth surfaces, tonsils, throat and stool samples. *Genome Biol.* **13**, R42 (2012).

113. V. K. Ridaura *et al.*, Gut microbiota from twins discordant for obesity modulate metabolism in mice. *Science*. **341**, 1241214 (2013).

114. K. Kurokawa *et al.*, Comparative metagenomics revealed commonly enriched gene sets in human gut microbiomes. *DNA Res.* **14**, 169–181 (2007).

115. J. Maukonen, J. Mättö, M.-L. Suihko, M. Saarela, Intra-individual diversity and similarity of salivary and faecal microbiota. *J. Med. Microbiol.* **57**, 1560–1568 (2008).

116. F. E. Dewhirst *et al.*, The human oral microbiome. *J. Bacteriol.* **192**, 5002–5017 (2010).

117. G. D. Wu *et al.*, Linking long-term dietary patterns with gut microbial enterotypes. *Science*. **334**, 105–108 (2011).

118. S. M. Huse, Y. Ye, Y. Zhou, A. A. Fodor, A core human microbiome as viewed through 16S rRNA sequence clusters. *PLoS ONE*. **7**, e34242 (2012).

119. I. Martínez, C. E. Muller, J. Walter, Long-term temporal analysis of the human fecal microbiota revealed a stable core of dominant bacterial species. *PLoS ONE*. **8**, e69621 (2013).

120. J. J. Faith *et al.*, The long-term stability of the human gut microbiota. *Science*. **341**, 1237439 (2013).

121. K. Li, M. Bihan, B. A. Methé, Analyses of the stability and core taxonomic memberships of the human microbiome. *PLoS ONE*. **8**, e63139 (2013).

122. M. J. Claesson *et al.*, Gut microbiota composition correlates with diet and health in the elderly. *Nature*. **488**, 178–184 (2012).

123. S. P. van Tongeren, J. P. J. Slaets, H. J. M. Harmsen, G. W. Welling, Fecal microbiota composition and frailty. *Appl. Environ. Microbiol.* **71**, 6438–6442 (2005).

124. M. J. Claesson *et al.*, Composition, variability, and temporal stability of the intestinal microbiota of the elderly. *Proc. Natl. Acad. Sci. U.S.A.* **108 Suppl 1**, 4586–4591 (2011).

125. C. C. Evans *et al.*, Exercise prevents weight gain and alters the gut microbiota in a mouse model of high fat diet-induced obesity. *PLoS ONE*. **9**, e92193 (2014).

126. R. E. Ley *et al.*, Obesity alters gut microbial ecology. *Proc. Natl. Acad. Sci. U.S.A.* **102**, 11070–11075 (2005).

127. P. J. Turnbaugh *et al.*, The effect of diet on the human gut microbiome: a metagenomic analysis in humanized gnotobiotic mice. *Sci Transl Med*. **1**, 6ra14 (2009).

128. F. Bäckhed, J. K. Manchester, C. F. Semenkovich, J. I. Gordon, Mechanisms underlying the resistance to diet-induced obesity in germ-free mice. *Proc. Natl. Acad. Sci. U.S.A.* **104**, 979–984 (2007).

129. B. J. Reid, D. S. Levine, G. Longton, P. L. Blount, P. S. Rabinovitch, Predictors of progression to cancer in Barrett's esophagus: baseline histology and flow cytometry identify low- and high-risk patient subsets. *Am. J. Gastroenterol.* **95**, 1669–1676 (2000).

130. P. S. Rabinovitch, G. Longton, P. L. Blount, D. S. Levine, B. J. Reid, Predictors of progression in Barrett's esophagus III: baseline flow cytometric variables. *Am. J. Gastroenterol.* **96**, 3071–3083 (2001).

131. D. S. Levine, P. L. Blount, R. E. Rudolph, B. J. Reid, Safety of a systematic endoscopic biopsy protocol in patients with Barrett's esophagus. *Am. J. Gastroenterol.* **95**, 1152–1157 (2000).

132. C. W. Nossa *et al.*, Design of 16S rRNA gene primers for 454 pyrosequencing of the human foregut microbiome. *World J. Gastroenterol.* **16**, 4135–4144 (2010).

133. J. M. Neefs, Y. Van de Peer, P. De Rijk, S. Chapelle, R. De Wachter, Compilation of small ribosomal subunit RNA structures. *Nucleic Acids Res.* **21**, 3025–3049 (1993).

134. M. Hamady, J. J. Walker, J. K. Harris, N. J. Gold, R. Knight, Error-correcting barcoded primers for pyrosequencing hundreds of samples in multiplex. *Nat. Methods*. **5**, 235–237 (2008).

135. F. A. Matsen, R. B. Kodner, E. V. Armbrust, pplacer: linear time maximum-likelihood and Bayesian phylogenetic placement of sequences onto a fixed reference tree. *BMC Bioinformatics*. **11**, 538 (2010).

136. Q. Wang, G. M. Garrity, J. M. Tiedje, J. R. Cole, Naive Bayesian classifier for rapid assignment of rRNA sequences into the new bacterial taxonomy. *Appl. Environ.*

Microbiol. **73**, 5261–5267 (2007).

137. S. N. Evans, F. A. Matsen, The phylogenetic Kantorovich-Rubinstein metric for environmental sequence samples. *J R Stat Soc Series B Stat Methodol*. **74**, 569–592 (2012).

138. F. A. Matsen, S. N. Evans, Edge principal components and squash clustering: using the special structure of phylogenetic placement data for sample comparison. *PLoS ONE*. **8**, e56859 (2013).

139. R. M. Warwick, K. R. Clarke, New "biodiversity" measures reveal a decrease in taxonomic distinctness with increasing stress. *Marine Ecology Progress Series*. **129**, 301–305 (1995).

140. D. Gevers, M. Pop, P. D. Schloss, C. Huttenhower, Bioinformatics for the Human Microbiome Project. *PLoS Comput. Biol.* **8**, e1002779 (2012).

141. J. D. Rudney, Y. Pan, R. Chen, Streptococcal diversity in oral biofilms with respect to salivary function. *Arch. Oral Biol.* **48**, 475–493 (2003).

142. R. C. Team, R, (available at http://www.R-project.org/).

143. C. R. Rao, Diversity and dissimilarity coefficients: A unified approach. *Theoretical Population Biology*. **21**, 24–43 (1982).

144. A. Gall, R. G. Gaudet, S. D. Gray-Owen, N. R. Salama, TIFA Signaling in Gastric Epithelial Cells Initiates the *cag* Type 4 Secretion System-Dependent Innate Immune Response to *Helicobacter pylori* Infection. *MBio*. **8** (2017), doi:10.1128/mBio.01168-17.

145. Y. Yamaoka, Mechanisms of disease: *Helicobacter pylori* virulence factors. *Nat Rev Gastroenterol Hepatol*. **7**, 629–641 (2010).

146. M. A. Monteiro *et al.*, Simultaneous expression of type 1 and type 2 Lewis blood group antigens by *Helicobacter pylori* lipopolysaccharides. Molecular mimicry between *H. pylori* lipopolysaccharides and human gastric epithelial cell surface glycoforms. *J. Biol. Chem.* **273**, 11533–11543 (1998).

147. A. X. Tran *et al.*, The lipid A 1-phosphatase of *Helicobacter pylori* is required for resistance to the antimicrobial peptide polymyxin. *J. Bacteriol.* **188**, 4531–4541 (2006).

148. P. B. Ernst, B. D. Gold, The disease spectrum of *Helicobacter pylori*: the immunopathogenesis of gastroduodenal ulcer and gastric cancer. *Annu. Rev. Microbiol.* **54**, 615–640 (2000).

149. S. Brandt, T. Kwok, R. Hartig, W. König, S. Backert, NF-kappaB activation and potentiation of proinflammatory responses by the *Helicobacter pylori* CagA protein.

Proc. Natl. Acad. Sci. U.S.A. **102**, 9300–9305 (2005).

150. Y. Hirata *et al.*, MyD88 and TNF receptor-associated factor 6 are critical signal transducers in *Helicobacter pylori*-infected human epithelial cells. *J. Immunol.* **176**, 3796–3803 (2006).

151. R. J. Gorrell *et al.*, A novel NOD1- and CagA-independent pathway of interleukin-8 induction mediated by the *Helicobacter pylori* type IV secretion system. *Cell. Microbiol.* **15**, 554–570 (2013).

152. H. Takatsuna *et al.*, Identification of TIFA as an adapter protein that links tumor necrosis factor receptor-associated factor 6 (TRAF6) to interleukin-1 (IL-1) receptor-associated kinase-1 (IRAK-1) in IL-1 receptor signaling. *J. Biol. Chem.* **278**, 12144–12150 (2003).

153. C.-K. Ea, L. Sun, J.-I. Inoue, Z. J. Chen, TIFA activates IkappaB kinase (IKK) by promoting oligomerization and ubiquitination of TRAF6. *Proc. Natl. Acad. Sci. U.S.A.* **101**, 15318–15323 (2004).

154. N. Ding *et al.*, TIFA upregulation after hypoxia-reoxygenation is TLR4- and MyD88-dependent and associated with HMGB1 upregulation and release. *Free Radic. Biol. Med.* **63**, 361–367 (2013).

155. R. G. Gaudet *et al.*, INNATE IMMUNITY. Cytosolic detection of the bacterial metabolite HBP activates TIFA-dependent innate immunity. *Science*. **348**, 1251–1255 (2015).

156. R. G. Gaudet, S. D. Gray-Owen, Heptose Sounds the Alarm: Innate Sensing of a Bacterial Sugar Stimulates Immunity. *PLoS Pathog.* **12**, e1005807 (2016).

157. M. Milivojevic *et al.*, ALPK1 controls TIFA/TRAF6-dependent innate immunity against heptose-1,7-bisphosphate of gram-negative bacteria. *PLoS Pathog.* **13**, e1006224 (2017).

158. R. G. Gaudet *et al.*, Innate Recognition of Intracellular Bacterial Growth Is Driven by the TIFA-Dependent Cytosolic Surveillance Pathway. *Cell Rep*. **19**, 1418–1430 (2017).

159. K. Kobayashi *et al.*, RICK/Rip2/CARDIAK mediates signalling for receptors of the innate and adaptive immune systems. *Nature*. **416**, 194–199 (2002).

160. H. Janouskova *et al.*, Activation of p53 pathway by Nutlin-3a inhibits the expression of the therapeutic target α5 integrin in colon cancer cells. *Cancer Lett.* **336**, 307–318 (2013).

161. L. F. Jiménez-Soto *et al.*, *Helicobacter pylori* type IV secretion apparatus exploits beta1 integrin in a novel RGD-independent manner. *PLoS Pathog.* **5**, e1000684 (2009).

162. V. Hornung *et al.*, Quantitative expression of toll-like receptor 1-10 mRNA in cellular subsets of human peripheral blood mononuclear cells and sensitivity to CpG oligodeoxynucleotides. *J. Immunol.* **168**, 4531–4537 (2002).

163. L. Lau, E. E. Gray, R. L. Brunette, D. B. Stetson, DNA tumor virus oncogenes antagonize the cGAS-STING DNA-sensing pathway. *Science*. **350**, 568–571 (2015).

164. M. A. Valvano, P. Messner, P. Kosma, Novel pathways for biosynthesis of nucleotide-activated glycero-manno-heptose precursors of bacterial glycoproteins and cell surface polysaccharides. *Microbiology (Reading, Engl.)*. **148**, 1979–1989 (2002).

165. C.-K. Yu *et al.*, Functional characterization of *Helicobacter pylori* 26695 sedoheptulose 7-phosphate isomerase encoded by hp0857 and its association with lipopolysaccharide biosynthesis and adhesion. *Biochem. Biophys. Res. Commun.* **477**, 794–800 (2016).

166. M. M. Shaik, G. Zanotti, L. Cendron, The crystal structure of ADP-L-glycero-D-manno-heptose-6-epimerase (HP0859) from *Helicobacter pylori*. *Biochim. Biophys. Acta*. **1814**, 1641–1647 (2011).

167. H. Li *et al.*, The redefinition of *Helicobacter pylori* lipopolysaccharide O-antigen and core-oligosaccharide domains. *PLoS Pathog.* **13**, e1006280 (2017).

168. K. Hiratsuka *et al.*, Identification of a D-glycero-D-manno-heptosyltransferase gene from *Helicobacter pylori*. *J. Bacteriol.* **187**, 5156–5165 (2005).

169. H. L. Mobley, G. L. Mendz, S. L. Hazell, A. P. Moran, Molecular Structure, Biosynthesis, and Pathogenic Roles of Lipopolysaccharides (2001).

170. D. A. Baltrus *et al.*, The complete genome sequence of *Helicobacter pylori* strain G27. *J. Bacteriol.* **191**, 447–448 (2009).

171. L. A. Kelley, S. Mezulis, C. M. Yates, M. N. Wass, M. J. E. Sternberg, The Phyre2 web portal for protein modeling, prediction and analysis. *Nat. Protocols*. **10**, 845–858.

172. P.-C. Chang, C.-J. Wang, C.-K. You, M.-C. Kao, Effects of a HP0859 (rfaD) knockout mutation on lipopolysaccharide structure of *Helicobacter pylori* 26695 and the bacterial adhesion on AGS cells. *Biochem. Biophys. Res. Commun.* **405**, 497–502 (2011).

173. A. Lamb, J. Chen, S. R. Blanke, L.-F. Chen, *Helicobacter pylori* activates NF-κB by inducing Ubc13-mediated ubiquitination of lysine 158 of TAK1. *J. Cell. Biochem.* **114**, 2284–2292 (2013).

174. M. Stein, P. Ruggiero, R. Rappuoli, F. Bagnoli, *Helicobacter pylori* CagA: From Pathogenic Mechanisms to Its Use as an Anti-Cancer Vaccine. *Front Immunol*. **4**,

328 (2013).

175. J. E. Crabtree *et al.*, Induction of interleukin-8 secretion from gastric epithelial cells by a cagA negative isogenic mutant of *Helicobacter pylori*. *J. Clin. Pathol.* **48**, 967–969 (1995).

176. S. A. Sharma, M. K. Tummuru, M. J. Blaser, L. D. Kerr, Activation of IL-8 gene expression by *Helicobacter pylori* is regulated by transcription factor nuclear factor-kappa B in gastric epithelial cells. *J. Immunol.* **160**, 2401–2407 (1998).

177. W. Fischer *et al.*, Systematic mutagenesis of the *Helicobacter pylori* cag pathogenicity island: essential genes for CagA translocation in host cells and induction of interleukin-8. *Mol. Microbiol.* **42**, 1337–1348 (2001).

178. A. Lamb *et al.*, *Helicobacter pylori* CagA activates NF-kappaB by targeting TAK1 for TRAF6-mediated Lys 63 ubiquitination. *EMBO Rep.* **10**, 1242–1249 (2009).

179. E. Altman, V. Chandan, J. Li, E. Vinogradov, A reinvestigation of the lipopolysaccharide structure of *Helicobacter pylori* strain Sydney (SS1). *FEBS J.* **278**, 3484–3493 (2011).

180. E. Altman, V. Chandan, J. Li, E. Vinogradov, Lipopolysaccharide structures of *Helicobacter pylori* wild-type strain 26695 and 26695 HP0826::Kan mutant devoid of the O-chain polysaccharide component. *Carbohydr. Res.* **346**, 2437–2444 (2011).

181. E. Altman, V. Chandan, J. Li, E. Vinogradov, Lipopolysaccharide structure of *Helicobacter pylori* serogroup O:3. *Carbohydr. Res.* **378**, 139–143 (2013).

182. H. Li *et al.*, Lipopolysaccharide Structure and Biosynthesis in *Helicobacter pylori*. *Helicobacter*. **21**, 445–461 (2016).

183. E. E. Gray *et al.*, The AIM2-like Receptors Are Dispensable for the Interferon Response to Intracellular DNA. *Immunity*. **45**, 255–266 (2016).

184. N. E. Sanjana, O. Shalem, F. Zhang, Improved vectors and genome-wide libraries for CRISPR screening. *Nat. Methods*. **11**, 783–784 (2014).

185. J. M. Kim, D. Kim, S. Kim, J.-S. Kim, Genotyping with CRISPR-Cas-derived RNA-guided endonucleases. *Nat Commun*. **5**, 3157 (2014).

186. A. Covacci *et al.*, Molecular characterization of the 128-kDa immunodominant antigen of *Helicobacter pylori* associated with cytotoxicity and duodenal ulcer. *Proc. Natl. Acad. Sci. U.S.A.* **90**, 5791–5795 (1993).

187. N. R. Salama, B. Shepherd, S. Falkow, Global transposon mutagenesis and essential gene analysis of *Helicobacter pylori*. *J. Bacteriol.* **186**, 7926–7935 (2004).

188. O. Humbert, N. R. Salama, The *Helicobacter pylori* HpyAXII restriction-

modification system limits exogenous DNA uptake by targeting GTAC sites but shows asymmetric conservation of the DNA methyltransferase and restriction endonuclease components. *Nucleic Acids Res.* **36**, 6893–6906 (2008).

189. L. C. Smeets, J. J. Bijlsma, S. Y. Boomkens, C. M. Vandenbroucke-Grauls, J. G. Kusters, comH, a novel gene essential for natural transformation of *Helicobacter pylori*. *J. Bacteriol.* **182**, 3948–3954 (2000).

190. M. L. Langford, J. Zabaleta, A. C. Ochoa, T. L. Testerman, D. J. McGee, *In vitro* and *in vivo* complementation of the *Helicobacter pylori* arginase mutant using an intergenic chromosomal site. *Helicobacter*. **11**, 477–493 (2006).

191. F. M. Ausubel *et al.*, *Short Protocols in Molecular Biology* (John Wiley & Sons, 1995).

192. S. E. Girardin *et al.*, Nod1 detects a unique muropeptide from gram-negative bacterial peptidoglycan. *Science*. **300**, 1584–1587 (2003).

193. W. Hoffmann, Stem cells, self-renewal and cancer of the gastric epithelium. *Curr. Med. Chem.* **19**, 5975–5983 (2012).

194. T. Sato *et al.*, Single Lgr5 stem cells build crypt-villus structures in vitro without a mesenchymal niche. *Nature*. **459**, 262–265 (2009).

195. H. Miyoshi, T. S. Stappenbeck, *In vitro* expansion and genetic modification of gastrointestinal stem cells in spheroid culture. *Nat Protoc*. **8**, 2471–2482 (2013).

196. J. R. Spence *et al.*, Directed differentiation of human pluripotent stem cells into intestinal tissue *in vitro*. *Nature*. **470**, 105–109 (2011).

197. M. Noben *et al.*, Human intestinal epithelium in a dish: Current models for research into gastrointestinal pathophysiology. *United European Gastroenterol J*. **5**, 1073–1081 (2017).

198. K. L. VanDussen *et al.*, Development of an enhanced human gastrointestinal epithelial culture system to facilitate patient-based assays. *Gut*. **64**, 911–920 (2015).

199. T. Watanabe *et al.*, NOD1 contributes to mouse host defense against *Helicobacter pylori* via induction of type I IFN and activation of the ISGF3 signaling pathway. *J. Clin. Invest.* **120**, 1645–1662 (2010).

200. D. N. Baldwin *et al.*, Identification of *Helicobacter pylori* genes that contribute to stomach colonization. *Infect. Immun.* **75**, 1005–1016 (2007).

201. G. M. Morrison *et al.*, Mouse beta defensin-1 is a functional homolog of human beta defensin-1. *Mamm. Genome*. **9**, 453–457 (1998).

202. G. M. Morrison, D. J. Davidson, J. R. Dorin, A novel mouse beta defensin, Defb2,

which is upregulated in the airways by lipopolysaccharide. *FEBS Lett.* **442**, 112–116 (1999).

203. R. Bals *et al.*, Mouse beta-defensin 3 is an inducible antimicrobial peptide expressed in the epithelia of multiple organs. *Infect. Immun.* **67**, 3542–3547 (1999).

204. J. Röhrl, D. Yang, J. J. Oppenheim, T. Hehlgans, Human beta-defensin 2 and 3 and their mouse orthologs induce chemotaxis through interaction with CCR2. *J. Immunol.* **184**, 6688–6694 (2010).

205. L. E. Martínez, thesis, University of Washington, Seattle (2016).

206. P. Schlaermann *et al.*, A novel human gastric primary cell culture system for modelling *Helicobacter pylori* infection in vitro. *Gut*. **65**, 202–213 (2016).

207. S. Bartfeld, H. Clevers, Organoids as Model for Infectious Diseases: Culture of Human and Murine Stomach Organoids and Microinjection of *Helicobacter pylori*. *J Vis Exp* (2015), doi:10.3791/53359.

208. S. Bartfeld *et al.*, In vitro expansion of human gastric epithelial stem cells and their responses to bacterial infection. *Gastroenterology*. **148**, 126–136.e6 (2015).

209. S. Omenetti, T. T. Pizarro, The Treg/Th17 Axis: A Dynamic Balance Regulated by the Gut Microbiome. *Front Immunol*. **6**, 639 (2015).

210. C. B. Hergott *et al.*, Peptidoglycan from the gut microbiota governs the lifespan of circulating phagocytes at homeostasis. *Blood*. **127**, 2460–2471 (2016).

211. N. R. Salama, G. Otto, L. Tompkins, S. Falkow, Vacuolating cytotoxin of *Helicobacter pylori* plays a role during colonization in a mouse model of infection. *Infect. Immun.* **69**, 730–736 (2001).

212. C. Moon, K. L. VanDussen, H. Miyoshi, T. S. Stappenbeck, Development of a primary mouse intestinal epithelial cell monolayer culture system to evaluate factors that modulate IgA transcytosis. *Mucosal Immunol*. **7**, 818–828 (2014).

213. R. M. Genta, G. M. Lew, D. Y. Graham, Changes in the gastric mucosa following eradication of *Helicobacter pylori*. *Mod. Pathol.* **6**, 281–289 (1993).

214. A. Mantovani, M. A. Cassatella, C. Costantini, S. Jaillon, Neutrophils in the activation and regulation of innate and adaptive immunity. *Nat Rev Immunol*. **11**, 519–531 (2011).

215. K. Otani *et al.*, Toll-like receptor 9 signaling has anti-inflammatory effects on the early phase of *Helicobacter pylori*-induced gastritis. *Biochem. Biophys. Res. Commun.* **426**, 342–349 (2012).

216. T. Decker, M. Müller, S. Stockinger, The yin and yang of type I interferon activity

in bacterial infection. *Nat Rev Immunol*. **5**, 675–687 (2005).

217. M. S. Dorer, I. E. Cohen, T. H. Sessler, J. Fero, N. R. Salama, Natural competence promotes *Helicobacter pylori* chronic infection. *Infect. Immun.* **81**, 209–215 (2013).

218. A. Lee *et al.*, A standardized mouse model of *Helicobacter pylori* infection: introducing the Sydney strain. *Gastroenterology*. **112**, 1386–1397 (1997).

219. J. Wu *et al.*, Cyclic GMP-AMP is an endogenous second messenger in innate immune signaling by cytosolic DNA. *Science*. **339**, 826–830 (2013).

220. B. L. Lee, G. M. Barton, Trafficking of endosomal Toll-like receptors. *Trends Cell Biol.* **24**, 360–369 (2014).

221. S. Zimmermann *et al.*, ALPK1- and TIFA-Dependent Innate Immune Response Triggered by the *Helicobacter pylori* Type IV Secretion System. *Cell Rep*. **20**, 2384–2395 (2017).

222. G. Wang, P. Alamuri, R. J. Maier, The diverse antioxidant systems of *Helicobacter pylori*. *Mol. Microbiol.* **61**, 847–860 (2006).

VITA

Alevtina Gall was born in Novosibirsk, Russia. At the age of ten, she immigrated with her family to the United States. In 2008, she received a Bachelor of Science in Molecular, Cellular and Developmental Biology and a Bachelor of Arts in International Studies with a minor in African Studies from the University of Washington. During her undergraduate career, she traveled to The Gambia and worked at the Medical Research Council investigating immune mechanisms of disease initiation in trachomatous trichiasis. After completing her undergraduate studies, she worked for three years as a research scientist at the University of Washington studying how misregulated antiviral responses can result in autoimmune disease. In 2011, she began her medical studies at the University of Washington School of Medicine. She joined Dr. Nina Salama's lab in 2013 to pursue her graduate thesis work focused on understanding how *Helicobacter pylori* interacts with host gastric epithelial cells and myeloid-derived cells to initiate disease. She received her doctoral degree in 2018.